Doing science with eLISA:

Astrophysics and cosmology in the millihertz regime

Pau Amaro-Seoane[1,13], Sofiane Aoudia[1], Stanislav Babak[1], Pierre Binétruy[2], Emanuele Berti[3,4], Alejandro Bohé[5], Chiara Caprini[6], Monica Colpi[7], Neil J. Cornish[8], Karsten Danzmann[1], Jean-François Dufaux[2], Jonathan Gair[9], Oliver Jennrich[10], Philippe Jetzer[11], Antoine Klein[11,8], Ryan N. Lang[12], Alberto Lobo[13], Tyson Littenberg[14,15], Sean T. McWilliams[16], Gijs Nelemans[17,18,19], Antoine Petiteau[2,1], Edward K. Porter[2], Bernard F. Schutz[1], Alberto Sesana[1], Robin Stebbins[20], Tim Sumner[21], Michele Vallisneri[22], Stefano Vitale[23], Marta Volonteri[24,25], and Henry Ward[26]

[1]Max Planck Institut für Gravitationsphysik (Albert-Einstein-Institut), Germany
[2]APC, Univ. Paris Diderot, CNRS/IN2P3, CEA/Irfu, Obs. de Paris, Sorbonne Paris Cité, France
[3]Department of Physics and Astronomy, The University of Mississippi, University, MS 38677, USA
[4]Division of Physics, Mathematics, and Astronomy, California Institute of Technology, Pasadena CA 91125, USA
[5]UPMC-CNRS, UMR7095, Institut d'Astrophysique de Paris, F-75014, Paris, France
[6]Institut de Physique Théorique, CEA, IPhT, CNRS, URA 2306, F-91191Gif/Yvette Cedex, France
[7]University of Milano Bicocca, Milano, I-20100, Italy
[8]Department of Physics, Montana State University, Bozeman, MT 59717, USA
[9]Institute of Astronomy, University of Cambridge, Madingley Road, Cambridge, CB3 0HA, UK
[10]ESA, Keplerlaan 1, 2200 AG Noordwijk, The Netherlands
[11]Institute of Theoretical Physics University of Zürich, Winterthurerstr. 190, 8057 Zürich Switzerland
[12]Washington University in St. Louis, One Brookings Drive, St. Louis, MO 63130, USA
[13]Institut de Ciències de l'Espai (CSIC-IEEC), Campus UAB, Torre C-5, parells, 2na planta, ES-08193, Bellaterra, Barcelona, Spain
[14]Maryland Center for Fundamental Physics, Department of Physics, University of Maryland, College Park, MD 20742
[15]Gravitational Astrophysics Laboratory, NASA Goddard Spaceflight Center, 8800 Greenbelt Rd., Greenbelt, MD 20771, USA
[16]Department of Physics, Princeton University, Princeton, NJ 08544, USA
[17]Department of Astrophysics, Radboud University Nijmegen, The Netherlands
[18]Institute for Astronomy, KU Leuven, Celestijnenlaan 200D, 3001 Leuven, Belgium
[19]Nikhef, Science Park 105, 1098 XG Amsterdam, The Netherlands
[20]NASA Liason, NASA GSFC, USA
[21]Imperial College, UK
[22]Jet Propulsion Laboratory, California Inst. of Technology, Pasadena, CA 91109, USA
[23]University of Trento, Department of Physics, I38050 Povo, Trento, Italy
[24]Institut d'Astrophysique de Paris, 98bis Boulevard Arago, 75014 Paris, France
[25]Astronomy Department, University of Michigan, Ann Arbor, MI 48109, USA
[26]Institute for Gravitational Research, Department of Physics & Astronomy Kelvin Building, University of Glasgow, Glasgow

Contents

Abstract

This document introduces the exciting and fundamentally new science and astronomy that the European New Gravitational Wave Observatory (NGO) mission (derived from the previous LISA proposal) will deliver. The mission (which we will refer to by its informal name "eLISA") will survey for the first time the low-frequency gravitational wave band (about 0.1 mHz to 1 Hz), with sufficient sensitivity to detect interesting individual astrophysical sources out to $z = 15$. The measurements described here will address the basic scientific goals that have been captured in ESA's "New Gravitational Wave Observatory Science Requirements Document"; they are presented here so that the wider scientific community can have access to them. The eLISA mission will discover and study a variety of cosmic events and systems with high sensitivity: coalescences of massive black holes binaries, brought together by galaxy mergers; mergers of earlier, less-massive black holes during the epoch of hierarchical galaxy and black-hole growth; stellar-mass black holes and compact stars in orbits just skimming the horizons of massive black holes in galactic nuclei of the present era; extremely compact white dwarf binaries in our Galaxy, a rich source of information about binary evolution and about future Type Ia supernovae; and possibly most interesting of all, the uncertain and unpredicted sources, for example relics of inflation and of the symmetry-breaking epoch directly after the Big Bang. eLISA's measurements will allow detailed studies of these signals with high signal-to-noise ratio, addressing most of the key scientific questions raised by ESA's Cosmic Vision programme in the areas of astrophysics and cosmology. They will also provide stringent tests of general relativity in the strong-field dynamical regime, which cannot be probed in any other way. This document not only describes the science but also gives an overview on the mission design and orbits. LISA's heritage in the eLISA design will be clear to those familiar with the previous proposal, as will its incorporation of key elements of hardware from the LISA Pathfinder mission, scheduled for launch by ESA in 2014. But eLISA is fundamentally a new mission, one that will pioneer the completely new science of low-frequency gravitational wave astronomy.

1 Introduction

Our view of the Universe has changed dramatically over the past century. Less than a hundred years ago our own Galaxy, the Milky Way, was believed to be our own island-Universe. The discovery of hundreds of billion galaxies like our own, and of billion luminous sources such as Quasi Stellar Objects (QSOs), changed our perception of the cosmic landscape. New astronomical objects were discovered with the advent of radio and X-ray Astronomy. Relativistic binaries composed of compact stars (such as white dwarfs or neutron stars) and stellar-mass black holes are among these sources of electromagnetic radiation. According to the accretion paradigm, supermassive black holes at galactic centres are the simplest explanation for the power emitted by distant, luminous QSOs, but a conclusive test of this hypothesis is still lacking.

The remarkable discovery of the recession of galaxies and of the fossil microwave background radiation, almost contemporary to the discovery of X-ray sources, has further led to the emergence of a cosmological paradigm, the Big Bang, that has revolutionized our description of the Universe. We now know that our Universe had a beginning and that its luminous components (in particular, galaxies and QSOs) evolve jointly and in concordance with the evolution of the underlying dark matter permeating the Universe.

According to General Relativity, black holes and compact binaries are expected to be powerful sources of *gravitational waves*. Rather than "seeing" electromagnetic radiation, as all of astronomy has done until present, eLISA will "hear" the vibrations of the fabric of spacetime itself, emitted coherently by macroscopic bodies. Studying these signals will convey rich new information about the behaviour, the structure and the history of the Universe, and it will clarify several issues in fundamental physics.

Gravitational waves travel undisturbed through spacetime, and when observed they offer a new and uniquely powerful way to probe the *very distant Universe*, from the extremely early Big Bang to the early epoch of galaxy and black hole seed formation. This may allow us to address deep questions. What powered the Big Bang? How did galaxies and their black holes form and evolve? What is the structure of spacetime around the massive objects we believe to be black holes? What is the nature of the mysterious dark matter and dark energy accelerating the expansion of the Universe?

eLISA is a space-based mission designed to measure gravitational radiation over a broad band at frequencies ranging between $f \sim 0.1$ mHz and $f \sim 1$ Hz. In this frequency band the Universe is richly populated by strong sources of gravitational waves. For binary systems the characteristic gravitational-wave frequency f is twice the Keplerian orbital frequency, which in turn is proportional to $(M/a^3)^{1/2}$, where M is the total mass of the binary and a its semi-major axis. In the eLISA frequency band, gravitational waves are produced by close binaries of stellar-mass objects with orbital periods of a few to several minutes. Massive black hole binaries with $M \sim 10^4\,M_\odot - 10^7\,M_\odot$ and mass ratio $0.01 \lesssim q \lesssim 1$ on the verge of coalescing have orbital frequencies sweeping to higher and higher values, until the binary separation a becomes as small as the scale of the event horizon GM/c^2. Finally, eLISA could observe binaries comprising a massive black hole and a stellar-mass compact object (e.g., a stellar-mass black hole) skimming the horizon of the larger black hole before being captured: these systems are commonly referred to as extreme mass ratio inspirals (EMRIs). Furthermore, a stochastic background in the eLISA frequency band can be generated by less conventional sources, such as phase transitions in the very early Universe and/or cosmic strings.

This note is a comprehensive survey of the eLISA science case. We consider all the relevant astrophysical and cosmological gravitational wave sources and explore eLISA detection performances in terms of sensitivity, SNR distributions, and parameter estimation.

In Section 2 we will briefly describe the *mission concept* and the basic design of the instrument, introducing the eLISA sensitivity curve that will be used throughout the study.

Our survey of the eLISA science case will start in Section 3 by exploring the nearest observable sources of gravitational waves, i.e. *compact stellar-mass binaries* in the Milky Way. eLISA will study the gravitational wave signals from thousands of stellar-mass close binaries in the Galaxy and will give information on the extreme endpoints of stellar evolution. eLISA will provide distances and detailed orbital and mass parameters for hundreds of these binaries. This is a rich trove of information for mapping and reconstructing the history of stars in the Galaxy, and it can reveal details of the tidal and non-gravitational influences on the binary evolution associated with the internal physics of the compact remnants themselves.

Then we will summarize the science objectives that are relevant for the *astrophysics of black holes* (Section 4). Current electromagnetic observations are probing only the tip of the black hole mass distribution in the Universe, targeting black holes with large masses, between $10^7\,\mathrm{M}_\odot$ and $10^9\,\mathrm{M}_\odot$. Conversely, eLISA will be able to detect the gravitational waves

emitted by black hole binaries with total mass (in the source rest frame) as small as $10^4\,M_\odot$ and up to $10^7\,M_\odot$, out to a redshift as large as $z \sim 20$. eLISA will detect fiducial sources out to redshift $z \sim 10$, and so it will explore almost all the mass-redshift parameter space relevant for addressing scientific questions on the evolution of the black hole population. Redshifted masses will be measured to an unprecedented accuracy, up to the 0.1 – 1 % level, whereas absolute errors in the spin determination are expected to be in the range 0.01 to 0.1, allowing us to reconstruct the cosmic evolution of massive black holes. Black holes are expected to transit into the mass interval to which eLISA is sensitive along the course of their cosmic evolution. Thus, eLISA will map and mark the loci where galaxies form and cluster, using black holes as clean tracers of their assembly.

eLISA will also bring a new revolutionary perspective to the study of *galactic nuclei*, as shown in Section 5. Orbits of stellar objects captured by the massive black hole at the galactic centre evolve by gravitational radiation. By capturing their signal, eLISA will offer the deepest view of nearby galactic nuclei, exploring regions that are invisible to electromagnetic techniques. eLISA will probe the dynamics of compact objects in the space-time of a Kerr black hole, providing information on the space density of those objects.

In Section 6 we address key questions concerning the nature of spacetime and gravity. GR has been extensively tested in the weak field regime, both in the solar system and via binary pulsar observations. eLISA will provide a unique opportunity to *probe GR in the strong field limit.* eLISA will observe the coalescence of massive black hole binaries moving at speeds close to the speed of light, and enable us to test the dynamics of curved spacetime when gravitational fields are strong. By observing a large number of orbital cycles during the last few years of the inspiral of a stellar mass object into a massive black hole, eLISA will allow us to measure precisely the parameters of the central object (including its quadrupole moment) in the near Universe. Any deviations in the orbital motion from GR predictions will leave an imprint in the gravitational wave phase. Thus, measurements of the mass, spin and quadrupole moment of the central object will allow us to check the Kerr nature of the central massive object, and to *test for the first time the black hole hypothesis.*

Lastly, as we describe in Section 7, eLISA will probe *new physics and cosmology* with gravitational waves, and search for unforeseen sources of gravitational waves. The eLISA frequency band in the relativistic early Universe corresponds to horizon scales where phase transitions or extra dimensions may have caused catastrophic, explosive bubble growth and efficient gravitational wave production. eLISA will be capable of detecting a stochastic background from such events from about 100 GeV to about 1000 TeV, if gravitational waves in the eLISA band were produced with sufficient efficiency.

In closing the note, we will present a summary of the science objectives of the eLISA mission. We summarize the key theoretical and observational goals of the eLISA science case in Section 8. There, in a schematic bullet-point form, we enumerate the scientific goals related to each class of gravitational wave sources and the observational performance of eLISA in achieving such goals. This could serve as a compact summary of eLISA science, as well as a reference point for other space-based gravitational wave detector proposals.

2 Description of the mission

eLISA is a European-led variant of LISA that can be launched before 2022 . The basic principle of gravitational wave detection for eLISA is the same as for LISA: it is a laser interferometer designed to detect the passage of a gravitational wave by measuring the time-varying changes of optical pathlength between free-falling masses. Many design and technological developments were migrated from LISA, however there are some substantial differences.

The two measurement arms are defined by three spacecraft orbiting the Sun in a triangular configuration (see figure 1). A key feature of the eLISA concept is a set of three orbits that maintain a near-equilateral triangular formation with an armlength $L = 10^9$m, without the need for station-keeping. Depending on the initial conditions of the spacecraft, the formation can be kept in an almost constant distance to the Earth or be allowed to slowly drift away to about 70×10^9 m, the outer limit for communication purposes. A very attractive feature of the eLISA orbits is the almost constant sun-angle of 30 degrees with respect to the normal to the top of the spacecraft, thereby resulting in an extremely stable thermal environment, minimizing the thermal disturbances on the spacecraft.

One of the three spacecraft serves as the “central hub” and defines the apex of a “V”. Two other, simpler spacecraft are positioned at the ends of the V-shaped constellation. The central spacecraft houses two free-falling “test masses” that define the endpoint of the two interferometer arms. The other spacecraft contain one test mass each, defining two more endpoints (see figure 2). Each spacecraft accommodates the interferometry equipment for measuring changes in the arm

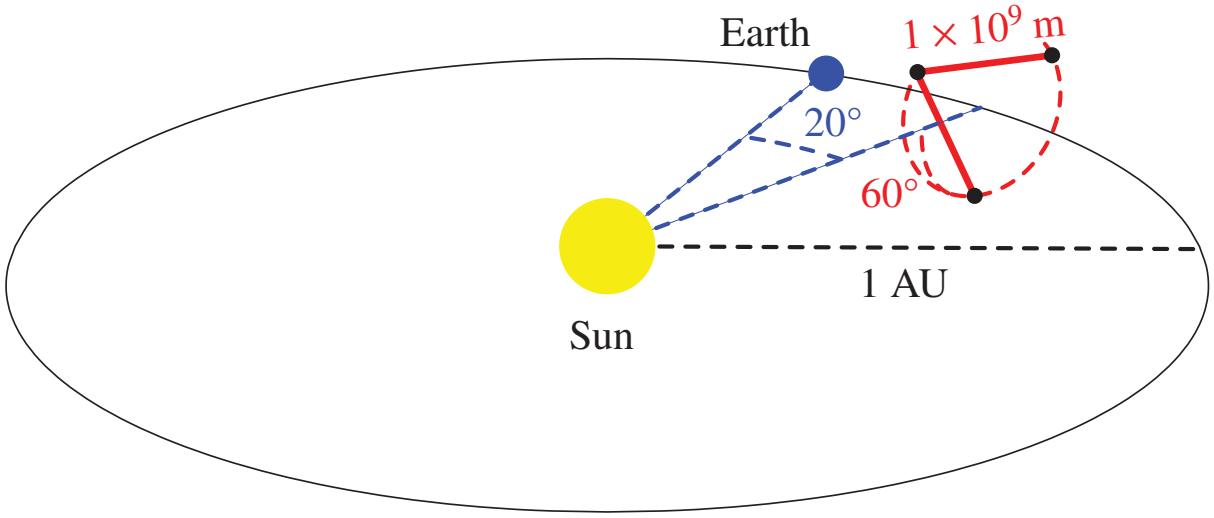

Figure 1: The eLISA orbits: The constellation is shown trailing the Earth by about 20 degrees (or 5×10^{10}km) and is inclined by 60 degrees with respect to the ecliptic. The trailing angle will vary over the course of the mission duration from 10 degrees to 25 degrees. The separation between the spacecraft is $L = 1 \times 10^9$ m.

length. For practical reasons, this measurement is broken up into three distinct parts (see figure 3): the measurement between the spacecrafts, i.e. between the optical benches that are fixed to each spacecraft, and the measurement between each of the test masses and its respective optical bench. Those measurements are recombined in a way that allows us to reconstruct the distance between the test masses which is insensitive to the noise in the position of the spacecraft with respect to the test masses.

A second key feature of the eLISA concept is that the test masses are protected from disturbances as much as possible by a careful design and the "drag-free" operation. To establish the drag-free operation, a housing around the test mass senses the relative position of test mass and spacecraft, and a control system commands the spacecraft thrusters to follow the free-falling mass. Drag-free operation reduces the time-varying disturbances to the test masses caused by force gradients arising in a spacecraft that is moving with respect to the test masses. The requirements on the power spectral density of the residual acceleration of the test mass is

$$S_{\mathrm{x,acc}}(f) = 2.13 \times 10^{-29} \left(1 + \frac{10^{-4}\mathrm{Hz}}{f}\right) \mathrm{m^2\,s^{-4}\,Hz^{-1}} \tag{1}$$

or

$$S_{\mathrm{x,acc}}(f) = 1.37 \times 10^{-32} \left(1 + \frac{10^{-4}\mathrm{Hz}}{f}\right) \frac{\mathrm{Hz}}{f^4} \mathrm{m^2\,Hz^{-1}}, \tag{2}$$

where f is the frequency.

The third key feature, the distance measuring system, is a continuous interferometric laser ranging scheme, similar to that used for radar-tracking of spacecraft. The direct reflection of laser light, such as in a normal Michelson interferometer, is not feasible due to the large distance between the spacecrafts. Therefore, lasers at the ends of each arm operate in a "transponder" mode. A laser beam is sent out from the central spacecraft to an end spacecraft. The laser in the end spacecraft is then phase-locked to the incoming beam thus returning a high-power phase replica. The returned beam is received by the central spacecraft and its phase is in turn compared to the phase of the local laser. A similar scheme is employed for the second arm. In addition, the phases of the two lasers serving the two arms are compared within the central spacecraft. The combined set of phase measurements together with some auxiliary modulation allows to determine the relative optical path changes with simultaneous suppression of the laser frequency noise and clock noise below the secondary (acceleration and displacement) noise. The displacement noise has two components: the shot noise, with a required power spectral density

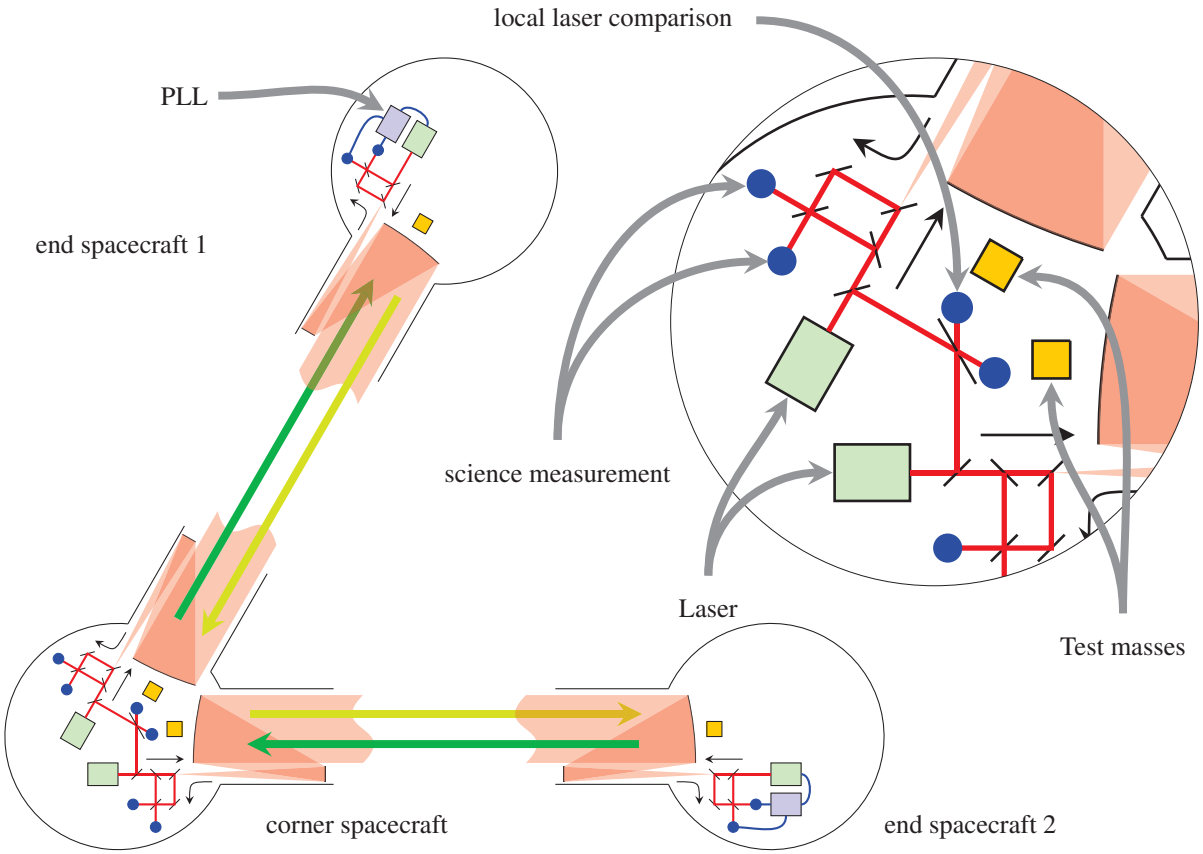

Figure 2: The constellation of the three eLISA spacecraft constitutes the science instrument. The central spacecraft harbors two send/receive laser ranging terminals, while the end spacecraft has one each. The laser in the end spacecraft is phase-locked to the incoming laser light. The blue dots indicate where interferometric measurements are taken. The sketch leaves out the test mass interferometers for clarity.

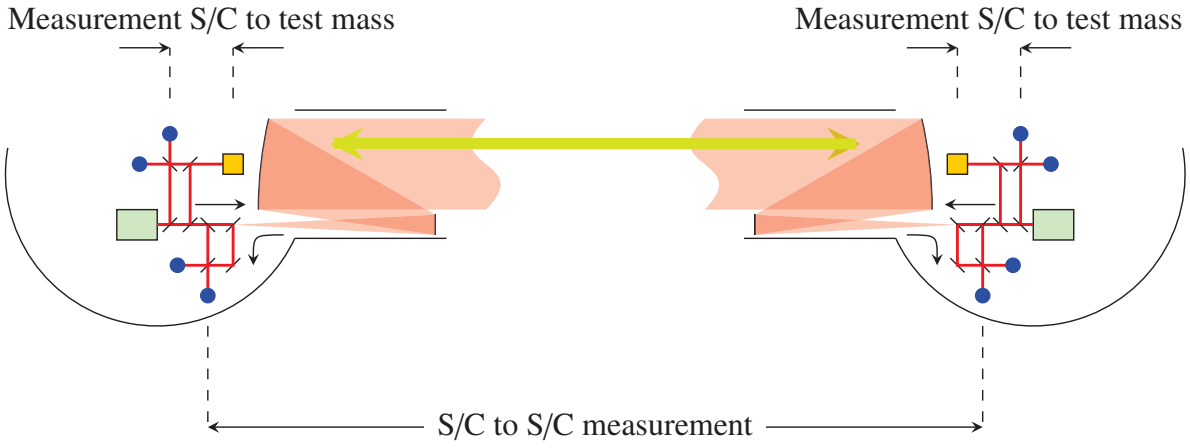

Figure 3: Partition of the eLISA measurement. Each measurement between two test masses is broken up into three different measurements: two between the respective test mass and the spacecraft and one between the two spacecraft (S/C). As the noise in the measurement is dominated by the shot noise in the S/C-S/C measurement, the noise penalty for the partitioning of the measurement is negligible. The blue (solid) dots indicate where the interferometric measurements are taken.

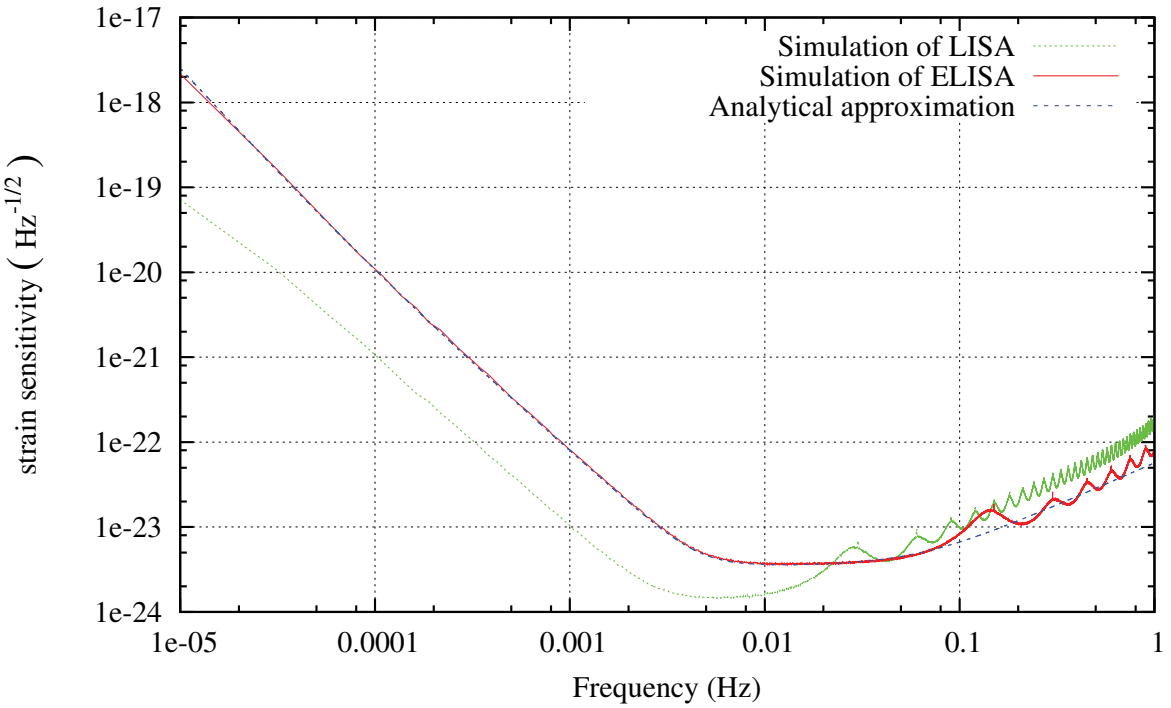

Figure 4: Sensitivity of eLISA (averaged over all sky locations and polarisations) versus frequency: the solid red curve is obtained numerically using the simulator LISACode 2.0 (Petiteau et al., 2008) and the dashed blue curve is the analytic approximation based on equation 5. For a reference, we also depict the sensitivity curve of LISA (dotted, green curve).

$$S_{\mathrm{x,sn}}(f) = 5.25 \times 10^{-23}\ \mathrm{m^2\,Hz^{-1}} \tag{3}$$

and the other (combined) measurement noise with a required power spectral density

$$S_{\mathrm{x,omn}}(f) = 6.28 \times 10^{-23}\ \mathrm{m^2\,Hz^{-1}}. \tag{4}$$

According to the requirements, eLISA achieves the strain noise amplitude spectral density (often called sensitivity) showed in figure 4 which can be analytically approximate as $\tilde{h}(f) = 2\,\widetilde{\delta L}(f)/L = \sqrt{S(f)}$, where :

$$S(f) = \frac{20}{3}\,\frac{4\,S_{\mathrm{x,acc}}(f) + S_{\mathrm{x,sn}}(f) + S_{\mathrm{x,omn}}(f)}{L^2}\left(1 + \left(\frac{f}{0.41\left(\frac{c}{2L}\right)}\right)^2\right), \tag{5}$$

This allows to detect a strain of about 3.7×10^{-24} in a 2-year measurement with an SNR of 1 (displacement sensitivity of $11 \times 10^{-12}\mathrm{m}/\sqrt{\mathrm{Hz}}$ over a path length of $1 \times 10^{9}\mathrm{m}$). The feasible reduction of disturbances on test masses and the displacement sensitivities achievable by the laser ranging system yield a useful measurement frequency bandwidth from 3×10^{-5} Hz to 1 Hz (the requirement is 10^{-4} Hz to 1 Hz; the goal is 3×10^{-5} Hz to 1 Hz).

3 Ultra-Compact Binaries

1 Overview

The most numerous sources in the low-frequency gravitational wave band are ultra-compact binary stars: double stars in which two compact objects, such as white dwarfs and neutron stars, orbit each other with short periods. They have

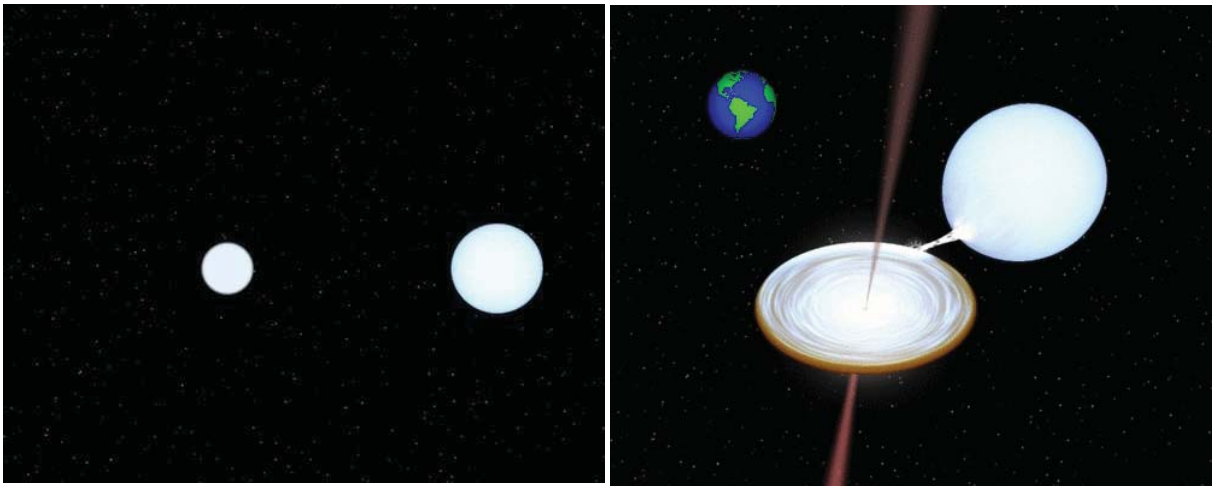

Figure 5: Artist impression of a detached double white dwarf binary (left) and an interacting binary in which a neutron star accretes material from a white dwarf donor. The Earth is shown to set the scale. Courtesy BinSim by Rob Hynes.

relatively weak gravitational wave signals in comparison to massive black hole binaries, but are numerous in the Galaxy and even the Solar neighbourhood.

Several thousand systems are expected to be detected individually, with their parameters determined to high precision, while the combined signals of the millions of compact binaries in the eLISA band will form a foreground signal. This is in contrast to less than 50 ultra-compact binaries known today. The number of detections will allow for detailed study of the entire WD binary population. In particular, the most numerous sources are double white dwarfs, which are one of the candidate progenitors of type Ia supernovae and related peculiar supernovae. eLISA will determine the merger rate of these binaries. The detailed knowledge of the ultra-compact binary population also constrains the formation of these binaries and thus many preceding phases in binary evolution. This has a strong bearing on our understanding of many high-energy phenomena in the Universe, such as supernova explosions, gamma-ray bursts and X-ray sources, as they share parts of the evolution history of the binaries detectable by eLISA.

As many of the Galactic sources are rather close (within a few kpc), they will be detectable at high SNR (often larger than 50), allowing detailed studies of individual binaries. For many hundreds, the frequency and phase evolution can be studied, enabling the study of the physics of tides and mass transfer in unprecedented detail. The extreme conditions of short orbital periods, strong gravitational fields and high mass-transfer rates are unique in astrophysics.

The information provided by eLISA will be different from what can be deduced by electromagnetic observations. In particular, eLISA's capability to determine distances and inclinations, as well as the fact that the gravitational wave signals are unaffected by interstellar dust, provide significant advantages over other detection techniques. Compared to Gaia, eLISA will observe a quite different population. Gravitational wave observations allow us to determine the distances to binaries that are right in the Galactic centre rather than to those close to the Sun. The distance determinations will make it possible to map the distribution of many compact binaries in the Galaxy, providing a new method to study Galactic structure. The inclination determinations allow the study of binary formation by comparing the average angular momentum of the binaries to that of the Galaxy. Electromagnetic observations and gravitational wave observations are complementary to one another; dedicated complementary observing programs as well as public data releases will allow simultaneous and follow-up electromagnetic observations of binaries identified by eLISA.

A number of guaranteed detectable sources are known to date from electromagnetic observations. Some of these can be used to verify instrument performance by looking for a gravitational signal at twice the orbital period and comparing the signal with expectations. In addition, once eLISA has detected several nearby binaries and determined their sky position they can be observed optically, thus providing an additional quantitative check on instrument sensitivity.

2 Instrument verification

There are currently about 50 know ultra-compact binaries. They come in two flavours: systems in which the two stars are well apart, called detached binaries, and systems in which the two stars are so close together that mass is flowing from one star to the other, called interacting binaries (see figure 5).

A subset of the known ultra-compact binaries have been recognised as instrument verification sources, as they should be detected in a few weeks to months and thus can be used to verify the performance of the instrument (Stroeer and Vecchio, 2006). The most promising verification binaries, shown as green squares in figure 6, are the shortest-period interacting binaries HM Cnc (RX J0806.3+1527), V407 Vul, ES Cet and the recently discovered 12 minute period detached system SDSS J0651+28 (Brown et al., 2011), whose lightcurve is shown in figure 8. For a decade it has remained unclear if the measured periods of HM Cnc and V407 Vul were actually orbital periods, but recent results from the Keck telescope on HM Cnc (Roelofs et al., 2010) show conclusively that this system has an orbital period of 5.4 minutes. As V407 Vul has almost identical properties, this implies that this also really is a binary with an orbital period of 9.5 minutes. As the signal from the verification binaries is essentially monochromatic with a well known frequency within the eLISA mission time, astrophysical effects such as those discussed in section 4 will not hamper their detection. As more and more wide field and synoptical surveys are completed, the number of ultra-compact binaries is gradually increasing and is expected to continue to do so in the future. Already several new binaries have been found in the SDSS and the PTF (Levitan et al., 2011, Rau et al., 2010) while surveys such as Pan-Starrs, the EGAPS and in the future LSST will also find new systems. However, most of the systems found so far have relatively long orbital periods (longer than about 30 minutes). Two pilot surveys in principle capable of finding ultra-compact binaries with periods less than 30 minutes are underway or will start soon: the RATS (Barclay et al., 2011) and the OmegaWhite survey.

Interacting ultra-compact binaries with neutron star accretors are strong X-ray sources and new discoveries are expected, both through the continued monitoring of the sky to search for X-ray transients with RXTE, MAXI and other satellites, as well as through dedicated X-ray and optical surveys of the Galactic bulge that are currently happening (Jonker et al., 2011). With these developments we expect that several tens of verification sources should be available for eLISA, allowing detailed tests of the performance of the instrument.

3 eLISA as a workhorse: thousands of new binaries

Ultra-compact binaries will completely dominate the number of source detections by eLISA. Current estimates suggest the numbers of resolved compact binaries that will be detected by eLISA to be in the thousands (Webbink, 2010). We provide a visual impression in figure 6 by showing the 100 (red dots) and 1000 (black dots) strongest binaries from a MonteCarlo realization of the galaxy compact white dwarf binary population. The shortest period systems will be the most numerous, the majority having periods between 5 and 10 minutes. eLISA will revolutionise our knowledge of such a population, especially given that only two of the known fifty sources have periods less than ten minutes. As these systems are relatively short lived and faint, there is no hope to detect them in significant numbers by any other means than via gravitational radiation, as there are only several thousand expected to exist in the whole Galaxy. Their detection will allow us to test different models for the common-envelope phase, a significant uncertainty in our understanding of binary evolution and many high-energy phenomena. The internal statistical accuracy delivered by the sheer number of detected sources will ensure that the common-envelope phase will be put to the most critical test expected in the midterm future. The same population can be used to constrain models for type Ia supernovae and peculiar supernovae, as well as the formation of ultra-compact binaries in globular clusters.

The outcome of the common envelope phase

Only a minority of the stars in the Universe are single, leaving the majority to be part of a binary, a triple or a higher-order system. On the order of half of the binaries formed with sufficiently small orbital separation, so that the stars will interact during the evolution of the components into giants or super giants. Especially for low-mass stars, the majority of interactions are unstable and will lead to runaway mass transfer. Based on the observed short orbital periods of binaries that have passed this stage it is argued that somehow the companion of the giant ends up inside the giant's outer layers. During that common envelope phase, (dynamical) friction reduces the velocity of the companion, leading to orbital shrinkage and transfer of angular momentum from the orbit into the envelope of the giant. Along with angular momentum, orbital energy is deposited in the envelope, whose matter is then unbound from the giant's core, leading to a very compact binary consisting of the core of the giant and the original companion (Paczynski, 1976).

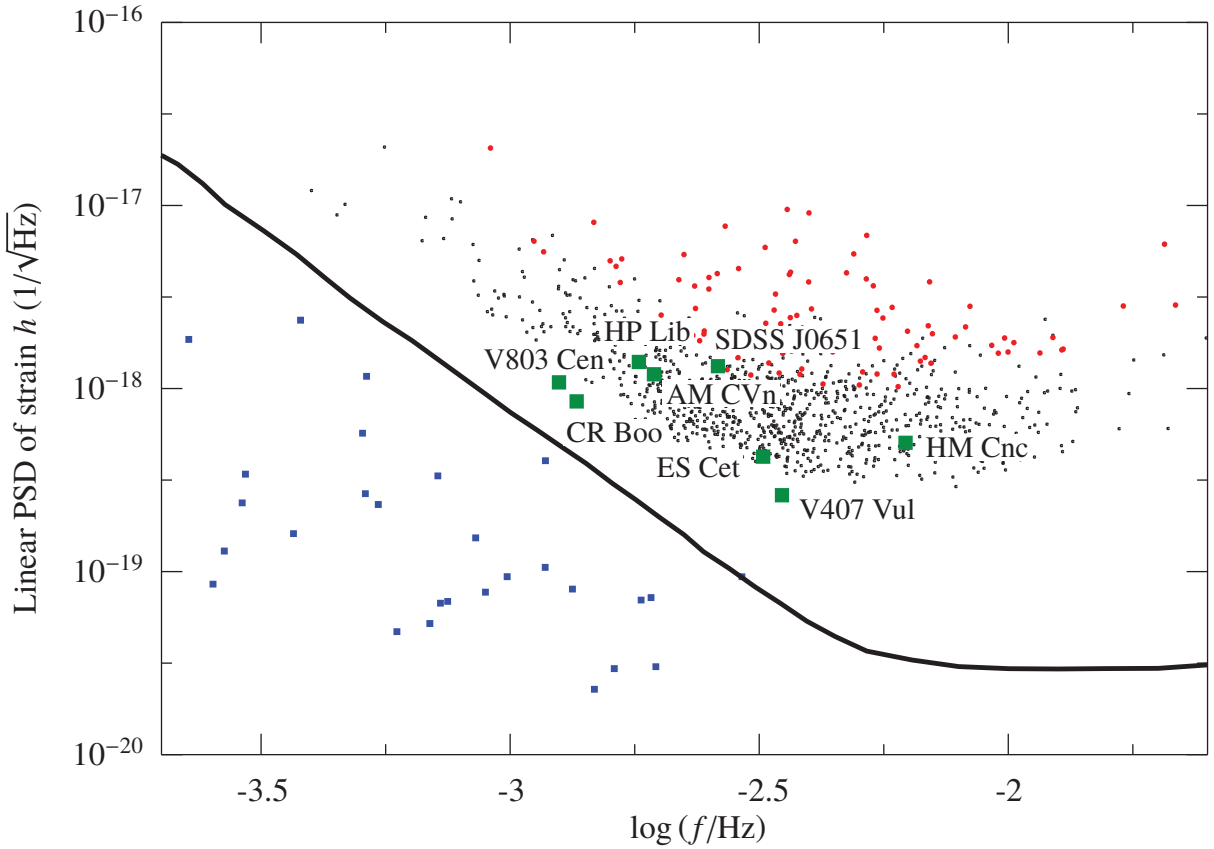

Figure 6: Strain amplitude spectral density versus frequency for the verification binaries and the brightest binaries,expected from a simulated Galactic population of ultra-compact binaries. The solid line shows the sensitivity of eLISA. Verification binaries are indicated as green squares with their names indicated, blue squares are other known binaries. Strongest 100 simulated binaries are shown in red, strongest 1000 as black dots. The integration time for the binaries is two years. Based on Brown et al. (2011), Roelofs et al. (2006, 2010) for the known binaries and Nelemans et al. (2004) for the simulation.

Virtually all compact binaries and most of the systems giving rise to high-energy phenomena (such as X-ray binaries, relativistic binary pulsars and possibly gamma-ray bursts) have experienced at least one common-envelope phase. Given the importance of this phase in high-energy astrophysics, our understanding of the physics and our ability to predict the outcome of the common-envelope phase are poor. Theoretical progress to understand the phase from first physical principles is slow (e.g. Taam and Ricker, 2010, Taam and Sandquist, 2000) and the standard formalism described above has been challenged by observational tests (De Marco et al., 2011, Nelemans and Tout, 2005). Comparison of the parameters of the thousands of binaries detected by eLISA with model predictions will provide a direct test of the different proposed outcomes of the common-envelope phase and our understanding of the preceding binary evolution in general.

3.1 Type Ia supernovae and sub-luminous supernovae

Type Ia supernovae have been the heralds of a new paradigm in Cosmology: cosmic acceleration (Perlmutter and Riess, 1999, Riess et al., 1998) for which the 2011 Nobel Prize in Physics was awarded. However, there are different scenarios proposed for the progenitors of SN Ia. One is the merger of two (carbon-oxygen) white dwarfs that are brought together via gravitational wave radiation (Pakmor et al., 2010) which is exactly the population eLISA will be probing. By determining the number of systems in the Galaxy and their period distribution, the rate at which they will merge will be measured. By comparing that to the inferred SNIa rate for an Sbc galaxy, the viability of this progenitor scenario will be determined. The significant efforts in the past decade to find more supernovae and the advent of wide field optical surveys have revealed a host of new types of supernovae (Kasliwal et al., 2010, Perets et al., 2011, 2010, Sullivan et al., 2011). Some of these have been suggested to originate in the interaction between two white dwarfs at very short periods, again exactly the population to which eLISA is sensitive (Perets et al., 2010, Waldman et al., 2011).

Formation of ultra-compact binaries in globular clusters

Globular clusters have a strong overabundance of bright X-ray sources per unit mass compared to the field, probably due to dynamical interactions. Many of these have turned out to be so-called ultra-compact X-ray binaries, in which a neutron star accreted material from a white dwarf companion is a very compact orbit, exactly the type of sources that eLISA may see. However, it is not clear if the same enhancement will operate for the much more numerous white dwarf binaries. The angular resolution that can be achieved with eLISA is such that globular clusters can be resolved, so that the cluster sources can be distinguished from the Galactic disc sources. This enables eLISA to determine the number of ultra-compact binaries in globular clusters and thus to provide a direct test of the overabundance of white dwarfs binaries in globular clusters. That in turn can be used to test models for dynamical interactions in clusters.

The foreground of Galactic gravitational waves

At frequencies below a few mHz the number of sources in the Galaxy is so large (6×10^7 to 8×10^7, see e.g. Ruiter et al., 2010, Yu and Jeffery, 2010) that only a small percentage, the brightest sources, will be *individually* detected. The vast majority will form an unresolved *foreground* signal in the detector, which is quite different from and much stronger than any diffuse extragalactic *background* (Farmer and Phinney, 2003).

This foreground is often described as an additional noise component, which is misleading for two reasons. The first is that there is a lot of astrophysical information in the foreground. The overall level of the foreground is a measure of the total number of ultra-compact binaries, which gives valuable information given the current uncertainty levels in the normalisation of the population models. The spectral shape of the foreground also contains information about the homogeneity of the sample, as simple models of a steady state with one type of binary predict a very distinct shape. In addition, the geometrical distribution of the sources can be detected by eLISA.

Due to the concentration of sources in the Galactic centre and the inhomogeneity of the eLISA antenna pattern, the foreground is strongly modulated over the course of a year (see figure 7), with time periods in which the foreground is more than a factor two lower than during other periods (Edlund et al., 2005). The characteristics of the modulation can be used to learn about the distribution of the sources in the Galaxy, as the different Galactic components (thin disk, thick disk, halo) contribute differently to the modulation and their respective amplitude can be used, for example, to set upper limits on the halo population (e.g. Ruiter et al., 2009).

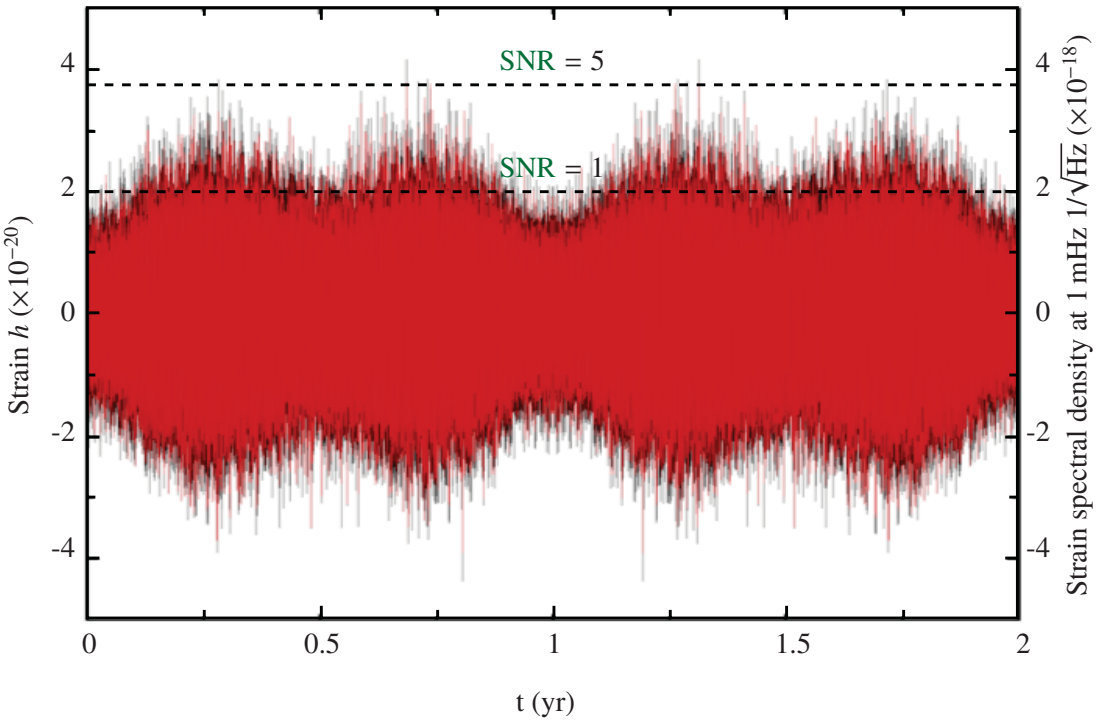

Figure 7: Level of the Galactic gravitational wave signal as a function of time. Black is the total signal, the red after removal of the resolved binaries. The yearly variation of the Galactic foreground is clearly seen. Based on the Ruiter et al. (2009) Galactic model.

4 Studying the astrophysics of compact binaries using eLISA

Although the effect of gravitational radiation on the orbit will dominate the evolution of the binaries detected by eLISA, additional physical processes will cause strong deviations from the simple point-mass approximation. The two most important interactions that occur are tides – when at least one of the stars in a binary system is not in co-rotation with the orbital motion or when the orbit is eccentric – and mass transfer. Because many binaries will be easily detected, these interactions do not hamper their discovery, but instead will allow tests of the physics underlying these deviations. By providing a completely complementary approach, gravitational wave measurements are optimal to the study of short period systems, in contrast to the current bias towards bright electromagnetic systems and events.

Physics of tidal interaction

eLISA measurements of individual short-period binaries will give a wealth of information on the physics of tides and the stability of the mass transfer. For detached systems with little or no interaction, the frequency evolution is well understood as that of two point masses. The strain amplitude h, the frequency f and its derivatives then are connected by

$$h \propto \mathcal{M}^{5/3} f^{2/3} D^{-1}\,, \tag{6}$$

$$\dot{f} \propto \mathcal{M}^{5/3} f^{11/3}\,, \tag{7}$$

$$\ddot{f} = \frac{11}{3}\frac{\dot{f}}{f}\,, \tag{8}$$

where $\mathcal{M} = (m_1 m_2)^{3/5} / (m_1 + m_2)^{1/5}$ is the chirp mass, m_1, m_2 are the masses of the binary constituents and D is the distance. Thus the measurement of h, f, $\dot{f}$ provides chirp mass and distance; the additional measurement of $\ddot{f}$ gives a direct test of the dominance of gravitational wave radiation in the frequency evolution. Tidal interaction between white dwarfs in detached systems before the onset of mass transfer will give rise to distinct deviations of the frequency evolution as compared to systems with no or little tidal interaction. The strength of the tidal interaction is virtually unknown, with

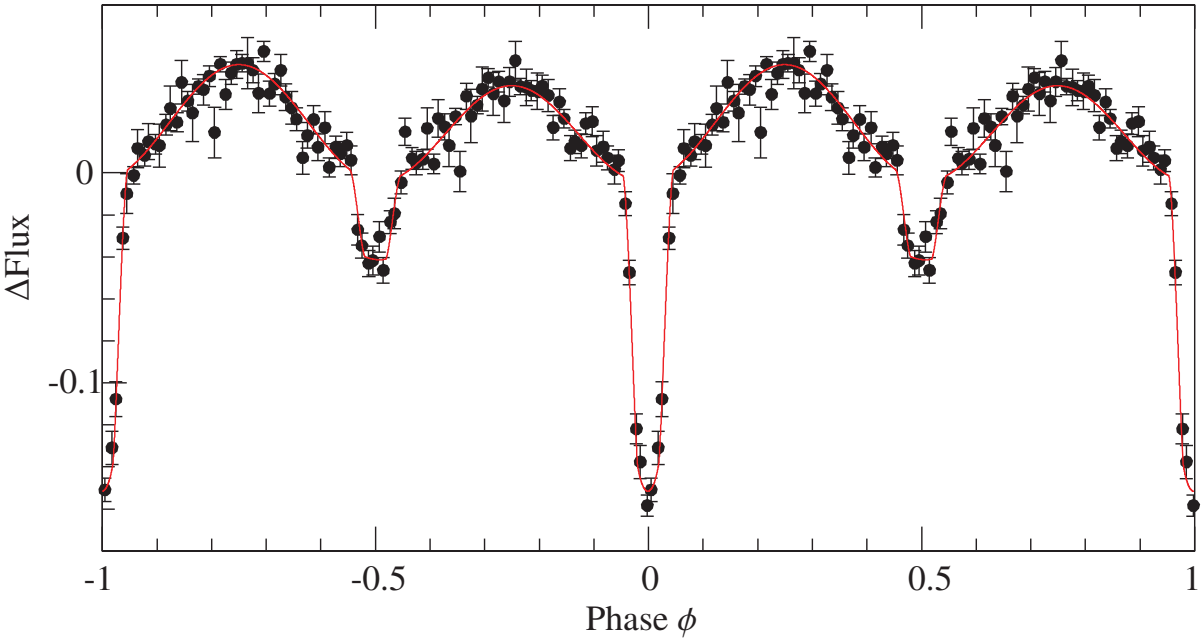

Figure 8: Lightcurve of SDSS J0651+28, folded on the 12 minute orbital period. Except for the two eclipses at phase $\phi = 0$ and $\phi = 0.5$, the sinusoidal variation due to the tidal distortion of the primary white dwarf. From Brown et al. (2011)

estimates ranging over many orders of magnitude (Marsh et al., 2004), although the high temperature of the white dwarf in the recently discovered 12 min double white dwarf may suggest efficient tidal heating (Piro, 2011). Knowledge of the strength of the tides is not only important for understanding the physics of tides in general and of white dwarf interiors, it also has important consequences for the tidal heating (and possibly optical observability) of eLISA sources and for the stability of mass transfer between white dwarfs (Fuller and Lai, 2011, Marsh, 2011, Racine et al., 2007, Willems et al., 2010).

In globular clusters, dynamical interactions may produce eccentric double white dwarf systems, which can be used to constrain white dwarf properties and masses (Valsecchi et al., 2011).

Physics of mass-transfer stability

Detached ultra-compact binaries will evolve to shorter and shorter periods due to the angular momentum loss through gravitational wave radiation. At sufficiently short orbital periods (a few minutes) one of the stars becomes larger than its Roche lobe – the equipotential surface that crosses the minimum of the potential between the two stars – and material leaks out of the potential well of one star upon the other star. Depending on the difference between the change of the radius of this star and the Roche lobe upon mass transfer, there may be positive or negative feedback, leading to either limited, stable mass transfer, or a runaway mass-transfer instability.

For double white dwarfs and white dwarf-neutron star binaries the stability of the ensuing mass transfer has important consequences, for the number of detectable sources, as well as for a number of open astrophysical questions. The stable systems will form interacting binaries, AM CVn systems or ultra-compact X-ray binaries, that can be detected through their gravitational wave emissions. eLISA will detect a number of detached double white dwarfs and AM CVn systems that are so close to the onset of mass transfer that the stability of the mass transfer can be tested directly by comparing their numbers. In addition, eLISA will detect several ultra-compact X-ray binaries at the very early stages of mass transfer, providing a test of the mass transfer stability in these systems as well (Marsh, 2011).

For AM CVn systems, a major uncertainty in the mass-transfer stability is again the tidal interaction between the two white dwarfs. Most likely the mass transfer will proceed via the direct impact configuration: due to the proximity of the two stars, the mass transfer stream lands directly on the surface of the accreting white dwarf, rather than wrapping around the accreting stars and interacting with itself to form a flat accretion disk in the plane of the orbit (Marsh and Steeghs,

2002, Webbink, 1984). The stability of the mass transfer depends critically on the tidal interaction between the two white dwarfs (Marsh et al., 2004): In the absence of any tidal interaction, there will be additional angular momentum loss from the orbit due to the transfer of angular momentum from the orbit to the accreting star which will consequently spin up. This is different from cases where the accretion is via a disc for which most of the angular momentum generally is stored in the disc and eventually via very efficient tidal interaction put back into the orbit. Efficient tidal coupling between the accreting star and the companion has the ability to return the angular momentum back to the orbit (see D'Souza et al., 2006, Racine et al., 2007), thus reducing the magnitude of the spin-up. The difference between efficient and inefficient tidal coupling is rather dramatic: the fraction of double white dwarfs estimated to survive the onset of mass transfer can drop from about 20 % to 0.2 % (Nelemans et al., 2001) depending on assumptions about the tidal coupling. This difference is easily measurable with eLISA. Short-term variations in the secular evolution of the systems experiencing mass transfer will change the frequency evolution, but are likely to be rare and will not prevent the detection of these systems (Stroeer and Nelemans, 2009).

For ultra-compact X-ray binaries (see e.g. figure 9), the stability issue is completely different. At the onset, the mass transfer is orders of magnitude above the Eddington limit for a neutron star (the mass transfer rate at which the potential energy liberated in the accretion can couple to the infalling gas to blow it away). For normal stars and white dwarfs, this would likely lead to a complete merger of the system, but the enormous amount of energy liberated when matter is falling into the very deep potential well of a neutron star allows matter to be dumped on it at rates up to a thousand times the Eddington limit if the white dwarf has a low mass (see Yungelson et al., 2002). This allows the formation of ultra-compact X-ray binaries from white dwarf-neutron star pairs. eLISA will unambiguously test this prediction by detecting several tens of ultra-compact X-ray binaries with periods between 5 and 20 minutes.

Double white dwarf mergers

The 80% to 99.8% of the double white dwarfs that experience run-away mass transfer and merger give rise to quite spectacular phenomena. Mergers of double white dwarfs have been proposed as progenitors of single subdwarf O and B stars, R Corona Borealis stars and maybe all massive white dwarfs (e.g. Webbink, 1984). In addition, the merger of a sufficiently massive double white dwarf can be a trigger for type Ia supernova events (see Pakmor et al., 2010). Alternatively, if the merger does not lead to an explosion, a (rapidly spinning) neutron star will be formed. This is one possible way to form isolated millisecond radio pulsars as well as magnetars, which have been proposed as sites for short gamma-ray bursts (e.g. Levan et al., 2006).

Although it is not expected that eLISA will witness the actual merger of a double white dwarf as the event rate in our Galaxy is too low, it will certainly detect the shortest-period binaries known, expected at a period of about two minutes, and give an extremely good estimate of their merger rate. In addition, if the actual merger takes many orbits as recently found in simulations (Dan et al., 2011), eLISA may observe them directly.

By measuring (chirp) masses and coalescence times, eLISA will directly determine the merger rate for double white dwarfs with different masses, which can then be compared with the rates and population of their possible descendants determined by other means (Stroeer et al., 2011).

Neutron star and black hole binaries

The current observational and theoretical estimates of the formation rate of neutron star binaries are highly uncertain and predict several tens of neutron star binaries to be detected by eLISA (e.g. Belczynski et al., 2010, Nelemans et al., 2001). The number of ultra-compact stellar-mass black hole binaries in the Galaxy is even more uncertain (e.g. Belczynski et al., 2002); furthermore, these binaries are likely to be detectable only through their gravitational wave emission as they are electromagnetically quiet.

eLISA will thus constrain the formation rate estimates and the numbers of neutron star binaries and ultra-compact stellar mass black hole binaries. As these systems can be seen throughout the Galaxy, the samples for all these populations will be *complete at the shortest periods*. Thus the sample will be independent of selection effects, such as those present in radio pulsar surveys and X-ray surveys, that pick up only transient X-ray sources. In addition, by the time eLISA will fly, Advanced LIGO and Virgo will likely have detected a number of double neutron star mergers from far away galaxies, so these measurements together will test our ability to extrapolate our population models from our own galaxy to the rest of the Universe.

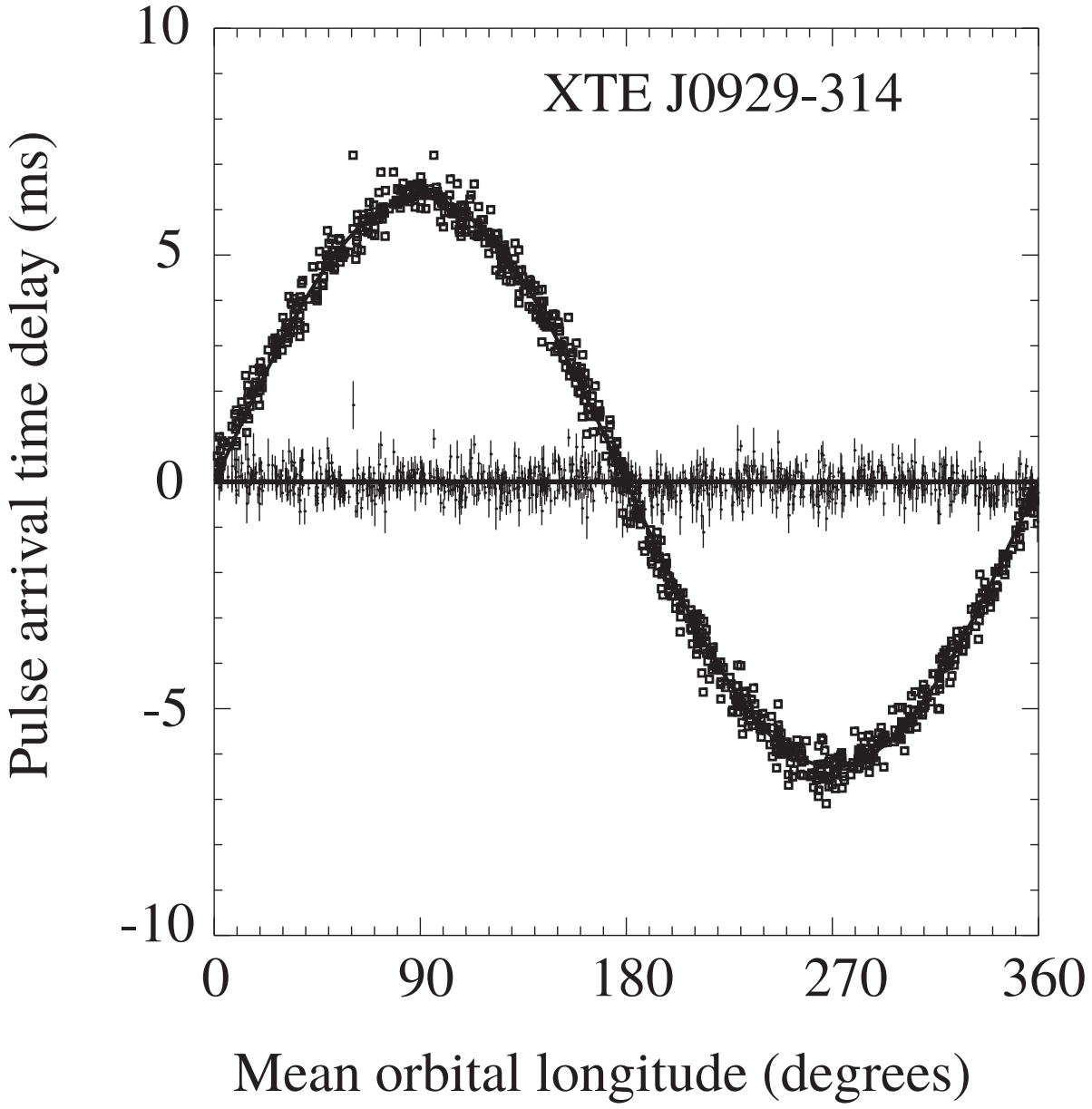

Figure 9: Imprint of the 40 min orbital period on the arrival times of the X-ray pulsations in the ultra-compact X-ray binary XTE J0929-314. From Galloway et al. (2002).

A special situation might arise for the case of millisecond X-ray pulsars, in ultra-compact X-ray binaries. In the last decade, observations of X-ray pulsations from many ultra-compact X-ray binaries have enabled astrophysicists to determine the rotation rate of the neutron star in the binary using the NASA mission RXTE (Wijnands, 2010). As had been expected on theoretical grounds, neutron stars are spinning rapidly (several hundred times per second) due to the angular momentum gained from infalling matter. The measurements give credence to the idea that these rapidly spinning neutron stars observed as millisecond radio pulsars are descendants of accreting neutron stars in binary systems (e.g. Bhattacharya and van den Heuvel, 1991). However, the exact role of ultra-compact binaries in the formation of these pulsars has yet to be established. The distribution of spin periods discovered in X-ray binaries suggests additional neutron star angular momentum loss on top of the plasma physics interaction between the accretion and magnetic field of the spinning neutron stars (Chakrabarty et al., 2003) which could be due to strong gravitational wave emission (Bildsten (1998); but see Watts et al. (2008) and Patruno et al. (2011)). In that case, ultra-compact X-ray binaries might be the only sources that could be studied simultaneously with eLISA and ground based detectors, with eLISA detecting the orbital period and the ground based detector detecting the neutron star spin period.

5 Studies of galactic structure with eLISA

One of the major capabilities of eLISA is that it will determine distances for hundreds of compact binaries by measuring their $\dot{f}$ (see equation 7). The ability of eLISA to determine distances depends on the mission lifetime, as larger life times lead to more accurate $\dot{f}$ measurements. The directional dependence of the Galactic foreground as well as the directional accuracy for the resolved systems allow a statistical assessment of the contributions of the different Galactic components, such as the Galactic bulge (with its bar), the thin and thick disc and the Galactic halo (for a realistic MW model, see in figure 10).

The Galactic center is one of the most interesting areas of the Galaxy, with a central massive black hole surrounded by a dense assembly of stars with intriguing properties. Dynamical effects, in particular mass segregation, will lead to many interactions close to the central black hole so that wide binaries will become tighter or will be disrupted (for a review see Alexander, 2005). This likely leads to an increase in the number of ultra-compact binaries as well as the possibility of EMRIs (see 2). eLISA will put much more stringent constraints on these populations than current observations (see e.g. Roelofs et al., 2007), which are limited by the electromagnetic faintness of the sources, or theoretical predictions, which are limited by our current understanding of the processes leading to compact binary formation. Distance determinations to the many ultra-compact binaries around the Galactic centre will allow for an independent distance determination.

The level and shape of the double white dwarf foreground as well as the distribution of resolved sources will provide information on the *scale height* of the ultra-compact binary population (Benacquista and Holley-Bockelmann, 2006) in the disc of the Galaxy.

The distribution of sources in the *Galactic halo* will be significantly different from the other Galactic components. In principle the halo population is expected to be much smaller than the rest of the Galaxy (Ruiter et al., 2009, Yu and Jeffery, 2010), but it might be enhanced as the formation and evolution of binaries in the halo may have been quite different. Such old and metal-poor population can be studied locally only in globular clusters, where the formation and evolution of binaries is generally completely altered by dynamical effects. Two of the known AMCVn systems may belong to the halo. They have very low metal abundances and have anomalous velocities. If true this implies that a large number of AMCVn stars are in the halo, maybe as many as in the rest of the Galaxy.

The eLISA directional sensitivity will immediately pick up any strong halo population if it exists.

Finally, for many of the resolved sources the eLISA measurements will also provide an accurate estimate of their orbital inclination. For the first time, this will give hints on the dynamics of the formation of binaries from interstellar clouds, because the angular momentum vectors of the binaries is related (in a statistical way) to the overall angular momentum of the Galaxy.

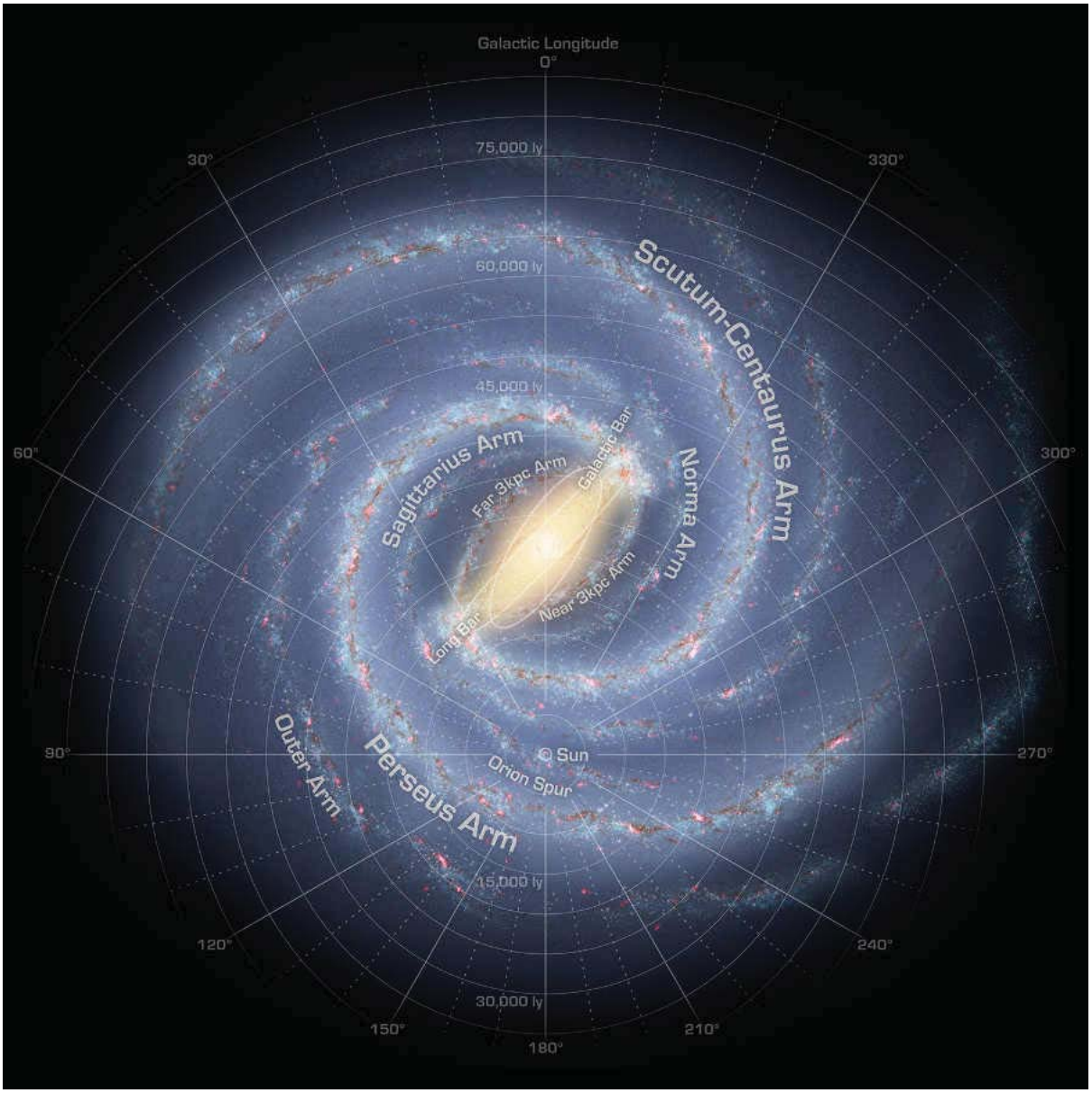

Figure 10: Spitzer GLIMPSE model of the Milky Way, showing bulge, bar and spiral arms. The resolved binaries are expected to trace the old stellar populations of the Milky Way. Courtesy NASA/JPL-Caltech/R. Hurt (SSC/Caltech)

4 Astrophysical Black Holes

1 Overview

Astrophysical black holes appear to come in nature into two flavours: the "stellar mass" black holes of $3\,M_\odot$ to approximately $100\,M_\odot$ resulting from the core collapse of very massive stars, and the "supermassive" black holes of $10^6\,M_\odot$ – $10^9\,M_\odot$ that, according to the accretion paradigm, power the luminous QSO. The former light up the X-ray sky, albeit only in our neighbourhood, as stellar mass black holes fade below detection limits outside our local group. The latter are detected as active nuclei, over the whole cosmic time accessible to our current telescopes. Electromagnetic evidence of black holes in the mass range $10^2\,M_\odot$– $10^6\,M_\odot$ is less common, due to the intrinsic difficulty of detecting such faint sources in external galaxies. However, it is in this mass interval, elusive to electromagnetic observations, that the history of supermassive black hole growth is imprinted.

Supermassive black holes inhabit bright galaxies, and are ubiquitous in our low-redshift Universe. The discovery of close correlations between the mass of the supermassive black hole with key properties of the host has led to the notion that black holes form and evolve in symbiosis with their galaxy host. In agreement with the current paradigm of hierarchical formation of galactic structures and with limits imposed by the cosmic X-ray background light, astrophysical black holes are believed to emerge from a population of *seed* black holes with masses in the range $100\,M_\odot$ – $10^5\,M_\odot$, customarily called *intermediate mass black holes*. The mass and spin of these black holes change sizably in these interactions as they evolve over cosmic time through intermittent phases of copious accretion and merging with other black holes in galactic halos. In a galactic merger, the black holes that inhabit the two colliding galaxies spiral in under the action of dynamical friction, and *pair* on sub-galactic scales forming a Keplerian binary: *binary black holes* thus appear as the inescapable outcome of galaxy assembly. When two massive black holes coalesce, they become one of the loudest sources of gravitational waves in the Universe.

eLISA is expected to target coalescing binaries of $10^5\,M_\odot$ – $10^7\,M_\odot$ during the epoch of widespread cosmic star formation and up to $z \sim 20$, and to capture the signal of a coalescing binary of $10^4\,M_\odot$ – $10^5\,M_\odot$ beyond the era of the earliest known QSO ($z \sim 7$). Gravitational waveforms carry information on the spins of the black holes that eLISA will measure with exquisite precision, providing a diagnostic of the mechanism of black hole growth. The detection of coalescing black holes not only will shed light into the phases of black hole growth and QSO evolution, but will pierce deep into the hierarchical process of galaxy formation.

2 Black holes in the realm of the observations

Dormant and active supermassive black holes

QSOs are active nuclei so luminous that they often outshine their galaxy host. They are sources of electromagnetic energy, with radiation emitted across the spectrum, almost equally, from X-rays to the far-infrared, and in a fraction of cases, from $\gamma-$rays to radio waves. Their variability on short timescales revealed that the emitting region is compact, only a few light hours across.

There is now scientific consensus that the electromagnetic power from QSO and from the less luminous AGN results from *accretion* onto a supermassive black hole of $10^6\,M_\odot$ – $10^9\,M_\odot$ (Krolik, 1999, Salpeter, 1964, Zel'dovich and Novikov, 1964). Escaping energy in the form of radiation, high velocity plasma outflows, and ultra relativistic jets can be generated with high efficiency ($\varepsilon \sim 10\,\%$, higher than nuclear reactions) just outside the event horizon, through viscous stresses on parcels of gas orbiting in the gravitational potential of the black hole. The accretion paradigm has thus been, and still is, at the heart of the hypothesis of black holes as being "real" sources in our cosmic landscape. eLISA will offer the new perspective of revealing these black holes as powerful sources of gravitational waves, probing the smallest volumes of the large scale Universe.

Massive black holes are tiny objects compared to their host galaxies. The event horizon of a Kerr black hole of mass $M_\bullet$ scales as $R_{\rm horizon} \sim GM_\bullet/c^2$, and it is far smaller than the optical radius of the galaxy host: $R_{\rm horizon} \sim 10^{-11}\,R_{\rm gal}$. The distance out to which a black affects the kinematic of stars and gas (the gravitational influence radius), $R_{\rm grav} \sim GM_\bullet/\sigma^2$, is also small compared to the optical radius of the host, $R_{\rm grav} \sim 10^{-4}\,R_{\rm gal}$ (where σ is the velocity dispersion of the stars of the galactic bulge).

For a long time, QSO and more generally the less luminous AGN phenomena were understood as caused by a process

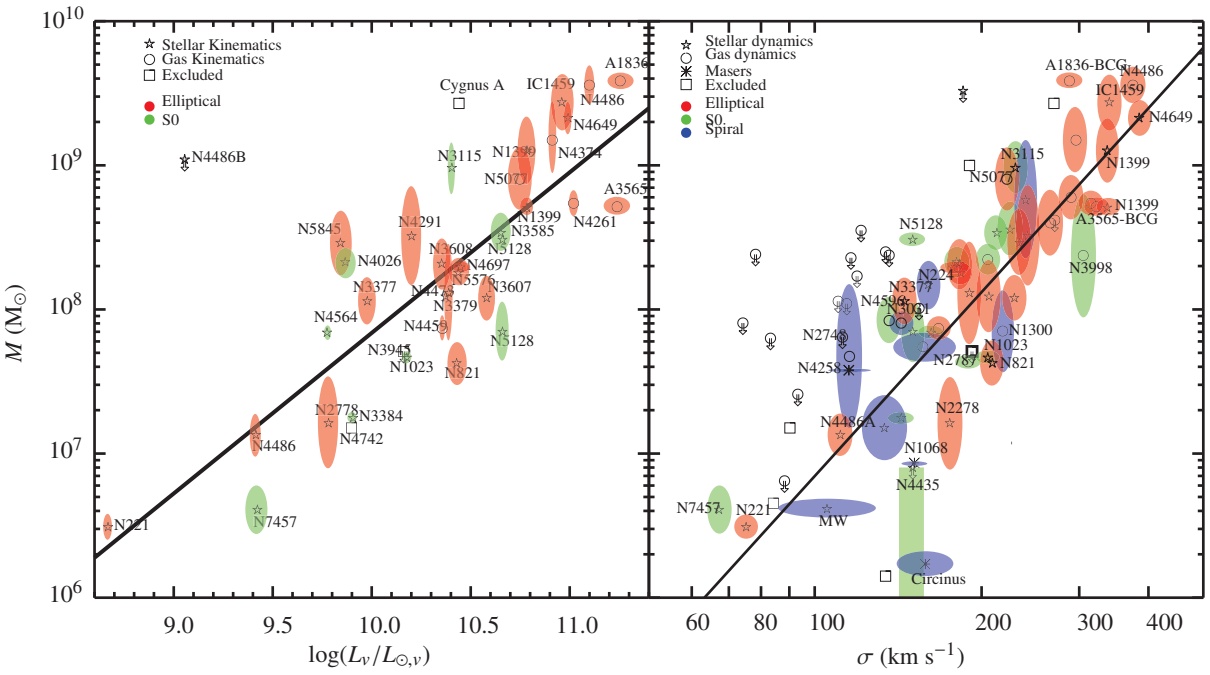

Figure 11: The correlation between the black hole mass $M_\bullet$ and the luminosity of the host galaxy's stellar bulge (left), and host galaxy's bulge velocity dispersion σ (right) for all detections in galaxies near enough for current instruments to resolve the region in which the black hole mass dominates the dynamics (adapted from Gültekin et al., 2009)

exclusively confined to the nuclear region of the host. This picture of disjoint black hole and galaxy evolution changed with the advent of the HST (Ferrarese and Ford, 2005).

Observations of almost all bright galaxy spheroids in the near universe reveal that the velocities of stars and gas start to rise in a Keplerian fashion at their centres, highlighting the presence of a dark point-mass which dominates the central gravitational potential. The same observations provide the mass of this dark object, hypothesised to be a quiescent black hole. The proximity of these galaxies to Earth allowed for a full optical characterisation of the host, and this ultimately led to the discovery of tight correlations – depicted in figure 11, from Gültekin et al. (2009) – between the black hole mass $M_\bullet$ and the optical luminosity and velocity dispersion σ of the stars measured far from the black hole (Ferrarese and Merritt, 2000, Gebhardt et al., 2000, Graham et al., 2011, Gültekin et al., 2009, Tremaine et al., 2002). The relations state that galaxy spheroids with higher stellar velocity dispersions, i.e. with deeper gravitational potential wells and higher stellar masses and luminosities, host heavier central black holes with little dispersion in the correlation. Thus more massive galaxies grow more massive black holes: the black hole sees the galaxy that it inhabits, and the galaxy sees the black hole at its centre despite its small influence radius (Häring and Rix, 2004, Magorrian et al., 1998, Marconi and Hunt, 2003).

Consensus is rising that the $M_\bullet - \sigma$ relation of figure 11 is fossil evidence of a *co-evolution of black holes and galaxies*. The relation may have been established along the course of galactic mergers and in episodes of self-regulated accretion (Croton et al., 2006, Di Matteo et al., 2005, Hopkins et al., 2006, 2008, 2009, Johansson et al., 2009, Lamastra et al., 2010, Mihos and Hernquist, 1996, Somerville et al., 2008). However, the origin of the $M_\bullet - \sigma$ relation (Ciotti et al., 2010, King, 2003, Silk and Rees, 1998, Wyithe and Loeb, 2003), and its evolution at look-back times is still unclear (Peng, 2007, Robertson et al., 2006, Treu et al., 2007, Woo et al., 2008). The similarity between the evolution, over cosmic time, of the luminosity density of QSOs and the global star formation rate (Boyle and Terlevich, 1998, Kauffmann and Haehnelt, 2000) points to the presence of a symbiotic growth, which is still under study (Schawinski et al., 2010, 2011).

The census of black holes, from the study of the kinematics of stars and gas in nearby galaxies, has further led to the estimate of the black hole local mass density: $\rho_\bullet \sim 2 \times 10^5\,\mathrm{M}_\odot\,\mathrm{Mpc}^{-3} - 5 \times 10^5\,\mathrm{M}_\odot\,\mathrm{Mpc}^{-3}$ (Aller and Richstone, 2002, Lauer et al., 2007, Marconi et al., 2004, Tundo et al., 2007). Whether this mass density traces the initial conditions, i.e. the mass since birth, obtained at most by rearranging individual masses via coalescences, or the mass acquired via major episodes of accretion in active AGN phases can only be inferred using additional information: that resulting from the AGN demographics and from studies of the X-ray cosmic background.

Two arguments provide information about how much of the black hole growth occurred through accretion of gas, in phases when the black hole is active as AGN. The first is the existence of a limiting luminosity for an accreting black hole, corresponding to when the radiation pressure force equals gravity. Above this limit material that would be responsible for the emission can not fall onto the black hole, as it is pushed away. This limit is the Eddington luminosity $L_{\rm E} = 4\pi G M_\bullet m_{\rm p} c/\sigma_T \sim 10^{46}\,{\rm erg\,s^{-1}} (M_\bullet/(10^8\,{\rm M}_\odot)$ (σ_T and $m_{\rm p}$ are the Thomson cross section and proton mass). The AGN luminosity L is normally a fraction $f_{\rm E} \lesssim 1$ of the Eddington luminosity, since as soon as L approaches $L_{\rm E}$ the radiation pressure force against gravity self-regulates the accretion flow to $L \sim L_{\rm E}$, providing also a lower bound on M. The second argument is that "light is mass", i.e. that any light output from accretion (at a luminosity level $L = \varepsilon \dot{M} c^2$) increases the black hole's mass at a rate ${\rm d}M_\bullet/{\rm d}t = (1-\varepsilon)\dot{M}$, where $\dot{M}$ is the rest-mass accreted per unit time and ε the accretion efficiency, i.e. how much of the accreted mass is converted into radiation. Accordingly, the black hole's mass increases exponentially in relation to the self-regulated flow, with an e-folding time $\tau_{\rm BH} \approx 4.7 \times 10^8\, \varepsilon [f_{\rm E}(1-\varepsilon)]^{-1}$yr. For $\varepsilon \approx 0.1$ – typical of radiatively efficient accretion onto a non-rapidly rotating black hole (Shapiro and Teukolsky, 1979) – and $f_{\rm E} \approx 0.1$, this timescale is short (about 3 %) compared to the age of the Universe, indicating that black holes can enhance their mass via accretion by orders of magnitude.

Active black holes in galaxies are known to contribute to the rise of a cosmic X-ray background resulting mostly from unresolved and obscured AGN of mass $10^8\,{\rm M}_\odot - 10^9\,{\rm M}_\odot$, in the redshift interval $0.5 < z < 3$ (Merloni, 2004). As energy from accretion is equivalent to mass, the X-ray light present in the background mirrors the increment experienced by the black holes over cosmic history due to accretion. This mass-density increment is found to be $\Delta\rho_\bullet \approx 3.5 \times 10^5\,(\varepsilon/0.1)^{-1}\,{\rm M}_\odot\,{\rm Mpc}^{-3}$ (Marconi et al., 2004, Soltan, 1982, Yu and Tremaine, 2002).

As the contribution to the local (zero redshift) black hole mass density $\rho_\bullet$ results from black holes of comparable mass $10^8\,{\rm M}_\odot - 10^9\,{\rm M}_\odot$, the close match between the two independent measures, $\rho_\bullet$ and $\Delta\rho_\bullet$, indicates that radiatively efficient accretion ($\varepsilon \approx 0.1$) played a large part in the building of supermassive black holes in galaxies, from redshift $z \sim 3$ to now. It further indicates that information residing in the initial mass distribution of the, albeit unknown, black hole seed population is erased during events of copious accretion, along the course of cosmic evolution.

Massive black holes in the cosmological framework

These key findings hint in favour of the existence, at any redshift, of an underlying population of black holes of a smaller variety, with masses of $10^4\,{\rm M}_\odot - 10^7\,{\rm M}_\odot$, that grew in mass along cosmic history inside their galaxies, through episodes of merging and accretion. The evolution of black holes mimics closely that of their host galaxies within the currently favoured cosmological paradigm: a Universe dominated by cold dark matter (CDM).

Observations show that the mass content of the Universe is dominated by CDM, with baryons contributing only at a 10 % level to the CDM, and that the spectrum of primordial density perturbations contains more power at lower masses (Mo et al., 2010). Thus, at the earliest epoch, the Universe was dominated by small density perturbations. Regions with higher density grow in time, to the point where they decouple from the Hubble flow and collapse and virialise, forming self gravitating halos. The first objects that collapse under their own self-gravity are small halos that grow bigger through mergers with other halos and accretion of surrounding matter. This is a bottom up path, and the process is known as hierarchical clustering. As halos cluster and merge to build larger ones, baryons follow the CDM halo potential well and, similarly, black holes form and evolve in the same bottom-up fashion (Haehnelt et al., 1998, Haiman and Loeb, 1998, Volonteri et al., 2003, White and Rees, 1978, Wyithe and Loeb, 2002).

State-of-the-art hydrodynamical cosmological simulations (Di Matteo et al., 2008) illustrate (figure 12) where and when the massive black holes form and how they are connected with the evolving background baryonic density field. As illustrated in figure 12 and as inferred in statistical models based on the extended Press-Schechter (EPS) formalism, most of the black holes transit into the mass interval for which eLISA is sensitive during their cosmic evolution (Volonteri et al., 2003). Figure 13 sketches and simplifies conceptually the complex net terminating with the formation of a bright galaxy at zero redshift, highlighting the sites where black holes form, cluster within halos, pair with other black holes, and eventually coalesce.

Black holes in the sensitivity window of eLISA

Is there any observational evidence of black holes of this variety in the Universe that may be observed by eLISA? The Milky Way hosts in its bulge a black hole of $(4 \pm 0.06 \pm 0.35) \times 10^6\,{\rm M}_\odot$ (Ghez et al., 2005, Gillessen et al., 2009), providing

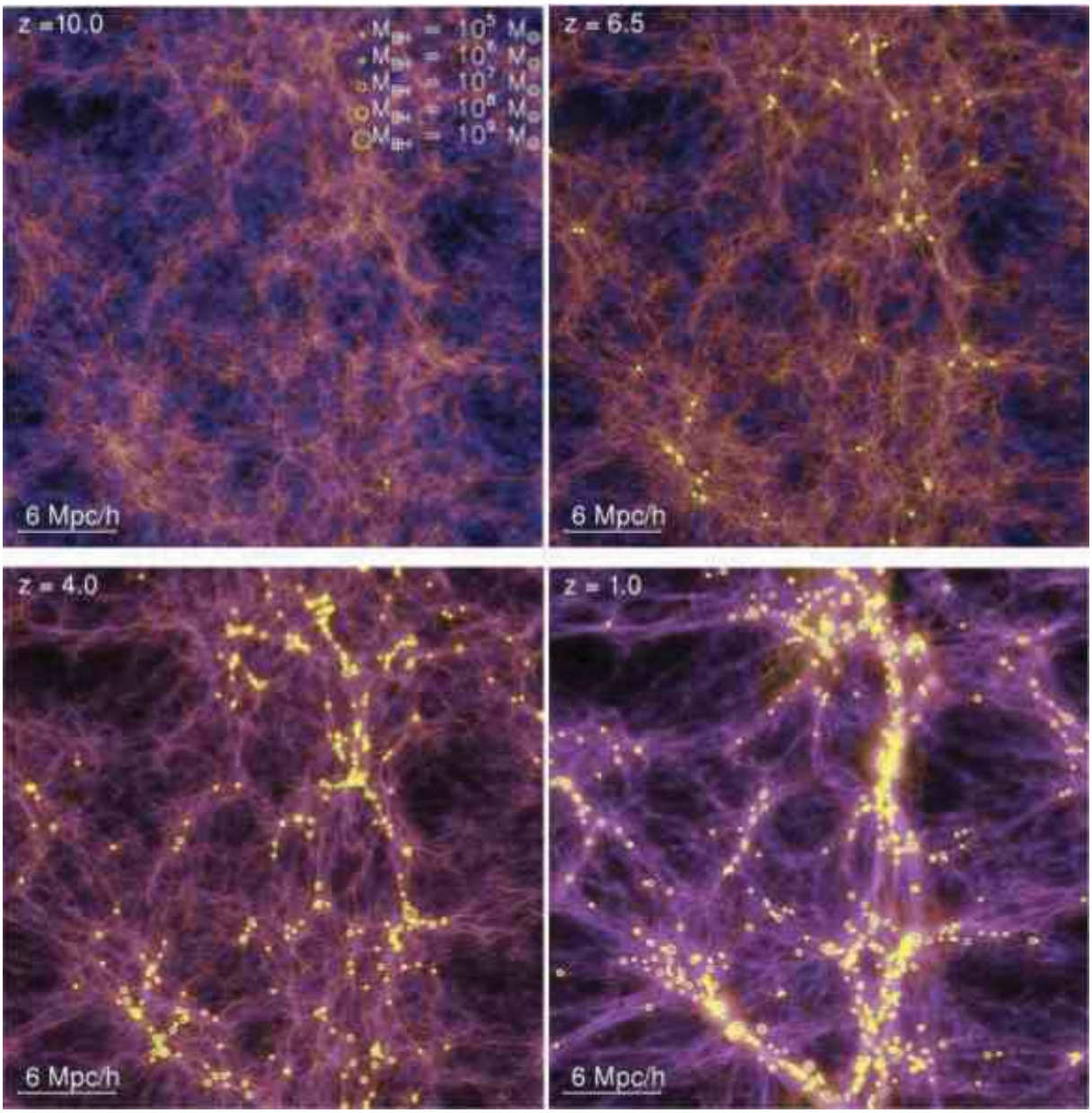

Figure 12: A state-of-art hydrodynamical simulation by Di Matteo et al. (2008) visualising the cosmic evolution of the baryonic density field and of their embedded black holes, in the ΛCDM cosmology. Each panel shows the same region of space ($33.75\,h^{-1}$ Mpc on a side) at different redshift, as labelled. The circles mark the positions of the black holes, with a size that encodes the mass, as indicated in the top left panel (numerical force resolution limits the lowest black hole mass to $10^5\,M_\odot$). The projected baryonic density field is colour-coded with brightness proportional to the logarithm of the gas surface density. The images show that the black holes emerge in halos starting at high redshift (as early as $z \sim 10$) and later grow by accretion driven by gas inflows that accompany the hierarchical build-up of ever larger halos through merging. As the simulation evolves the number of black holes rapidly increases and larger halos host increasingly larger black holes. No black holes as massive as $10^9\,M_\odot$ are present in the simulated box because they are extremely rare.

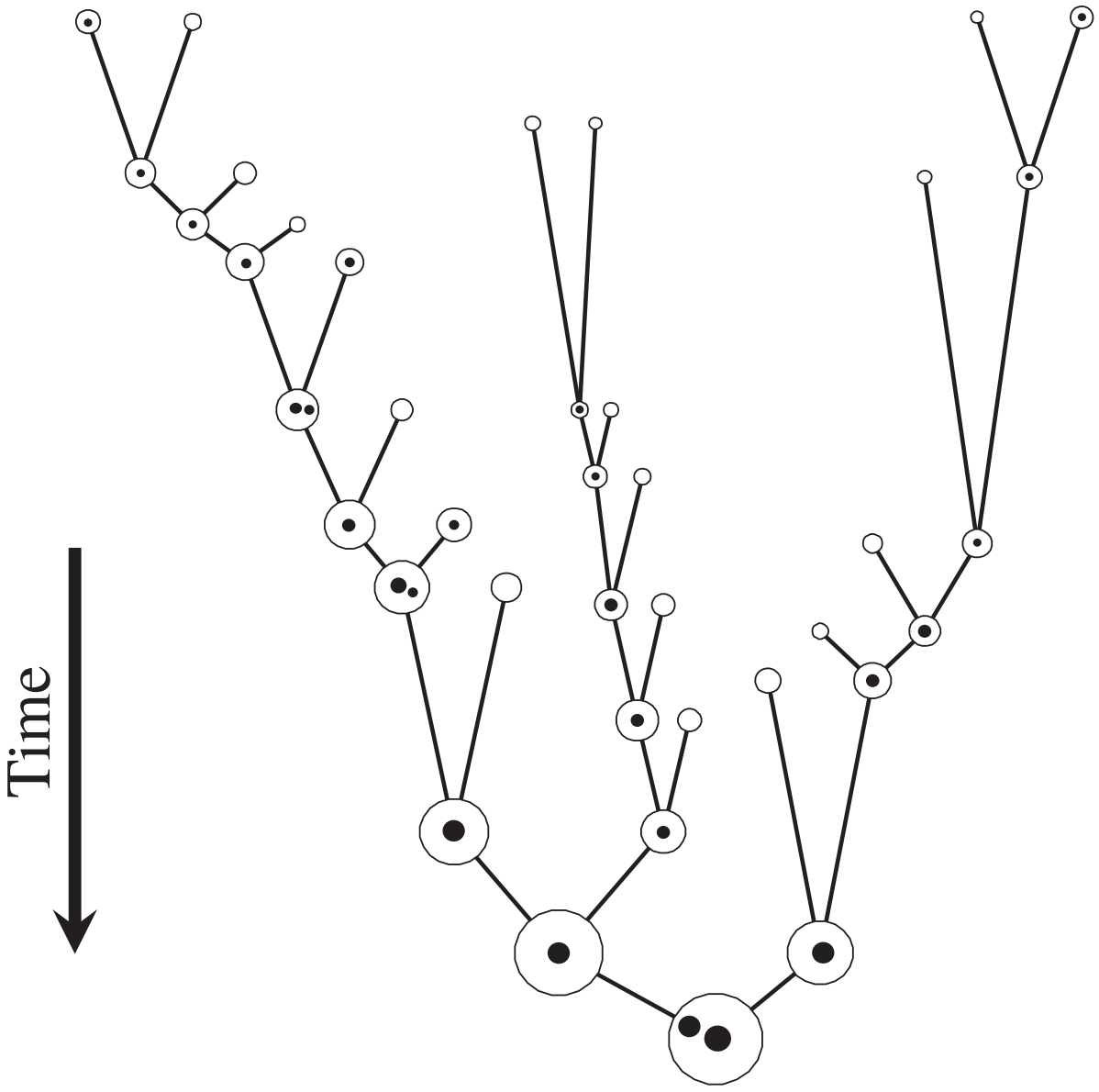

Figure 13: A cartoon of the merger-tree history for the assembly of a galaxy and its central black holes. Time increases along the arrow. Here the final galaxy is assembled through the merger of twenty smaller galaxies housing three seed black holes, and four coalescences of binary black holes.

an example of a black hole that does not fall into the population that can be traced by luminous QSO. Black holes in the mass range $10^5\,M_\odot - 10^7\,M_\odot$ are now increasingly found in low mass spiral galaxies and dwarfs with and without a bulge (Barth et al., 2004, Greene and Ho, 2004, Greene et al., 2008, Jiang et al., 2011a,b, Kuo et al., 2011, Xiao et al., 2011) and evidence exists that some of these low mass black holes of $M < 10^5\,M_\odot$ cohabit nuclear star clusters (Barth et al., 2009, Bekki and Graham, 2010, Ferrarese et al., 2006, Graham and Spitler, 2009, Seth et al., 2008, Wehner and Harris, 2006).

Dwarf galaxies in the galactic field are believed to undergo a quieter merger and accretion history than their brighter analogues. They may represent the closest example of low mass halos from which galaxy assembly took off. Late type dwarfs are thus the preferred site for the search of *pristine* black holes (Volonteri and Natarajan, 2009). NGC 4359, a close-by bulgeless, disky dwarf houses in its centre a black hole of only $3.6 \times 10^5\,M_\odot$ (Peterson et al., 2005). This key discovery shows that nature provides a channel to black hole formation also in potential wells much shallower than that of the massive spheroids.

These middleweight mass black holes are numerous at high redshifts (Di Matteo et al., 2008), but are invisible with today instrumentation, given their low intrinsic luminosity and far-out distance. Furthermore, they become invisible to electromagnetic observations near $z \gtrsim 11$ as close to this redshift the intergalactic medium becomes opaque to their light, due to intervening absorption of the neutral hydrogen (Fan et al., 2006a, Miralda-Escude, 1998). ULAS J1120+0641 holds the record of being the further distant known QSO, at redshift $z = 7.085 \pm 0.003$, and hosts a bright, very massive black hole of $\sim 2 \times 10^9\,M_\odot$ (Mortlock et al., 2011). Its light was emitted before the end of the reionisation, i.e. before the theoretically predicted transition of the interstellar medium from an electrically neutral to an ionised state (Fan et al., 2006a).

3 Galaxy mergers and black hole coalescence

A grand collision between two galaxies of comparable mass (called major merger) is not destructive event, but rather a transformation, as the two galaxies, after merging, form a new galaxy with a new morphology. Individual stars do not collide during the merger, as they are tiny compared to the distances between them. The two galaxies pass through each other and complex, time-varying gravitational interactions redistribute the energy of each star in such a way that a new bound galaxy forms. Gas clouds instead collide along the course of the merger: new stars form, and streams of gas flow in the nuclear region of the newly forming galaxy. The massive black holes in the grand collision behave like stars. A key question for the eLISA science case is: *do black holes coalesce as their galaxies merge?*

The fate of black holes in merging galaxies can only be traced using numerical simulations at the limits of current numerical resolution. Not only isolated black holes are tiny, but also binary black holes are. They form a tight binary system within a galaxy when the mass in stars enclosed in the binary orbit becomes negligible compared to the total mass of the binary M, and their Keplerian velocity exceeds the velocity of the stars, σ. This occurs when their relative separation a_B decays below about GM/σ^2, i.e. when $a_\mathrm{B} \lesssim 10^{-4} - 10^{-5}\,R_\mathrm{gal}$. Binary black holes on the verge of coalescing within less than a Hubble time are even smaller, as they touch when their separation is of the size of the event horizon. The timescale for coalescence by gravitational waves only is a sensitive function of the binary separation, scaling as a^4 (Peters, 1964). Therefore, gravitational waves guide the inspiral only when a is less than a critical value $a_\mathrm{GW} \sim 0.003\,a_\mathrm{B}(M/10^6\,M_\odot)^{1/4}$ (using scaling relations) that is of 0.01 pc – 0.001 pc for a circular binary in the eLISA mass interval. Typical orbital periods at a_GW are of a few years to tens of years, and the hole's relative velocities are as high as 3000 km/s – 5000 km/s.

Black holes have to travel a distance from 0.1 kpc – 10 kpc down to 0.01 pc – 0.001 pc, before entering the gravitational wave inspiral regime, in a galaxy. Given the huge dynamical range, different physical mechanisms are guiding their sinking (Colpi and Dotti, 2011). We can distinguish four phases for the dynamics of black holes on their way to and after merging:

1. the *pairing phase*, when the black holes pair on galactic scales following the dynamics of the galaxies they inhabit until they form a Keplerian binary (on pc scales);
2. the *binary phase*, when the Keplerian binary continues to harden at the centre of the galaxy remnant;
3. the *gravitational wave phase*, when black hole inspiral is dominated by loss of energy and angular momentum by gravitational waves; and finally
4. the *recoiling phase*, when the now single black hole either oscillates or escapes the galaxy following gravitational recoil.

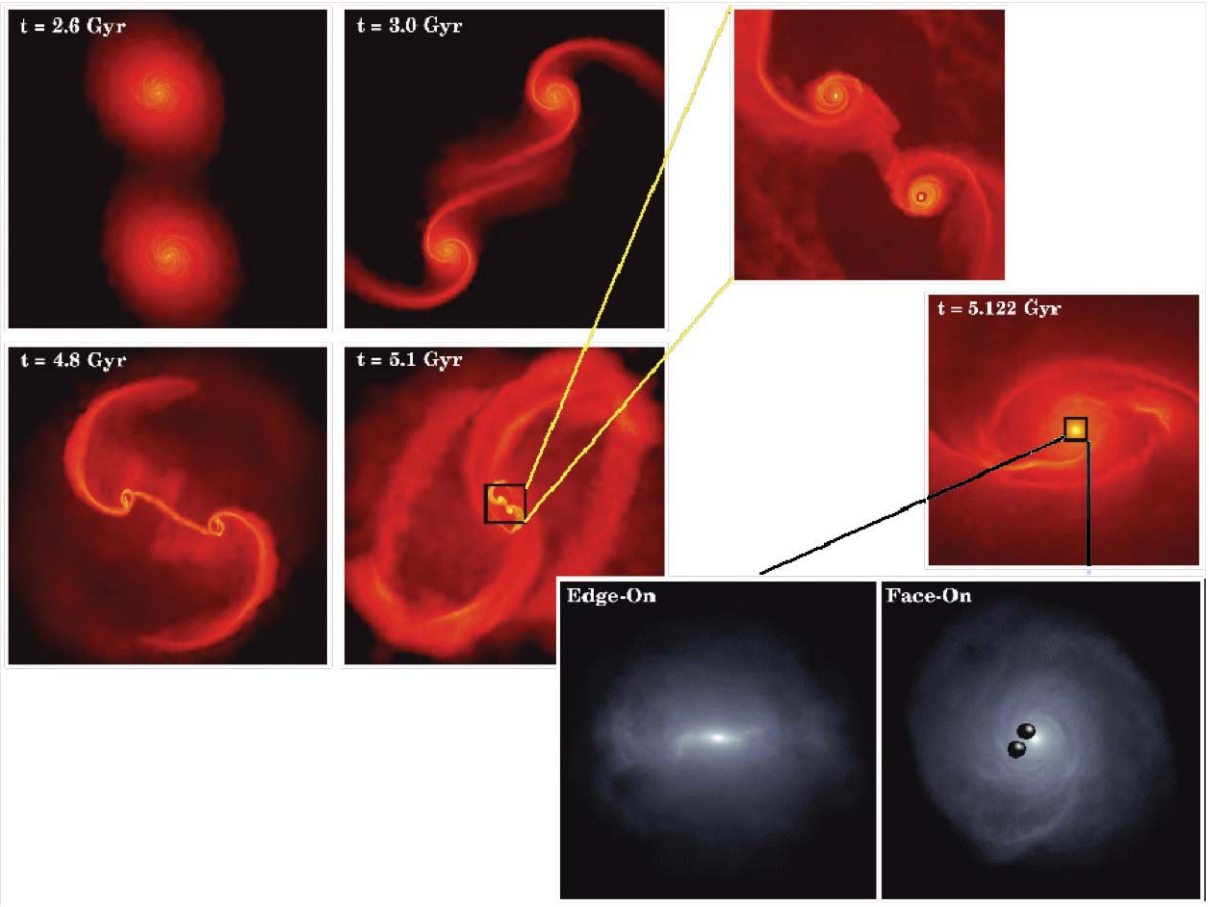

Figure 14: The different stages of the merger between two identical Milky-Way-like gas-rich disc galaxies (from Mayer et al., 2007). The panels show the density maps of the gas component in logarithmic scale, with brighter colours for higher densities. The four panels to the left show the large-scale evolution at different times. The boxes are 120 kpc on a side (top) and 60 kpc on a side (bottom). During the interaction tidal forces tear the galactic disks apart, generating spectacular tidal tails and plumes. The panels to the right show a zoom in of the very last stage of the merger, about 100 million years before the two cores have fully coalesced (upper panel), and 2 million years after the merger (middle panel), when a massive, rotating nuclear gaseous disc embedded in a series of large-scale ring-like structures has formed. The boxes are now 8 kpc on a side. The two bottom panels, with a grey colour scale, show the detail of the inner 160 pc of the middle panel; a massive nuclear disc, shown edge-on (left) and face-on (right), forms in the aftermath of the merger (of 10^9 $M_\odot$). The two black holes continue to sink inside the disc and form a Keplerian binary; they are shown in the face-on image.

In major merger of galaxies the black holes pair under the action of dynamical friction against the dark matter background, that brakes the disc/bulge which they inhabit (Begelman et al., 1980, Chandrasekhar, 1943, Colpi et al., 1999, Ostriker, 1999). Pairing occurs on the typical timescale of a galactic merger of a few billion years. A few million years after the new galaxy has formed, a Keplerian binary forms on the scale of 1 pc – 10 pc, under the action of dynamical friction by stars and gas (Mayer et al., 2007). Figure 14 shows the evolution of the two gas-discs in merging galaxies similar to the Milky Way. The galaxies host a central black hole, and the black holes end forming a Keplerian binary embedded in a massive nuclear disc (Mayer et al., 2007). The subsequent hardening of the binary orbit (phase II) is controlled by the inflow of stars from larger radii, and by the gas rotating in a circum-binary disc (Callegari et al., 2009, Colpi and Dotti, 2011, Dotti et al., 2006, 2007, 2009b, Escala et al., 2004, Merritt and Milosavljević, 2005). In gas rich environments, and for black holes of mass smaller than about $10^7\,M_\odot$, gas-dynamical torques on the binary suffice to drive the system down to the gravitational wave inspiral domain (Armitage and Natarajan, 2005, Cuadra et al., 2009, Gould and Rix, 2000, Hayasaki et al., 2008, Hayasaki and Okazaki, 2009, Ivanov et al., 1999, MacFadyen and Milosavljević, 2008) if the gas does not fragment in stars (Lodato et al., 2009).

Stars are ubiquitous, and in stellar bulges the black holes lose orbital energy and angular momentum by ejecting stars that scatter individually off the black holes (Berczik et al., 2005, Makino and Funato, 2004, Merritt, 2006, Merritt et al., 2007, Merritt and Milosavljević, 2005, Merritt and Poon, 2004, Milosavljević and Merritt, 2001, Perets and Alexander, 2008, Quinlan, 1996, Sesana et al., 2006, 2007a, 2008a). These stars approach the binary from nearly radial orbit, and shrink the binary down to the gravitational wave phase, if they are present in sufficient number to carry away the energy for the binary to decay down to $a_{\rm GW}$. These stars, ejected with high velocities, are lost by the galaxy, and the timescale of sinking of the binary depends on the rate at which new stars are supplied from far-out distances. Self-consistent high resolution direct N-body simulations (Berczik et al., 2006, Khan et al., 2011, Preto et al., 2011) indicate that the stellar potential of the remnant galaxy retains, in response to the anisotropy of the merger, a sufficiently high degree of rotation and triaxiality to guarantee a large reservoir of stars on centrophilic orbits that can interact with the black holes down to the transit from the binary phase to the gravitational wave phase. This seems to be a universal process. When coalescence occurs, the merger remnant "recoils"because of the anisotropic emission of gravitational waves (Baker et al., 2008), moving away from the gravitational centre of the galaxy. The kicked black hole, may return after a few oscillations down to the nuclear regions of the host galaxy, or escape the galaxy depending on the magnitude of the kick (Blecha et al., 2011, Blecha and Loeb, 2008, Gualandris and Merritt, 2008, Guedes et al., 2011).

4 Dual, binary and recoiling AGN in the cosmic landscape

Surprisingly, the closest example of an imminent merger is in our Local Group. Andromeda (M31) along with a handful of lesser galaxies does not follow Hubble's law of cosmic expansion: it is falling toward us at a speed of about 120 km/s. M31 is a member of a group of galaxies, including the Milky Way, that form a gravitationally bound system, the Local Group. M31 and the Milky Way each house a massive black hole (van der Marel et al., 1994) and are on a collision course, with a merger possibly before the Sun expands into a red giant ($\sim$ 4 billion years) (Cox and Loeb, 2008). Observations are now revealing the presence of many colliding galaxies in the Universe, and in a number of cases two active black holes are visible through their X-ray or radio emission.

The existence of binary AGN, i.e. of two active black holes bound in a Keplerian fashion, is still debatable at the observational level, as they are rare objects (Volonteri et al., 2009). Two cases deserve attention. The first case is 0402+379, a radio source in an elliptical galaxy showing two compact flat-spectrum radio nuclei, only 7 pc apart (Rodriguez et al., 2006, 2009). The second case is OJ 287, a source displaying a periodic variability of 12 years (Valtonen et al., 2008, 2011, 2010, 2006) that has been interpreted as being a Keplerian binary with evidence of orbital decay by emission of gravitational waves. A number of sub-parsec binary black hole candidates have been proposed (Eracleous et al., 2011, Tsalmantza et al., 2011) based on the recognition that gas clouds orbiting one/two black hole(s) can leave an imprint in the optical spectra of the AGN (Barrows et al., 2011, Bogdanović et al., 2008, Boroson and Lauer, 2009, Decarli et al., 2010, Montuori et al., 2011, Shen and Loeb, 2010, Shields et al., 2009). Follow-up observations will be necessary to assess their true nature.

Recoiling AGN, i.e. recoiling black holes observed in an active phase (Devecchi et al., 2009, Loeb, 2007, Merritt et al., 2009b, O'Leary and Loeb, 2009), have been searched recently, and there has been a claim of a discovery (Komossa et al., 2008), even though alternative interpretations are also viable (Bogdanović et al., 2009, Dotti et al., 2009a). Two spatially off-set AGN have been found in deep surveys with kinematic properties that are consistent with being two recoiling black holes (Civano et al., 2010, Jonker et al., 2010).

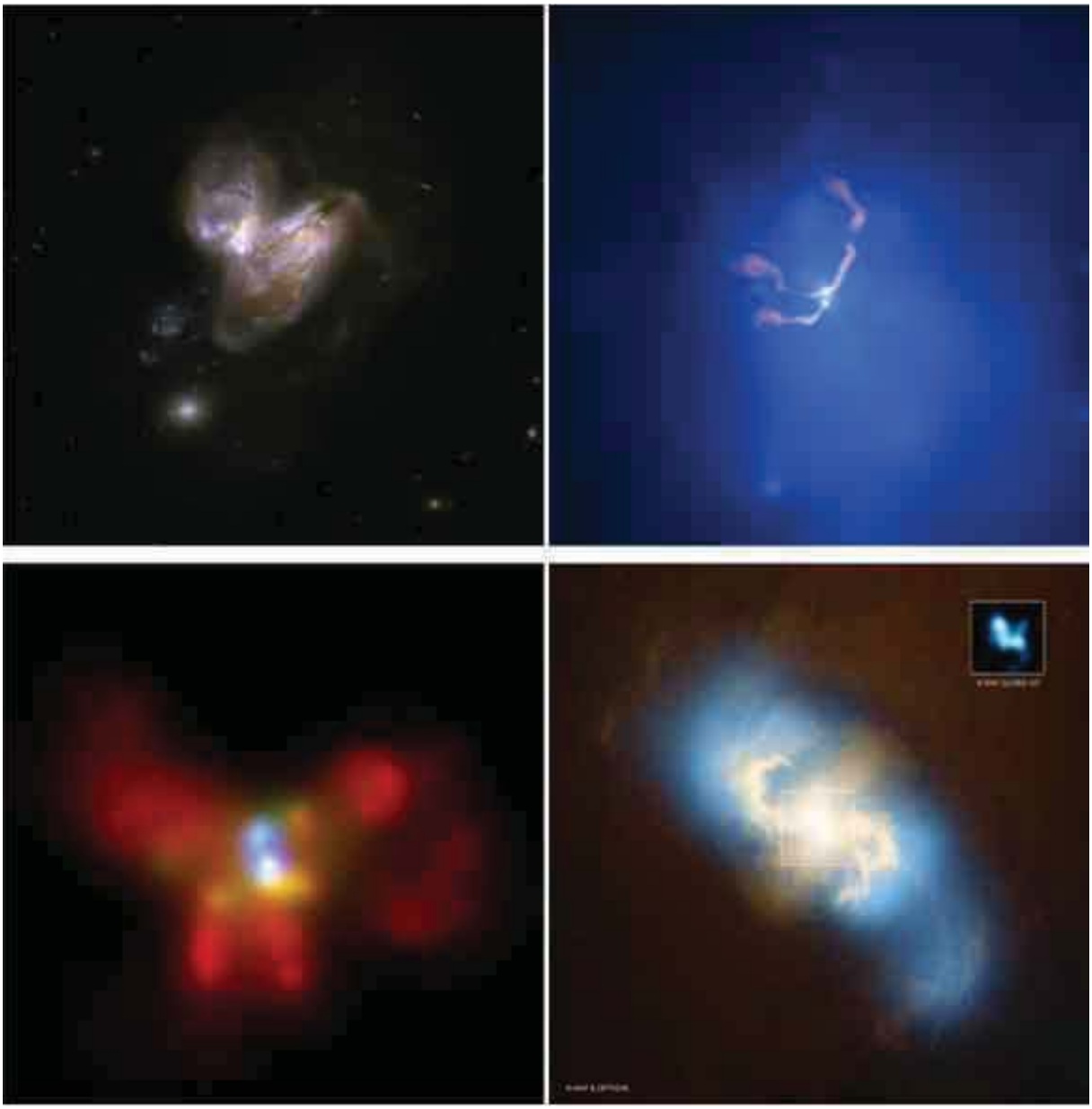

Figure 15: Active black holes in colliding galaxies. Arp 299 (upper left panel) is the interacting system resulting from the collision of two gas-rich spirals, and hosts a dual AGN, i.e. two black holes "active" during the pairing phase. The accreting black holes are visible in the X-rays and are located at the optical centres of the two galaxies, at a separation of 4.6 kpc(Ballo et al., 2004). X-ray view of NGC6240 (lower left panel) an ultra luminous infrared galaxy considered to be a merger in a well advanced phase (Komossa et al., 2003). X-ray observations with the Chandra Observatory let to the discovery of two strong hard X-ray unresolved sources embedded in the diluted soft X-ray emission (red) of a starburst. The dual AGN are at a separation of 700 pc. Composite X-ray (blue)/radio (pink) image of the galaxy cluster Abell 400 (upper right panel) showing radio jets immersed in a vast cloud of multimillion degree X-ray emitting gas that pervades the cluster. The jets emanate from the vicinity of two supermassive black holes (a dual radio-loud AGN) housed in two elliptical galaxies in the very early stage of merging. Composite optical and X-ray image of NGC 3393 (lower right panel), a spiral galaxy with no evident signs of interaction. In its nucleus, two active black holes have been discovered at a separation of only 150 pc (Fabbiano et al., 2011). The closeness of the black holes embedded in the bulge, provide a hitherto missing observational point to the study of galaxy-black hole evolution: the phase when the black holes are close to forming a Keplerian binary. The regular spiral morphology and predominantly old circum-nuclear stellar population of this galaxy, indicates that a merger of a dwarf with a large spiral led to the formation of the binary (Callegari et al., 2011, 2009).

The most remarkable, albeit indirect, evidence of coalescence events is found in bright elliptical galaxies that are believed to be product of mergers. Bright elliptical galaxies show light deficits (cores) in their surface brightness profiles, i.e. lack of stars in their nuclei (Kormendy and Bender, 2009), and this missing light correlates with the mass of the central black hole (Merritt, 2006, Merritt et al., 2007). Thus, cores are evidence of binary black holes scouring out the nuclear stars via three-body scattering (Merritt et al., 2007) or even via post-merger relaxation following a kick (Boylan-Kolchin et al., 2004, Gualandris and Merritt, 2008, Guedes et al., 2009). Lastly, mergers change the black hole's spin directions due to conservation of angular momentum. Reorientation of the black hole spin following coalescence is now believed to be at the heart of X-shaped radio galaxies, where an old jet coexists with a new jet of different orientation (Liu, 2004, Merritt and Ekers, 2002). This would be again a sign of a fully accomplished coalescence event.

5 Seed black holes

Models of hierarchical structure formation predict that galaxy sized dark matter halos start to become common at redshift $z \sim 10 - 20$ (Mo et al., 2010). This is the beginning of the nonlinear phase of density fluctuations in the Universe, and hence also the epoch of baryonic collapse leading to star and galaxy formation. Different populations of seed black holes have been proposed in the range $100\,\mathrm{M}_\odot - 10^6\,\mathrm{M}_\odot$ (Volonteri, 2010).

Small mass seeds ($100\,\mathrm{M}_\odot - 1000\,\mathrm{M}_\odot$) may result from the core collapse of the first generation of massive stars (Pop III) that form from unstable metal-free gas clouds, at $z \sim 20$ and in halos of $10^6\,\mathrm{M}_\odot$ (Abel et al., 2002, Bromm et al., 2002, Haiman et al., 1996, Omukai and Palla, 2001, 2003, Ripamonti et al., 2002, Tegmark et al., 1997). Pop III stars as massive as $260\,\mathrm{M}_\odot$ or larger collapse into a black hole of similar mass after only about 2 Myr (Heger et al., 2003, Madau and Rees, 2001). The formation of Pop III stars remains a poorly understood process (Zinnecker and Yorke, 2007) and the maximum mass reached by individual stars is unknown (see, e.g., Clark et al., 2011).

Large seeds form in heavier halos (of $10^8\,\mathrm{M}_\odot$) from the collapse of unstable gaseous discs of $10^4\,\mathrm{M}_\odot - 10^6\,\mathrm{M}_\odot$. This route, ending with the formation of a very massive quasi-star, assumes that fragmentation is suppressed possibly by turbulence and by an intense ultraviolet background light, in an environment of low metallicity (Begelman et al., 2006, Bromm and Loeb, 2003, Dijkstra et al., 2008, Dotan et al., 2011, Haehnelt and Rees, 1993, Koushiappas et al., 2004, Lodato and Natarajan, 2006, Loeb and Rasio, 1994). Collapsing clouds can have significant angular momentum (Bullock et al., 2001), and thus additional momentum transport is required for the self-gravitating disc to form a supermassive star (Begelman and Shlosman, 2009, Shlosman et al., 1989). The very massive quasi-star of about $10^5\,\mathrm{M}_\odot$, burns hydrogen and helium in its core and once formed, the star collapses into a black hole when metallicity is below some threshold, as the alternative is its entire explosion (Montero et al., 2011, Shibata and Shapiro, 2002). Recently, other formation routes have been explored for the large seeds ($10^3\,\mathrm{M}_\odot - 10^4\,\mathrm{M}_\odot$). They comprise the formation of a massive star via stellar runaway collisions in young dense star clusters (Devecchi and Volonteri, 2009, Gürkan et al., 2004, Portegies Zwart and McMillan, 2002), and the relativistic collapse of stellar mass black holes in nuclear star clusters invaded by a large inflow of gas (Davies et al., 2011). Lastly, much heavier seeds resulting from direct collapse of nuclear gas in a gas-rich galactic merger have been proposed as the origin of black holes (Mayer et al., 2010).

The subsequent step is to follow the evolution of the black hole seeds according to the growth of the halos they inhabit, and the mode of accretion (Devecchi and Volonteri, 2009, Volonteri and Begelman, 2010, Volonteri et al., 2008). This is an inherently model dependent process. Observations of nearby dormant black holes and of AGN at higher redshift help in constraining their evolution, but theoretical models still have some unconstrained degrees of freedom.

6 Evolving massive black hole spins via coalescence and accretion events

Astrophysical black holes are fully described by the mass $M_\bullet$ and angular momentum $\mathbf{J}$, referred to as spin. The modulus J of $\mathbf{J}$ is usually specified in terms of the dimensionless spin parameter $a_\bullet$ defined so that $J = a_\bullet(GM_\bullet^2/c)$. For a specified mass $M_\bullet$, a black hole described by GR cannot have $a_\bullet > 1$, without showing a naked singularity (and this is forbidden by the Cosmic Censorship conjecture).

Both coalescences and accretion change $M_\bullet$, J (or $a_\bullet$) and the orientation of $\mathbf{J}$ in a significant manner (Berti and Volonteri, 2008, Volonteri et al., 2007).

Spins in black hole coalescences

With the advent of numerical relativity, it became possible to accurately determine the evolution of the initial spins of the black holes to the final spin of the remnant black hole in a merger event (Baker et al., 2006, Campanelli et al., 2006, Centrella et al., 2010, Pretorius, 2005, Rezzolla et al., 2008a).

Numerical relativity simulations for equal mass, non spinning black holes find a spin $a_\bullet = 0.686\,46 \pm 0.000\,04$ (Scheel et al., 2009) for the merged black hole, resulting from the angular momentum of the orbit. Extrapolation of black hole coalescences with large initial spins (larger than approximately 0.9) exactly aligned with the orbital angular momentum find a final $a_\bullet = 0.951 \pm 0.004$ (Marronetti et al., 2008). When mergers occur with retro- and pro-grade orbits equally distributed, as it is expected in the case of astrophysical black holes (Hughes and Blandford, 2003), the average spin of the merger remnant is about 0.7, close to the expectation for non spinning holes (Berti and Volonteri, 2008).

For almost any configuration of spins and mass ratio, the emission pattern of the gravitational wave is anisotropic, leading to a *gravitational recoil* (Campanelli et al., 2007, González et al., 2007, Lousto and Zlochower, 2011b).

Numerical studies show that initially nonspinning black holes or binaries with spins aligned with the orbital angular momentum are recoiling with a velocity below about 200 km/s. By contrast, the recoil is dramatically larger, up to approximately 5000 km/s, for binaries of comparable mass and black holes with large spins in peculiar non-aligned configurations (Lousto and Zlochower, 2011a). Thus, unexpectedly, spins (regulated by coalescence and accretion) affect the retention fraction of black holes in galactic halos, and this has consequences on the overall evolution of black holes in galaxies (Kesden et al., 2010, Schnittman, 2007, Schnittman and Buonanno, 2007, Volonteri et al., 2010).

Spins and black hole accretion

The evolution of mass and spin of astrophysical black holes are strongly correlated, also when considering accretion. Spins determine directly the radiative efficiency $\varepsilon(a_\bullet)$, and so the rate at which mass is increasing. In radiatively efficient accretion discs (Shakura and Sunyaev, 1973) ε varies from 0.057 (for $a_\bullet = 0$) to 0.151 (for $a_\bullet = 0.9$) and 0.43 (for $a_\bullet = 1$). Accretion on the other hand determines black hole spins since matter carries with it angular momentum (the angular momentum at the innermost stable circular orbit of a Kerr black hole). A non-rotating black hole is spun-up to $a_\bullet = 1$ after increasing its mass by a factor $\sqrt{6}$, for prograde accretion (Bardeen, 1970). Conversely, a maximally rotating black hole is spun-down by retrograde accretion to $a_\bullet \sim 0$, after growing by a factor $\sqrt{3/2}$.

Accretion imposes limits on the black hole spin. Gas accretion from a geometrically thin disc limits the black-hole spin to $a_\bullet^{\rm acc} = 0.9980 \pm 0.0002$, as photons emitted by the disc and with angular momentum anti-parallel to the black hole spin are preferentially captured, having a larger cross section, limiting its rotation (Thorne, 1974). The inclusion of a jet, as studied in magneto-electrodynamic simulations, reduces this limit to $a_\bullet^{\rm jet} \simeq 0.93$ (Gammie et al., 2004), and changes in the accretion geometry produce a similar effect (Popham and Gammie, 1998).

How black holes are fed from the large scale down to the hole's influence radius ($R_{\rm grav}$) is presently unknown, and the spin is sensitive to the way gas is accreted with time (Volonteri et al., 2007). Two limiting modes of accretion can occur. *Coherent accretion* refers to accretion from a geometrically thin disc, lasting longer than a few black hole mass growth *e*-folding times. During coherent accretion the black hole can more than double its mass, bringing its spin up to the limit imposed by basic physics, either $a_\bullet^{\rm acc}$ or $a_\bullet^{\rm jet}$. By contrast, *chaotic accretion* refers to a succession of accretion episodes that are incoherent, i.e. randomly oriented. The black hole can then spin-up or down, and spin-down occurs when counter-rotating material is accreted, i.e. when the angular momentum $\mathbf{L}$ of the disc is strongly misaligned with respect to $\mathbf{J}$ (i.e. $\mathbf{J}\cdot\mathbf{L} < \mathbf{0}$). If accretion proceeds via short-lived, uncorrelated episodes with co-rotating and counter-rotating material equally probable, spins tend to be small (King and Pringle, 2006, 2007, Moderski et al., 1998): counter-rotating material spins the black hole down more than co-rotating material spins it up, as the innermost stable orbit of a counter-rotating test particle is located at a larger radius than that of a co-rotating particle, and accordingly carries a larger orbital angular momentum.

The direction of the black hole spin is also an important element in the study of black holes. In a viscous accretion disc that is misaligned with the spin of the black hole, Lense-Thirring precession of the orbital plane of fluid elements warps the disc, forcing the gas close to the black hole to align (either parallel or anti-parallel) with the spin of the black hole. Warping is a rapid process that causes alignment of the disc out to $100\,R_{\rm horizon} - 10^3\,R_{\rm horizon}$, depending on $a_\bullet$ (Bardeen and Petterson, 1975). Following conservation of total angular momentum, the black hole responds to the warping through precession and alignment, due to dissipation in the disc (Perego et al., 2009, Scheuer and Feiler, 1996) evolving into a

configuration of minimum energy where the black hole and disc are aligned (King et al., 2005). This process is short (10^5 yrs) compared to the typical accretion time scale, allowing astrophysical black holes to evolve into a quasi-aligned spin-orbit configuration prior to coalescence (Dotti et al., 2010).

According to these theoretical findings, masses and spins evolve dramatically following coalescence and accretion events. The spin offers the best diagnostics on whether the black holes prior to coalescence have experienced either coherent or chaotic accretion episodes. Both, mass and spin, are directly encoded into the gravitational waves emitted during the the merger process. eLISA will measure the masses and spins of the black holes prior to coalescence, offering unprecedented details on how black hole binaries have been evolving along of the course of the galactic merger and along cosmic history.

7 Cosmological massive black hole merger rate

As eLISA creates a new exploratory window on the evolution of black holes, covering a mass and redshift range that is out of the reach of current (and planned) instruments, its expected detection rate is observationally unconstrained. Today we can probe dormant black holes down to masses of about $10^5\,\mathrm{M}_\odot$ (Magorrian et al., 1998, Xiao et al., 2011) in the local Universe only, and their massive (i.e. heavier than $10^8\,\mathrm{M}_\odot$) active counterparts out to redshift $\gtrsim 6$ (Fan et al., 2004, 2001, 2006b, 2003). Any estimate of the eLISA detection rate necessarily has to rely on extrapolations based on theoretical models matching the properties of the observable black hole population.

Observationally, the black hole merger rate can be inferred only at relatively low redshift, by counting the fraction of close pairs in deep galaxy surveys. Given a galaxy density per co-moving megaparsec cube n_G, a fraction of close pairs ϕ, and a characteristic merger timescale $\mathcal{T}_M$, the merger rate density *of galaxies* (number of mergers per year per co-moving megaparsec cube), is given by $\dot{n}_M = \phi n_G/(2\mathcal{T}_M)$.

Estimates of $\dot{n}_M$ have been produced by several groups in the last decade (Bell et al., 2006, De Propris et al., 2007, de Ravel et al., 2009, Lin et al., 2004, 2008, Patton et al., 2002, Xu et al., 2011), using deep spectroscopic galaxy surveys like COMBO, COSMOS and DEEP2. Surveys are obviously flux limited, and usually an absolute magnitude cutoff (which translate into a stellar mass lower limit) is applied to obtain a complete sample of galaxy pairs across a range of redshifts. The galaxy merger rate is therefore fairly well constrained only at redshift $z \lesssim 1$ for galaxies with stellar mass larger than approximately $10^{10}\,\mathrm{M}_\odot$. From compilation of all the measurement (Xu et al., 2011), typical average massive galaxy merger rates $\dot{n}_M$ at $z < 1$ lie in the range $5 \times 10^{-4} < \dot{n}_M < 2 \times 10^{-3} h_{100}^3 \mathrm{Mpc}^{-3}\,\mathrm{Gyr}^{-1}$. By applying the black hole-host relations (Gültekin et al., 2009), the galaxy stellar mass cutoff is converted into a lower limit to the hosted black hole mass. Assuming a black hole occupation fraction of one (appropriate for massive galaxies) and integrating over the appropriate co-moving cosmological volume, this translates into an *observational* estimate of the *massive black hole merger rate* for $z < 1$ and $M >$ few $\times\, 10^6\,\mathrm{M}_\odot$.

These estimates can be compared to the rate predicted by Monte Carlo merger trees (Volonteri et al., 2003) based on the EPS formalism (Lacey and Cole, 1993, Press and Schechter, 1974, Sheth and Tormen, 1999), which are used to reconstruct the black hole assembly, and thus to infer eLISA detection rates, in the ΛCDM cosmology. The evolutionary path (outlined in the previous sections) can be traced back to very high redshift ($z > 20$) with high resolution via numerical EPS Monte Carlo realisations of the merger hierarchy. Sesana et al. (2008b) carried a detailed comparison of the merger rate predicted by such models in the $z < 1$ and $M >$ few $\times\, 10^6\,\mathrm{M}_\odot$ range with those inferred by galaxy pair counting, finding a generally broad consistency within a factor of 2.

On the theoretical side, massive black hole merger rates can be computed from semi-analytic galaxy formation models coupled to massive N-body simulations tracing the cosmological evolution of dark matter halos (Bertone et al., 2007, De Lucia et al., 2006, Guo et al., 2011), such as the Millennium Run (Springel et al., 2005). Such models are generally bound to the limiting resolution of the underlying N-body simulations, and are therefore complete only for galaxy masses larger than approximately $10^{10}\,\mathrm{M}_\odot$. In a companion study, Sesana et al. (2009) also showed that the merging black hole mass functions predicted by EPS based merger trees is in excellent agreement with those extracted by semi-analytic galaxy formation model in the mass range $M > 10^7\,\mathrm{M}_\odot$, where semi-analytic models can be considered complete.

Merger rates obtained by EPS merger trees are therefore firmly anchored to low redshift observations and to theoretical galaxy formation models. Nevertheless, the lack of observations in the mass range of interest for eLISA leaves significant room for modelling, and theoretical astrophysicists have developed a large variety of massive black holes formation scenarios that are compatible with observational constraints (Begelman et al., 2006, Koushiappas et al., 2004, Lodato and Natarajan, 2006, Volonteri et al., 2003). The predicted coalescence rate in the eLISA window depends on the peculiar

details of the models, ranging from a handful up to few hundred events per year (Enoki et al., 2004, Haehnelt, 1994, Koushiappas and Zentner, 2006, Rhook and Wyithe, 2005, Sesana et al., 2004, 2005, 2007b, Wyithe and Loeb, 2003). A recent compilation, encompassing a wide variety of assembly history models, can be found in (Sesana et al., 2011).

8 Massive black hole binaries as gravitational waves sources: what can eLISA discover?

In the eLISA window of detectability massive black hole binary coalescence is a three-step process comprising the *inspiral, merger, and ring-down* (Flanagan and Hughes, 1998). The inspiral stage is a relatively slow, adiabatic process in which the black holes spiral together on nearly circular orbits. The black holes have a separation wide enough so that they can be treated analytically as point particles through the Post Newtonian (PN) expansion of their binding energy and radiated flux (Blanchet, 2006). The inspiral is followed by the dynamical coalescence, in which the black holes plunge and merge together, forming a highly distorted, perturbed remnant. At the end of the inspiral, the black hole velocities approach $v/c \sim 1/3$. At this stage the PN approximation breaks down, and the system can only be described by a numerical solution of the Einstein equations. The distorted remnant settles into a stationary Kerr black hole as it *rings down*, by emitting gravitational radiation. This latter stage can be, again, modelled analytically in terms of black hole perturbation theory. At the end of the ring-down the final black hole is left in a quiescent state, with no residual structure besides its Kerr spacetime geometry.

In recent years there has been a major effort in constructing accurate waveforms inclusive of the inspiral merger and ring-down phases (Baker et al., 2006, Campanelli et al., 2006, Pretorius, 2005). Even a few orbital cycles of the full waveform are computationally very demanding. "Complete" waveforms can be designed by stitching together analytical PN waveforms for the early inspiral with a (semi)phenomenologically described merger and ring-down phase (Damour et al., 2011, Pan et al., 2011, Santamaría et al., 2010), calibrated against available numerical data. In the following estimations we will mostly employ phenomenological waveforms constructed in frequency domain, as described in Santamaría et al. (2010). Self-consistent waveforms of this type (the so called PhenomC waveforms) are available for non-spinning binaries and for binaries with aligned spins. In the case of binaries with misaligned spins, we use "hybrid" waveforms obtained by stitching precessing PN waveforms for the inspiral with PhenomC waveforms for the merger/ring-down. This stitching is performed by projecting the orbital angular momentum and individual spins onto the angular momentum of the distorted black hole after merger. Given a waveform model, a first measure of the eLISA performance is the SNR of a binary merger with parameters in the relevant astrophysical range.

Detector performance

Figure 16 shows eLISA SNRs for equal mass, non-spinning coalescing binaries. Here we use PhenomC waveforms and we compute the SNR as a function of the rest-frame total binary mass M and of the redshift z, averaging over all possible source sky locations and wave polarisation, for two-year observations. The plot highlights the exquisite capabilities of the instrument in covering almost all the mass-redshift parameter space relevant to massive black hole astrophysics. It is of importance to emphasise that current electromagnetic observations are probing only the tip of the massive black hole distribution in the Universe. Our current knowledge of massive black holes is bound to instrument flux limits, probing only the mass range $10^7\,\mathrm{M}_\odot - 10^9\,\mathrm{M}_\odot$ at $0 \lesssim z \lesssim 7$. Conversely, eLISA will be able to detect the gravitational waves emitted by sources with total mass (in the source rest frame) as small as $10^4\,\mathrm{M}_\odot$ at cosmological distances inaccessible to any other astrophysical probe. A binary with total mass in the interval $10^4\,\mathrm{M}_\odot - 10^7\,\mathrm{M}_\odot$ can be detected out to a redshift as remote as $z \sim 20$ with a SNR ≥ 10. By contrast, a binary as massive as a few $10^8\,\mathrm{M}_\odot$ can be detected with high SNR in our local Universe ($z \lesssim 1$). Binaries with total mass between $10^5\,\mathrm{M}_\odot - 10^7\,\mathrm{M}_\odot$ can be detected with a SNR $\gtrsim 100$, between $0 \lesssim z \lesssim 5$. These intervals in mass and redshift can be considered as optimal for a deep and extensive census of the black hole population in the Universe.

Figure 17 shows constant-contour levels of the SNR expected from binaries with different mass ratios q (defined as $q = m_2/m_1$, where m_2 is the mass of the less massive black hole in the binary) located at redshift $z = 1$ and $z = 4$. The plots show the SNR reduction that occurs with decreasing q, as unequal mass binaries have lower strain amplitudes than equal mass binaries. They also show how SNR decreases with increasing redshift, and thus with increasing luminosity distance. Notice however that even at $z = 4$, binaries in the mass range $10^5\,\mathrm{M}_\odot - 10^7\,\mathrm{M}_\odot$ with mass ratio $q \lesssim 10^{-1}$ can be detected with SNR > 20.

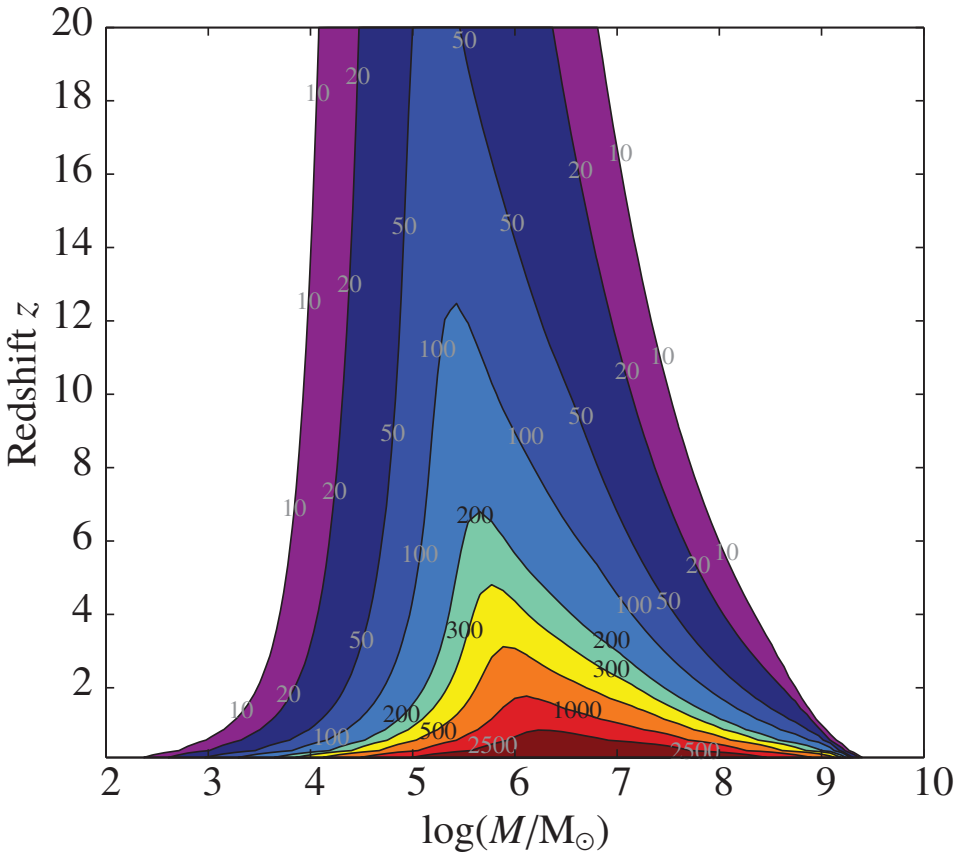

Figure 16: Constant-contour levels of the sky and polarisation angle-averaged signal-to-noise ratio (SNR) for equal mass non-spinning binaries as a function of their total mass M and cosmological redshift z. The total mass M is measured in the rest frame of the source. The SNR is computed using PhenomC waveforms (Santamaría et al., 2010), which are inclusive of the three phases of black hole coalescence (in jargon: inspiral, merger, and ring-down, as described in the text).

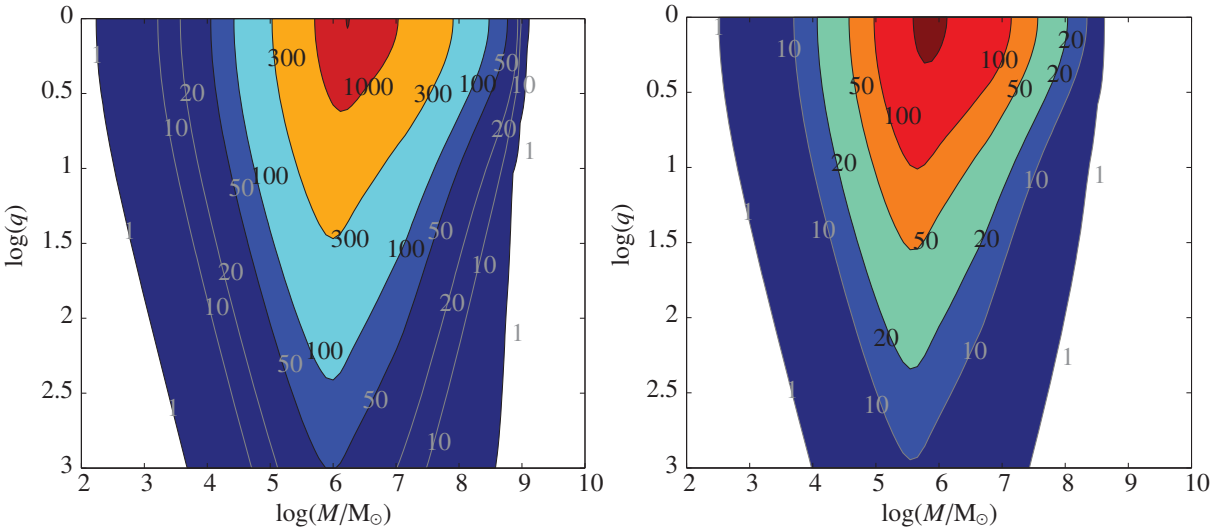

Figure 17: The figure shows constant-contour levels of the sky and polarisation angle averaged signal-to-noise ratio (SNR) for non-spinning binaries, at cosmological redshift $z = 1$ (left panel) and $z = 4$ (right panel) in the M–q plane. Here M is the total mass of the binary in the source rest frame, and q is the mass ratio. The SNR is computed from the full non spinning PhenomC waveform inclusive of inspiral, merger and ring-down, as in figure 16.

Parameter estimation

Figures 16 and 17 describe the detectability of single events, and for these individual events, it is possible to extract information on the physical parameters of the source. Waveforms carry information on the redshifted mass (the mass measured at the detector is $(1 + z)$ times the mass at the source location) and on the spin of the individual black holes prior to coalescence. The measure of the mass and spin is of importance in astrophysics. Except for the Galactic centre (Ghez et al., 2005, Gillessen et al., 2009), the mass of astrophysical black holes is estimated with uncertainties ranging from 15 % to a factor of about 2, depending on the technique used and the type of source. As far as spin is concerned, its measure is only indirect, and it is derived through modelling of the spectrum, or of the shape of emission lines, mainly by fitting the skewed relativistic Kα iron line. There are few notable examples, but uncertainties are still large. By contrast, spins leave a distinctive peculiar imprint in the waveform.

In section 5 and 6 we explored different routes to seed black hole formation and to their subsequent assembly and growth through mergers and accretion episodes. Different physically motivated assumptions lead to different black hole evolution scenarios, and, as we highlighted above, the lack of observational constraints allowed theoretical astrophysicists to develop a large variety of massive black holes formation scenarios. To assess the astrophysical impact of eLISA, we simulate observations assuming a fiducial set of four cosmological black hole evolution scenarios: SE refers to a model where the seeds have small (S) mass about 100 $M_\odot$ (from Pop III stars only) and accretion is coherent, i.e. resulting from extended (E) accretion episodes: SC refers to a model where seeds are small but accretion is chaotic (C), i.e., resulting from uncorrelated episodes; and finally, LE and LC refer to models where the seed population is heavy (L stands for large seeds of 10^5 $M_\odot$) and accretion is extended and chaotic, respectively. The models are almost the same used in previous studies by the LISA Parameter Estimation Task Force (Arun et al., 2009). The only difference is that in the extended accretion model, spins are not assumed to be perfectly aligned to the binary orbital angular momentum. The angles of misalignment relative to the orbit are drawn randomly in the range 0 to 20 degree, consistent with the finding of recent hydrodynamical simulations of binaries forming in wet mergers (Dotti et al., 2010). These models encompass a broad range of plausible massive black hole evolution scenarios, and we use them as a testbed for eLISA capabilities in a fiducial astrophysical context. Each massive black hole binary, coalescing at redshift z, is characterised by the (rest frame) total mass $M = m_1 + m_2$ (with m_1 and m_2 the mass of the primary and secondary black hole), mass ratio $q = m_2/m_1$, spin vectors $\mathbf{J_1}$ and $\mathbf{J_2}$; spin magnitudes are denoted by a_1 and a_2. The orientations of the spins are drawn as described above for the extended (E) accretion models, and completely random for the chaotic (C) accretion models. Here we generate several Monte Carlo realisations of each model and we sum up all the generated sources in a single "average" catalogue (we will consider models separately in the next section). Catalogues are generated by selecting M, q, z, a_1, a_2 according to the distribution predicted by the individual models, and by randomising other source parameters (sky location, polarisation, inclination, initial phase, coalescence time) according to the appropriate distribution.

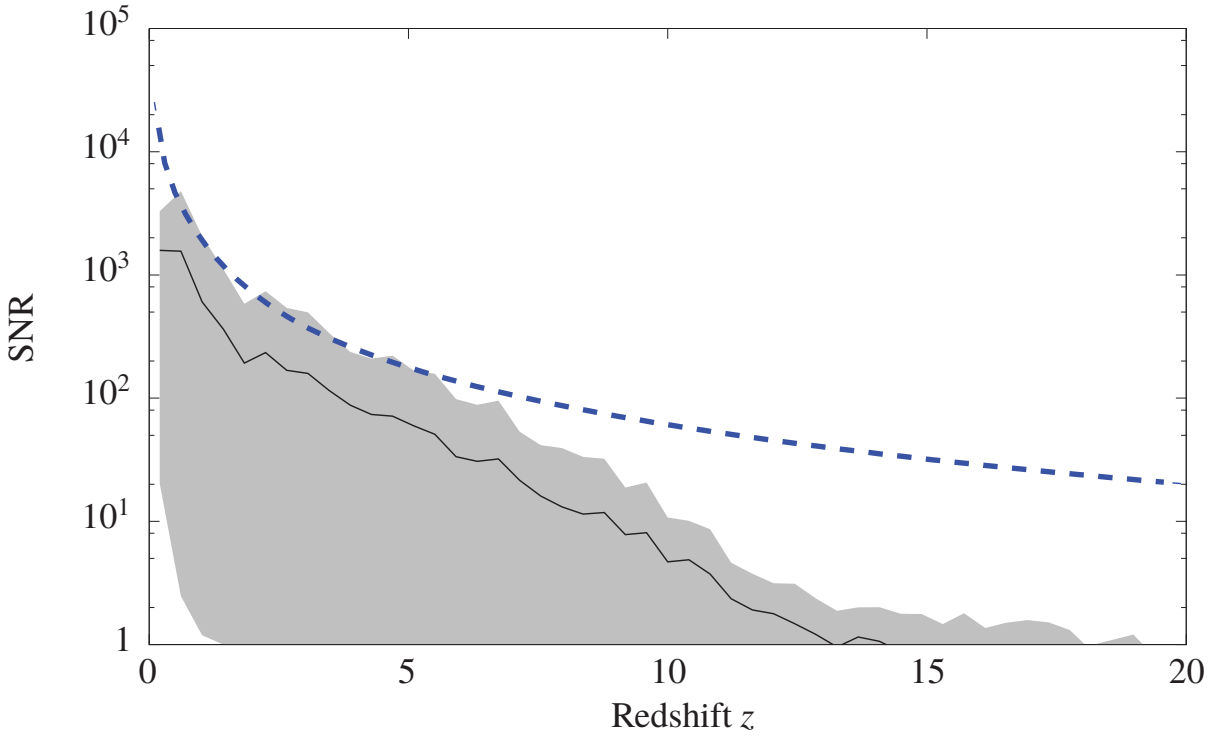

Figure 18: SNR distribution as a function of cosmological redshift, computed using the inspiral, merger and ring-down waveform PhenomC for spinning binaries (Santamaría et al., 2010). The solid line corresponds to the mean value, and the grey area to the distribution corresponding to 10th and 90th percentile of SNR distribution. These results are based on a catalogue of 15360 sources obtained combining 25 realisations of each of the four fiducial massive black hole evolution models. For reference, the dashed-blue line indicates the sky-averaged SNR, for one year of integration, computed for an equal mass coalescing binary of $10^6\,M_\odot$.

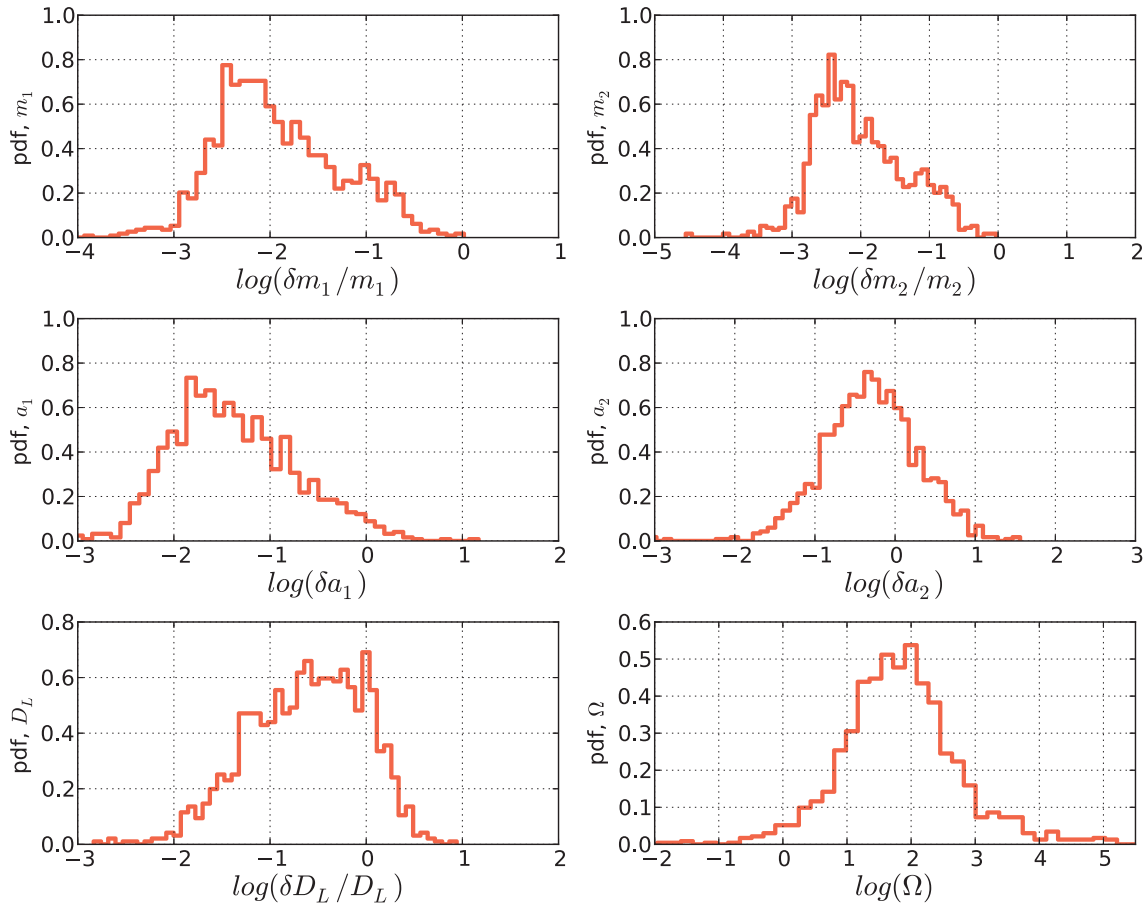

Figure 19: Parameter estimation accuracy evaluated on a source catalogue, obtained combining ten Monte Carlo realisations of the coalescing massive black hole binary population, predicted by the four SE-SC-LE-LC models. The top panels show the distributions of the fractional errors in the estimation of the redshifted masses of the primary (left) and secondary (right) black hole. The middle panels show the absolute error distributions on the measurement of the primary (left) and secondary (right) black hole spin, while the bottom panels show the D_L fractional error distribution on the luminosity distance D_L, and the sky location accuracy $\Delta\Omega$ (in deg^2). Errors are evaluated considering full waveforms.

Figure 18 shows the average source SNR as a function of the source redshift. According to the simulated models, eLISA will detect sources with SNR $\gtrsim 10$ out to $z \lesssim 10$. Note that the astrophysical capabilities of eLISA are not limited by the detector design, but by the population of astrophysical sources. If there were a coalescing black hole binary of $10^4\,M_\odot - 10^6\,M_\odot$ out to redshift $z \sim 20$, eLISA would reveal such a source. Our models, and accordingly our SNR distribution, do not have such an event.

Figure 19 shows *error distributions* in the source parameter estimation, for all the events in the combined catalogue. We used a hybrid approach of joining inspiral with PhenomC waveforms, as described above, to evaluate uncertainties based on the Fisher matrix approximation.

The figure illustrates the importance and power of including the full waveform modelling, comprising all the stages of the binary merger, in order to reach a high level of precision measurements. It is found that individual black hole redshifted masses can be measured with unprecedented precision, i.e. with an error of 0.1 % – 1 %, on both components. No other astrophysical tool has the capability of reaching a comparable accuracy. As far as spins are concerned, the analysis shows that the spin of the primary massive black hole can be measured with an exquisite accuracy, to a 0.01 – 0.1 absolute uncertainty. This precision in the measure mirrors the fact that the primary black hole leaves a bigger imprint in the waveform. The measurement is more problematic for a_2 that can be either determined to an accuracy of 0.1, or remain completely undetermined, depending on the source mass ratio and spin amplitude. We emphasise that the spin measure is a neat, direct measurement, that does not involve complex, often degenerate, multi-parametric fits of high energy emission processes.

The source luminosity distance error D_L has a wide spread, usually ranging from 50% to only few percent. Note that this is a direct measurement of the luminosity distance to the source, which, again, cannot be directly obtained (for cosmological objects) at any comparable accuracy level by any other astrophysical means. eLISA is a full sky monitor, and the localisation of the source in the sky is also encoded in the waveform pattern. Sky location accuracy is typically estimated in the range 10 – 1000 square degrees.

9 Reconstructing the massive black hole cosmic history through eLISA observations

eLISA will be an *observatory*. The goal is not only to detect sources, but also to extract valuable astrophysical information from the observations. While measurements for individual systems are interesting and potentially very useful for making strong-field tests of GR (see section 2), it is the properties of the set of massive black hole binary mergers that are observed which will carry the most information for astrophysics. Gravitational wave observations of multiple binary mergers may be used together to learn about their formation and evolution through cosmic history.

As any observatory, eLISA will observe a set of signals. After signal extraction and data analysis, these observations will provide a catalogue of coalescing binaries, with measurements of several properties of the sources (masses, mass ratio, spins, distances, etc) and estimated errors. The interesting questions to ask are the following: *can we discriminate among different massive black hole formation and evolution scenarios on the basis of gravitational wave observations alone?* Given a set of observed binary coalescences, what information can be extracted about the underlying population? For example, will gravitational wave observations alone tell us something about the mass spectrum of the seed black holes at high redshift, that are inaccessible to conventional electromagnetic observations, or about the poorly understood physics of accretion? These questions were extensively tackled in (Sesana et al., 2011) in the context of LISA.

Selection among a discrete set of models

First we consider a discrete set of models. As argued above, in the general picture of massive black hole cosmic evolution, the population is shaped by the *seeding process* and the *accretion history*. The four models we study here are the SE, SC, LE, and LC models introduced in the previous section (Arun et al., 2009). As a first step, we test here if eLISA observations will provide enough information to enable us to discriminate between those models, assuming that the Universe is well described by one of them.

Each model predicts a *theoretical* distribution of coalescing massive black hole binaries. A given dataset D of observed events can be compared to a given model A by computing the likelihood $p(D|A)$ that the observed dataset D is a realisation of model A. When testing a dataset D against a pair of models A and B, we assign probability $p_A = p(D|A)/(p(D|A) + p(D|B))$ to model A, and probability $p_B = 1 - p_A$ to model B. The probabilities p_A and p_B are a measure of the relative confidence we have in model A and B, given an observation D. Once eLISA data is available, each model comparison will

Table 1: Summary of all possible comparisons of the pure models. Results are for one year of observation with eLISA. We take a fixed confidence level of $p = 0.95$. The numbers in the upper-right half of each table show the fraction of realisations in which the *row* model will be chosen at more than this confidence level when the *row* model is true. The numbers in the lower-left half of each table show the fraction of realisations in which the *row* model *cannot be ruled out* at that confidence level when the *column* model is true. In the left table we consider the trivariate M, q, and z distribution of observed events; in the right table we also include the observed distribution of remnant spins, S_r.

	Without spins					With spins			
	SE	SC	LE	LC		SE	SC	LE	LC
(l) SE	×	0.48	0.99	0.99	SE	×	0.96	0.99	0.99
SC	0.53	×	1.00	1.00	SC	0.13	×	1.00	1.00
LE	0.01	0.01	×	0.79	LE	0.01	0.01	×	0.97
LC	0.02	0.02	0.22	×	LC	0.02	0.02	0.06	×

yield this single number, p_A, which is our confidence that model A is correct. Since the eLISA data set is not currently available, we can only work out how likely it is that we will achieve a certain confidence with future eLISA observations.

We therefore generate 1000 independent realisations of the population of coalescing massive black hole binaries in the Universe predicted by each of the four models. We then simulate gravitational wave observations by producing datasets D of observed events (including measurement errors), which we statistically compare to the theoretical models. We consider only sources that are observed with SNR larger than eight in the detector. We set a confidence threshold of 0.95, and we count what fraction of the 1000 realisations of model A yield a confidence $p_A > 0.95$ when compared to an alternative model B. We repeat this procedure for every pair of models. For simplicity, in modelling gravitational wave observations, we focus on circular, non-spinning binaries; therefore, each coalescing black hole binary in the population is characterised by only three intrinsic parameters – redshift z, mass M, and mass ratio q – and we compare the *theoretical* trivariate distribution in these parameters predicted by the models to the observed values in the dataset D. In terms of gravitational waveform modelling, our analysis can therefore be considered extremely conservative.

Results are shown in the left-hand panel of table 1, for a one year observation. The vast majority of the pair comparisons yield a 95 % confidence in the true model for almost all the realisations — we can perfectly discriminate among different models. Similarly, we can always rule out the alternative (false) model at a 95 % confidence level. Noticeable exceptions are the comparisons of models LE to LC and SE to SC, i.e., among models differing by accretion mode only. This is because the accretion mode (efficient versus chaotic) particularly affects the spin distribution of the coalescing systems, which was not considered here. To extend this work, we added to our analysis the distribution of the merger remnant spins S_r, and compared the *theoretical* distribution predicted by the models to the observed values (including determination errors once again). The spin of the remnant can be reasonably determined in about 30 % of the cases only; nevertheless, by adding this information, we are able to almost perfectly discriminate between the LE and LC and the SE and SC models, as shown in the right hand panel of table 1.

Constrains on parametric models

In the preceding section we demonstrated the potential of eLISA to discriminate among a discrete set of "pure" models given a priori. However, the true massive black hole population in the Universe will probably result from a mixing of known physical processes, or even from a completely unexplored physical mechanism. A meaningful way to study this problem is to construct parametric models that depend on a set of key physical parameters, λ_i, describing, for instance, the seed mass function and redshift distribution, the accretion efficiency etc. and to investigate the potential of eLISA to constrain these parameters. Such a parametric family of models is not available at the moment, but we can carry out a similar exercise by mixing two of our pure models, A and B, to produce a model in which the number of events of a particular type is given by $\mathcal{F}$[A]+$(1-\mathcal{F})$[B], where [A] is the number of events of that type predicted by model A, [B] is the corresponding number predicted by model B and $\mathcal{F}$ is the "mixing fraction". In this case we generate datasets D from a mixed model with a certain unknown $\mathcal{F}$, and we estimate the $\mathcal{F}$ parameter by computing the likelihood that the data D is drawn from a mixed distribution, as a function of $\mathcal{F}$. A specific example is shown in figure 20. Here the underlying model is $\mathcal{F}$[SE]+$(1-\mathcal{F})$[LE], with $\mathcal{F} = 0.45$. eLISA observations will allow us to pin-down the correct value of the mixing parameter with an uncertainty of ~ 0.1. More complex examples of multi-model mixing can be found in (Sesana et al., 2011). Although highly idealised, this exercise demonstrate the potential of eLISA observations to constrain the physics and astrophysics of massive black hole along their entire cosmic history, in a mass and redshift range inaccessible

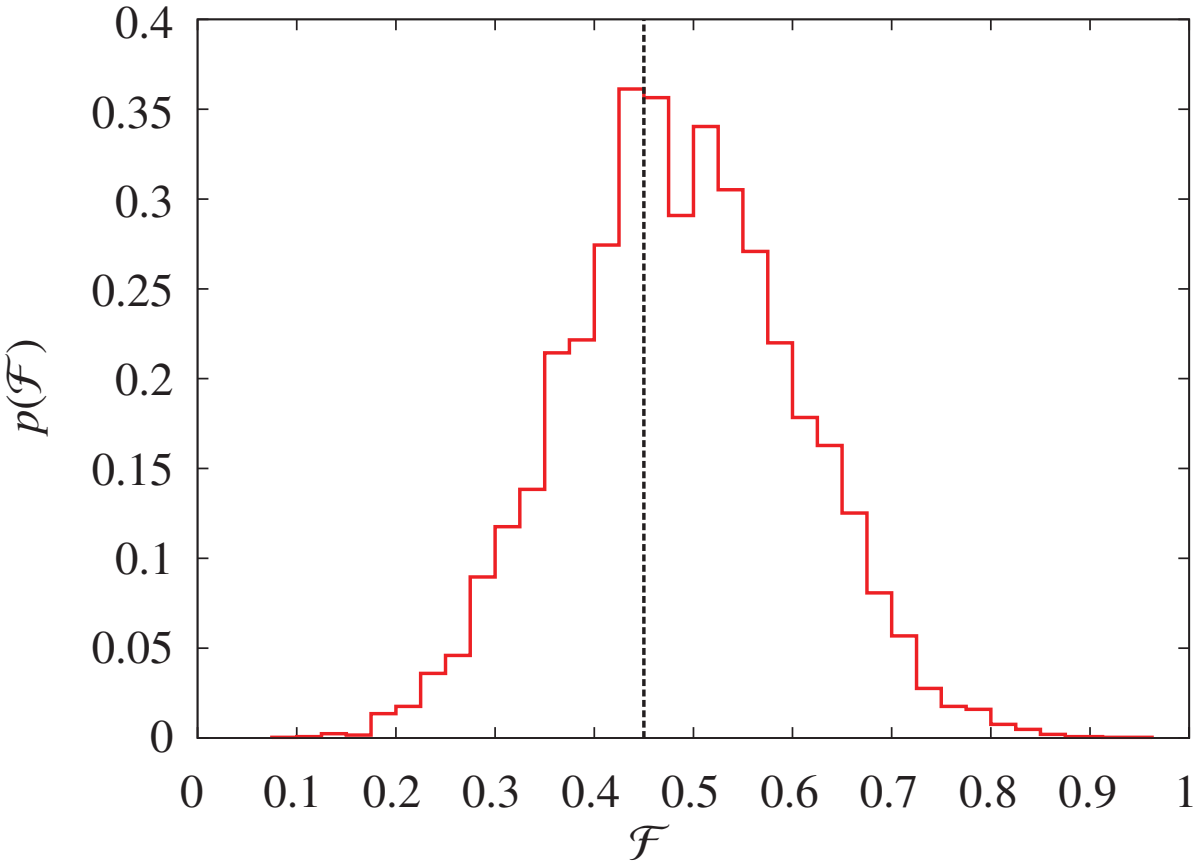

Figure 20: Likelihood distribution of the mixing fraction $\mathcal{F}$, for a particular realisation of the model $\mathcal{F}[SE]+(1-\mathcal{F})[LE]$. The true mixing parameter, marked by a dashed vertical line, was $\mathcal{F} = 0.45$.

to conventional electromagnetic observations.

5 Extreme mass ratio inspirals and astrophysics of dense stellar systems

1 The Galactic Centre: a unique laboratory

The discovery, in the local Universe, of dark, massive objects lurking at the centres of nearly all bright galaxies is one of the key findings of modern-day astronomy, the most spectacular being the case of the dark object in our own Galaxy (Eisenhauer et al., 2005, Ghez et al., 2003, 2005, 2008, Gillessen et al., 2009, Schödel et al., 2003). The nucleus of the Milky Way is one hundred times closer to Earth than the nearest large external galaxy Andromeda, and one hundred thousand times closer than the nearest QSO. Due to its proximity, it is the only nucleus in the Universe that can be studied and imaged in great detail. The central few parsecs of the Milky Way house gas cloud complexes in both neutral and hot phases, a dense luminous star cluster, and a faint radio source SgrA* of extreme compactness (3 – 10 light minutes across). Observations, using diffraction-limited imaging and spectroscopy in the near-infrared, have been able to probe the densest region of the star cluster and measure the stellar dynamics of more than two hundred stars within a few light days of the dynamic centre. The latter is coincident, to within 0.1 arcsec, with the compact radio source SgrA*. The stellar velocities increase toward SgrA* with a Kepler law, implying the presence of a $(4 \pm 0.06 \pm 0.35) \times 10^6$ M$_\odot$ central dark mass (Gillessen et al., 2009). This technique has also led to the discovery of nearly thirty young stars that orbit the innermost region: the so called S0 (or S) stars. These young stars are seen to move on Keplerian orbits, with S02 (or S2) the showcase star orbiting the putative black hole on a highly eccentric (0.88) orbit with a period of 15.9 years. The periapsis of this orbit requires a lower limit on the density of the dark point-like mass concentration of more than 10^{13} M$_\odot$ pc^{-3} (Maoz, 1998). Additionally, a lower limit of more than 10^{18} M$_\odot$ pc^{-3} can be inferred from the compactness of the radio source (Genzel et al., 2010). These limits provide compelling evidence that the dark point-mass at SgrA* is a black hole. A cluster of dark stars of this mass and density (e.g. composed of neutron stars, stellar black holes or sub-stellar entities such as brown dwarfs, planets and rocks) can not remain in stable equilibrium for longer than 10^7 years (Genzel et al., 2000, 2006, Maoz, 1998), and the only remaining, albeit improbable, hypothesis is a concentration of heavy bosons (a boson star, (Colpi et al., 1986)) or of hyperlight black holes (Maoz, 1998, $M_\bullet < 0.005\,\mathrm{M}_\odot$,). Overall, the measurements at the Galactic Centre are consistent with a system composed of a massive black hole and an extended close-to-isotropic star cluster, with the young S0 (or S) stars the only population showing a collective rotation pattern in their orbits (Genzel et al., 2010).

2 Extreme Mass Ratio Inspirals in galactic nuclei

Can we probe the nearest environs of a massive black hole other than the Galactic Centre? Massive black holes are surrounded by a variety of stellar populations, and among them are compact stars (stellar black holes, neutron stars and white dwarfs). White dwarfs, neutron stars, and stellar-mass black holes all share the property that they reach the last stable orbit around the central massive black hole before they are tidally disrupted. A compact star can either plunge directly toward the event horizon of the massive black hole, or gradually spiral in and fall into the hole, emitting gravitational waves. The latter process is the one of primary interest for eLISA. Gravitational waves produced by inspirals of stellar-mass compact objects into massive black holes are observable by eLISA. The mass of the compact object is typically of the order of a few solar masses, while the mass of the central black holes detectable by eLISA is from 10^4 M$_\odot$ to 10^7 M$_\odot$. Because the mass ratio for these binaries is typically around 10^5, these sources are commonly referred to as EMRI.

The extreme mass ratio ensures that the inspiralling object essentially acts as a test particle in the background space-time of the central massive black hole. EMRI detections thus provide the best means to probe the environment of an astrophysical black hole and its stellar surroundings. White dwarfs, neutron stars, and stellar-mass black holes can all in principle lead to observable EMRI signals. However, stellar-mass black holes, being more massive, are expected to dominate the observed rate for eLISA, for two reasons: mass segregation tends to concentrate the heavier compact stars nearer the massive black hole, and black hole inspirals have higher signal-to-noise, and so can be seen within a much larger volume.

Three different mechanisms for the production of EMRI have been explored in the literature. The oldest and best-understood mechanism is the diffusion of stars in angular-momentum space, due to two-body scattering. Compact stars in the inner 0.01 pc will sometimes diffuse onto very high eccentricity orbits, such that gravitational radiation will then shrink the orbit's semi-major axis and eventually drive the compact star into the massive black hole. Important physical

effects setting the overall rate for this mechanism are mass segregation, which concentrates the more massive stellar-mass black holes ($\simeq 10\,M_\odot$) close to the central black hole, and resonant relaxation, which increases the rate of orbit diffusion in phase-space (Hopman and Alexander, 2006b): the orbits of stars close to a massive black hole are nearly Keplerian ellipses, and these orbits exert long term torques on each other, which can modify the angular momentum distribution of the stars and enhance the rate of EMRI formation (Gürkan and Hopman, 2007). However, subtle relativistic effects can reduce the estimated rates from relaxation processes (Merritt et al., 2011). In addition to the two-body scattering mechanism, other proposed channels for EMRI are tidal disruption of binaries that pass close to the central black hole (Miller et al., 2005), and creation of massive stars (and their rapid evolution into black holes) in the accretion discs surrounding the central massive black hole (Levin, 2007). Tidal break up of incoming stellar binaries may already have been seen in the Milky Way following the remarkable discovery of a number of so-called hypervelocity stars observed escaping from our Galaxy (e.g., Brown et al., 2009). They are believed to be the outcome of an ejection following the break-up of two bound stars by the tidal field of SgrA*. All these mechanisms give specific predictions on the eccentricity and inclination of EMRI events that can be extracted from the gravitational wave signal (Miller et al., 2005).

When the orbiting object is close enough (within a few horizon radii from the large black hole) gravitational radiation dominates energy losses from the system, and the semimajor axis of the orbit shrinks. Radiation is emitted over hundreds of thousand of orbits as the object inspirals to the point where it is swallowed by the central massive black hole. Over short periods of time, the emitted radiation can be thought of as a snapshot that contains detailed information about the physical parameters of the binary. The detection of the emitted gravitational wave signal will give us very detailed information about the orbit, the mass, and spin of the massive black hole as well as the mass of the test object (Gair et al., 2010, Hopman, 2009, Preto and Amaro-Seoane, 2010).

The measurement of even *a few* EMRI will give astrophysicists a totally new and different way of probing dense stellar systems determining the mechanisms that shape stellar dynamics in the galactic nuclei and will allow us to recover information on the emitting system with a precision which is not only unprecedented in the history of astrophysics, but beyond that of any other technique (Amaro-Seoane et al., 2007, Babak et al., 2010, Porter, 2009).

3 A probe of galactic dynamics

The centre-most part of the stellar spheroid, i.e. the *galactic nucleus*, constitutes an extreme environment in terms of stellar dynamics. With stellar densities higher than $10^6\,M_\odot\,pc^{-3}$ and relative velocities exceeding 100 km/s, collisional processes (i.e. collective gravitational encounters among stars) are important in shaping the density profiles of stars. The mutual influence between the massive black hole and the stellar system occurs thanks to various mechanisms. Some are global, like the capture of stars via collisional relaxation, or accretion of gas lost by stars through stellar evolution, or adiabatic adaptation of stellar orbits to the increasing mass of the black hole. Others involve a very close interaction, like the tidal disruption of a star or the formation of an EMRI.

The distribution of stars around a massive black hole is a classical problem in stellar dynamics (Bahcall and Wolf, 1976, 1977), and of importance for EMRI is the distribution of stellar black holes. Objects more massive than the average star, such as stellar black holes, tend to segregate at the centre of the stellar distribution in the attempt to reach, through long-distance gravitational encounters, equipartition of kinetic energy. A dense, strongly mass-segregated cusp of stellar black hole is expected to form near a massive black hole, and such a cusp plays a critical role in the generation of EMRI. The problem of the presence of a dark cusp has been addressed, for the Galactic Centre, by different authors, from a semi-analytical and numerical standpoint (Freitag et al., 2006a,b, Hopman and Alexander, 2006a, Miralda-Escudé and Gould, 2000, Sigurdsson and Rees, 1997). A population of stellar black holes can leave an imprint on the dynamics of the S0 (or S) stars at the Galactic Centre, inducing a Newtonian retrograde precession on their orbits (Mouawad et al., 2005). Current data are not sufficient to provide evidence of such deviations from Keplerian orbits, so that the existence of a population of stellar black holes is yet to be confirmed (Gillessen et al., 2009, Merritt et al., 2009a).

4 A probe of the masses of stellar and massive black holes

It is very difficult to measure the mass of black holes, both of the massive and stellar variety. In the case of massive black holes, methods based on following the innermost kinematics are difficult for low-mass black holes in the range $10^5\,M_\odot - 10^7\,M_\odot$. These black holes have low intrinsic luminosities even when they are active, making detection hard. Performing dynamical measurements at these masses through stellar kinematics requires extremely high spatial resolution. Nowadays with adaptive optics we could optimistically hope to get a handful of measurements through stellar kinematics

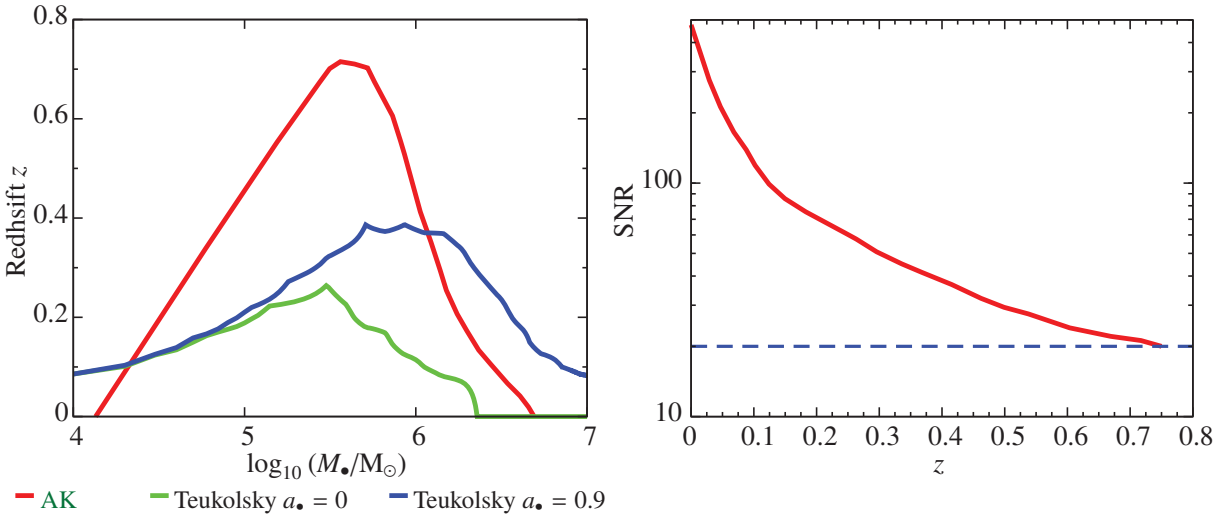

Figure 21: *Left*: The maximum detectable redshift z (or horizon) for EMRIs assuming a two year mission lifetime, and a SNR = 20. The red curve is computed using the analytic waveform model and has a maximum redshift of $z \sim 0.7$ for black hole masses at the source rest-frame of $4 \times 10^5\,\mathrm{M}_\odot$. The green and blue curves are sky-averaged horizons, computed using the Teukolsky waveform model, for two different values of the spin of the central black holes, $a_\bullet = 0$ (green) and $a_\bullet = 0.9$ (blue).
Right: The distribution of maximum EMRI SNRs versus redshift for eLISA. The dashed horizontal line denotes the SNR threshold of 20.

about 5 kpc away, although future 20 m – 30 m telescopes can reach out to the Virgo cluster (16.5 Mpc). Exquisite gas-dynamical measurements are possible for only a handful of active black holes using water megamaser spots in a Keplerian circumnuclear disk (Kuo et al., 2011). Still, the black hole in the centre of our own galaxy lies in this range, and placing constraints on the mass function of low-mass black holes has key astrophysical implications. Observations show that the masses of black holes correlate with the mass, luminosity and the stellar velocity dispersion of the host (Gültekin et al., 2009). These correlations imply that black holes evolve along with their hosts throughout cosmic time. One unanswered question is whether this symbiosis extends down to the lowest galaxy and black hole masses due to changes in the accretion properties (Mathur and Grupe, 2005), dynamical effects (Volonteri et al., 2007), or cosmic bias (Volonteri and Natarajan, 2009). eLISA will discover the population of massive black holes in galaxies smaller than the Milky Way, that are difficult to access using other observational techniques, and provide insights on the co-evolution of black holes and their hosts.

Difficulties, albeit of a different nature, exist in measuring the masses and mass distribution of stellar black holes. Stellar black holes are observed as accreting X-ray sources in binaries. According to stellar evolution, black holes result from the core collapse of very massive stars, and their mass is predicted to be in excess of the maximum mass of a neutron star, which is still not fully constrained. Depending on the state of nuclear matter, this limit varies from about $1.6\,\mathrm{M}_\odot$ to about $3\,\mathrm{M}_\odot$ (Shapiro and Teukolsky, 1986). The maximum mass of a stellar black hole is not constrained theoretically, and is known to depend sensitively on the metallicity of the progenitor star. The masses of stellar black holes are inferred using Kepler's third law, or through spectral analysis of the emission from the hole's accretion disc. These techniques can be used only for black holes in a binary system. Current measurements of the black hole mass indicate a range for stellar black holes from about $5\,\mathrm{M}_\odot$ up to $20\,\mathrm{M}_\odot$, but uncertainties in the estimate can be as large as a factor of two (Orosz, 2003). In addition, stellar black holes in interacting binaries are a very small and probably strongly biased fraction of the total stellar black hole population. They are formed from stars that have lost their hydrogen mantle due to mass transfer (and thus formed in a different way than the vast majority of stellar black holes. eLISA will measure the mass of the stellar black holes again with unprecedented precision providing invaluable insight on the process of star formation in the dense nuclei of galaxies, where conditions appear extreme.

5 Detecting extreme mass ratio inspirals with eLISA

EMRI are compact stars moving on relativistic orbits around a massive black hole. As the compact object spends most of its time in the strong field regime, its orbit is very complex and difficult to model. While not fully realistic, a set of

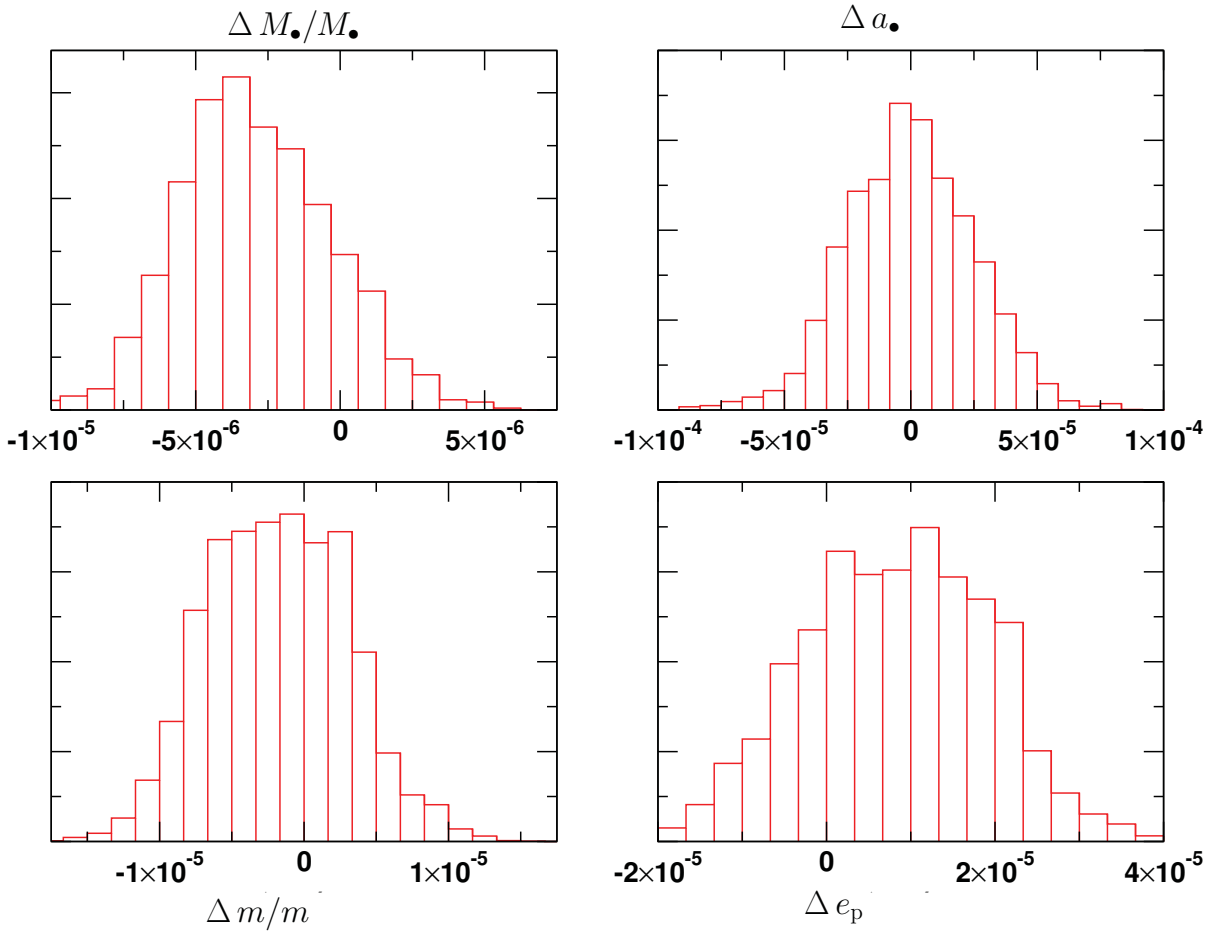

Figure 22: The distribution of errors from a Markov Chain Monte Carlo analysis for a source at $z = 0.55$ with an SNR of 25. The plot shows the error distributions for the central black holes mass $M_\bullet$ and spin $a_\bullet$, the mass of the compact object m and the eccentricity at plunge e_p.

phenomenological waveforms have been developed (Barack and Cutler, 2004), the AK waveforms, which fully capture the complexity of the model. These waveforms are defined by a 14 dimensional parameter set, of which the most physically relevant are the masses of the central black hole and of the compact object, $M_\bullet$ and m respectively, the spin of the massive black hole $a_\bullet$, the eccentricity of the orbit at plunge, e_p, the sky position of the source with respect to the detector, and the luminosity distance to the source, D_L. In addition to these approximate models, more accurate EMRI waveform models have been computed using black hole perturbation theory, in which the inspiraling object is regarded as a small perturbation to the background spacetime of the large black hole. The perturbation theory framework was first outlined in (Teukolsky, 1973) and gave rise to the Teukolsky equation. However, the solution of this equation is computationally expensive, and results have only recently been obtained for a selection of generic orbits (Drasco and Hughes, 2006). Nonetheless, results have been fully tabulated for certain restricted types of orbit. For the calculations described here we will use data for circular-equatorial orbits (Finn and Thorne, 2000, Gair, 2009a). We can use both models to compute the maximum detectable redshift, or the horizon for EMRI detection, as a function of mass.

To calculate the detection limit of EMRI for eLISA using the AK waveforms, we must perform a Monte Carlo simulation over the waveform parameters. We explore the mass range $10^4\,\mathrm{M}_\odot \lesssim M \lesssim 5\times10^6\,\mathrm{M}_\odot$. As not much is known about the distribution of spins or eccentricities for EMRI, we consider uniform distributions for the spins in the range $-0.95 \le a \le 0.95$, and for eccentricities at plunge in the interval $0.05 \le e_p \le 0.4$. We fix the mass of the inspiraling body to $10\,\mathrm{M}_\odot$ to represent the inspiral of a stellar black hole, as these are expected to dominate the event rate (Gair et al., 2004). The detection horizon for neutron star and white dwarf inspirals is significantly less than for black holes. The final assumption required is to set a threshold of detection. While a SNR threshold of 30 was thought to be justified in the past, advances in search algorithms have recently demonstrated that EMRI with SNR about 20 is sufficient for detection (Babak et al., 2010, Cornish, 2011, Gair et al., 2008), allowing us to assume an SNR threshold of 20 in this analysis. Assuming a mission lifetime T of two years, and plunge times between $0\,\mathrm{yr} \le t_p \le 5\,\mathrm{yr}$, a large scale Monte Carlo simulation was run over all 14 parameters. In figure 21 (left) we plot the maximum detectable redshift z (also referred to as horizon) as a function of intrinsic mass of the massive black hole. Systems with intrinsic mass in the range from $10^4\,\mathrm{M}_\odot \le M \le 5\times10^6\,\mathrm{M}_\odot$ are detectable in the local Universe at redshift of $z \lesssim 0.1$, while systems in the range from $10^5\,\mathrm{M}_\odot \le M \le 10^6\,\mathrm{M}_\odot$ should be detectable by eLISA to $z \sim 0.7$, corresponding to a co-moving volume of about $70\,\mathrm{Gpc}^3$.

Figure 21 (left) also shows the maximum detectable redshift z as a function of the mass of the central massive black hole, computed for circular-equatorial inspirals using the Teukolsky equation for the same masses of the inspiralling compact object and massive black holes. This curve shows the sky-averaged horizon, i.e., the maximum redshift at which the SNR averaged over inclinations and orientations of the EMRI system reaches the threshold value of 20. Tabulated Teukolsky results are only available for selected values of the spin of the central black hole, so we show the horizon assuming all the central black holes have either spin $a_\bullet = 0$ or $a_\bullet = 0.9$. The Teukolsky horizon appears significantly lower than the AK horizon, but this is a result of the sky-averaging approximation – the sky averaged SNR is expected to be a factor of about 2.5 lower than the SNR of an "optimally oriented" binary. The AK horizon was computed using a Monte Carlo simulation over orientations and sky locations for the source and will therefore approach the value for an optimally-oriented binary. The difference between the sky-averaged Teukolsky horizon and the AK horizon is therefore consistent with the expected level of difference. The maximum horizon for the Teukolsky curves is at a similar value for the mass of the central black hole as the AK results – somewhat lower for $a_\bullet = 0$ and higher for $a_\bullet = 0.9$, as we would expect since inspirals into more rapidly spinning black holes emit radiation at higher frequencies, which shifts the peak sensitivity to higher masses. For the same reason, we see that the eLISA horizon is at a higher redshift for more rapidly spinning central black holes.

In figure 21 (right) we plot the distribution of maximum SNR as a function of redshift for the Monte Carlo simulation performed using the AK waveforms. A nearby EMRI will be detectable with SNR of many tens, with SNRs of 30 being available out to $z = 0.5$. EMRI can be detected with an SNR of 20 up to $z \simeq 0.7$, up to a volume of about $70\,\mathrm{Gpc}^3$, encompassing the last 6 billion years of the Universe.

EMRIs are the most complex sources to model and to search for. However, if they can be detected, this complexity will allow us to estimate the parameters of the system with great accuracy (Babak et al., 2010, Cornish, 2011, Gair et al., 2008). For an EMRI detected with a certain SNR, the parameter estimation accuracy does not strongly depend on the detector configuration, since any detected EMRI will be observed for many waveform cycles. For this reason the parameter estimation accuracy achievable with eLISA is essentially the same as reported in the published LISA literature (Barack and Cutler, 2004, Huerta and Gair, 2009). For any EMRI observed with SNR above the detection threshold of 20, we expect to measure the mass $M_\bullet$ and spin $a_\bullet$ of the central massive black hole with a precision to better than a part in 10^4. This is illustrated in Figure 22, that shows the results from a Markov Chain Monte Carlo analysis (Cornish and Porter, 2006) of a source at $z = 0.55$ with SNR = 25. The plots show the distribution of errors for a particular source that would be recovered by analysing the data from the detector. Results are shown for the mass $M_\bullet/\mathrm{M}_\odot$ and spin $a_\bullet$ of central

Table 2: Estimated number of EMRI events detectable by eLISA. The first three columns shows the results computed using the Teukolsky waveform model, assuming all black holes have fixed spin of 0, 0.5 or 0.9. The last column shows results computed using the analytic kludge waveform model.

Waveform model	Teukolsky with black hole spin			Analytic Kludge
	$a_\bullet = 0$	$a_\bullet = 0.5$	$a_\bullet = 0.9$	
Number of events	30	35	55	50

black hole, the mass $m/M_\bullet$ of the stellar black hole, and the eccentricity at plunge e_p. Our analysis also shows that the luminosity distance D_L to the source is determined with an accuracy of less than 1 % and the source sky location can be determined to around 0.2 square degrees. While the SNR is quite low for this source, the accuracy in the estimation of parameters is very good.

6 Estimating the event rates of extreme mass ratio inspirals for eLISA

We can use the horizon distances described in the preceding section to compute the likely number of EMRI events that eLISA will detect, if we make further assumptions about the EMRI occurring in the Universe. This depends on the black hole population and on the rate at which EMRI occur around massive black holes with particular properties. The latter is poorly known, and we will use results from Hopman (2009) and Amaro-Seoane and Preto (2011) for the rate of inspirals involving black holes. The rate $\Gamma_\bullet$ is found to scale with the central black hole mass, $M_\bullet$, as $\Gamma_\bullet \sim 400\,\mathrm{Gyr}^{-1}\left(M_\bullet/3\times10^6\,\mathrm{M}_\odot\right)^{-0.19}$. We do not consider neutron star and white dwarf inspirals in these rate estimates as the expected number of detections with eLISA is less than one in both cases, due to the considerably reduced horizon distance for these events. We therefore fix the mass of the inspiraling body at $10\,\mathrm{M}_\odot$, as in the previous section.

To model the black hole population, we take the mass function of black holes to be in the intrinsic mass range $10^4\,\mathrm{M}_\odot \lesssim M_\bullet \lesssim 5\times10^6\,\mathrm{M}_\odot$. Using the assumption that there is no evolution in the black hole mass function, we sampled sources from a uniform distribution in co-moving volume. These assumptions are consistent with the mass function derived from the observed galaxy luminosity function using the $M_\bullet - \sigma$ relation, and excluding Sc-Sd galaxies (Aller and Richstone, 2002, Gair, 2009a, Gair et al., 2004). For the results using the AK waveform model, we choose the spin of the central object uniformly in the range $0 \le a \le 0.95$, the eccentricity of the orbit at plunge uniformly in the range $0.05 \le e_p \le 0.4$ and all angles to be uniform or uniform in cosine as appropriate. For the Teukolsky based results we do not need to specify the angles, as we use a sky and orientation averaged sensitivity, and we do not specify the eccentricity or inclination as the orbits are all circular and equatorial (although we assume equal numbers of prograde and retrograde inspirals). As before, the Teukolsky results are available for fixed values of the spin only, so we estimate the event rate assuming that all the black holes have spin 0, 0.5 or 0.9.

It is important also to correctly randomise over the plunge time of the EMRI. For the AK calculation, we choose the plunge time uniformly in $0\,\mathrm{yr} \le t_p \le 5\,\mathrm{yr}$, with time measured relative to the start of the eLISA observation and assuming an eLISA lifetime of 2 years. Although sufficiently nearby events with plunge times greater than 5 years in principle could be detected, it was found that such events contribute less than one event to the total event rate. For the Teukolsky calculation, we evaluated the observable lifetime for every event, which is the amount of time during the inspiral that eLISA could start to observe that will allow sufficient SNR to be accumulated over the mission lifetime to allow a detection (Gair, 2009a).

In table 2 we give the results of this calculation for different waveform models and black hole spins. The predicted number of events depends on the assumptions about the waveform model and the spin of the black holes, but it is in the range of 25 – 50 events in two years. The number of events predicted for the AK model is higher because the presence of eccentricity in the system tends to increase the amount of energy radiated in the eLISA band. The analytic kludge estimates include randomisation over the black hole spin, orbital eccentricity and inclination, so the true detection rate is likely to be closer to this number, although this depends on the unknown astrophysical distribution of EMRI parameters. Even with as few as 10 events, Gair et al. (2010) show that the slope of the mass function of massive black holes in the mass range $10^4\,\mathrm{M}_\odot$ – $10^6\,\mathrm{M}_\odot$ can be determined to a precision of about 0.3, which is the current level of observational uncertainty.

7 Black hole coalescence events in star clusters

In closing this section on astrophysical black holes, we explore briefly the possibility that an instrument like eLISA will detect coalescences between low-mass massive black holes (called also intermediate-mass black holes) in the mass range $10^2\,M_\odot - 10^4\,M_\odot$. These coalescence events do *not* result from the assembly of dark matter halos, but rather they are *local* coalescence events occurring in star clusters under extreme (and largely unexplored) astrophysical conditions. Given the tiny radius of gravitational influence (about 0.01 pc) of such light black holes on the surrounding dense stellar environment, their detection is extremely difficult, and their existence has never been confirmed, though evidence has been claimed in a number of globular clusters (see Miller, 2009, Miller and Colbert, 2004, and references therein).

An intermediate-mass black hole may form in a young cluster if the most massive stars sink to the cluster's centre due to mass segregation before they evolve and explode. There, they start to physically collide. The most massive star gains more and more mass and forms a runaway star that may collapse to form an intermediate-mass black hole (Freitag et al., 2006a,c, Gürkan et al., 2004, Portegies Zwart et al., 2004, Portegies Zwart and McMillan, 2000). Intermediate-mass black holes can be observed by eLISA via the inspiral of compact objects such as stellar mass black holes (Konstantinidis et al., 2011), or when they form a binary. The formation of an intermediate-mass black hole binary can occur via star-cluster star-cluster collisions like those found in the Antennæ galaxy (Amaro-Seoane et al., 2010a, Amaro-Seoane and Freitag, 2006a), or via formation in situ (Gürkan et al., 2006).

eLISA will observe intermediate-mass black hole binaries with SNR > 10 out to a few Gpc (Santamaría et al., 2010), and it will detect stellar-mass black holes plunging into an intermediate-mass black hole in a massive star cluster in the local Universe (Konstantinidis et al., 2011). Event rates are hard to predict due to large uncertainties in the dynamical formation of intermediate mass black holes in star clusters, but we may observe as many as a few events per year (Amaro-Seoane and Freitag, 2006a). The detection of even a single event would have great importance for astrophysics, probing the existence of black holes in this unexplored mass range and shedding light on the complex dynamics of dense stellar clusters.

6 Confronting General Relativity with Precision Measurements of Strong Gravity

1 Setting the stage

GR is a theory of gravity in which gravitational fields are manifested as curvature of spacetime. GR has no adjustable parameters other than Newton's gravitational constant, and it makes solid, specific predictions. Any test can therefore potentially be fatal to its viability, and any failure of GR can point the way to new physics. Confronting GR with experimental measurements, particularly in the strong gravitational field regime, is therefore an essential enterprise. In fact, despite its great successes, we know that GR cannot be the final word on gravity, since it is a classical theory that necessarily breaks down at the Planck scale. As yet there is no complete, quantum theory of gravity, and gravitation is not unified with the other fundamental forces. Under such a premise, several stress tests of GR have been proposed, each of them potentially fatal to the theory, however all of them involve low energies and length-scales much larger than the Planck scale.

Although so far GR has passed all the tests to which it has been subjected (Will, 2006), most of these tests were set in the weak-field regime, in which the parameter $\epsilon = v^2/c^2 \sim GM/(Rc^2)$ is much smaller than one. Here v is the typical velocity of the orbiting bodies, M their total mass, and R their typical separation.

For the tests of GR that have been carried out in our Solar System, expected second-order GR corrections to the Newtonian dynamics are of the order $\epsilon \sim 10^{-6} - 10^{-8}$, and so to date it has been sufficient to expand GR equations to the first Post-Newtonian (PN) order. Solar System tests are completely consistent with GR to this order of approximation.

Binary pulsars, which are essentially very stable and accurate clocks with typical orbital velocities $v/c \sim 10^{-3}$ ($\epsilon \sim 10^{-6}$), are excellent laboratories for precision tests of GR (Lorimer, 2008). Current observations of several binary pulsars are perfectly consistent with the GR predictions, with orbits again calculated to the first PN order. Observations of the first binary pulsar to be discovered, PSR 1913+16, also provided the first astrophysical evidence for gravitational radiation, a 2.5-PN-order effect. Loss of energy due to gravitational-wave emission (radiation reaction) causes the binary orbit to shrink slowly; its measured period derivative $\dot{P}$ agrees with GR predictions to within 0.2 %, consistent with measurement

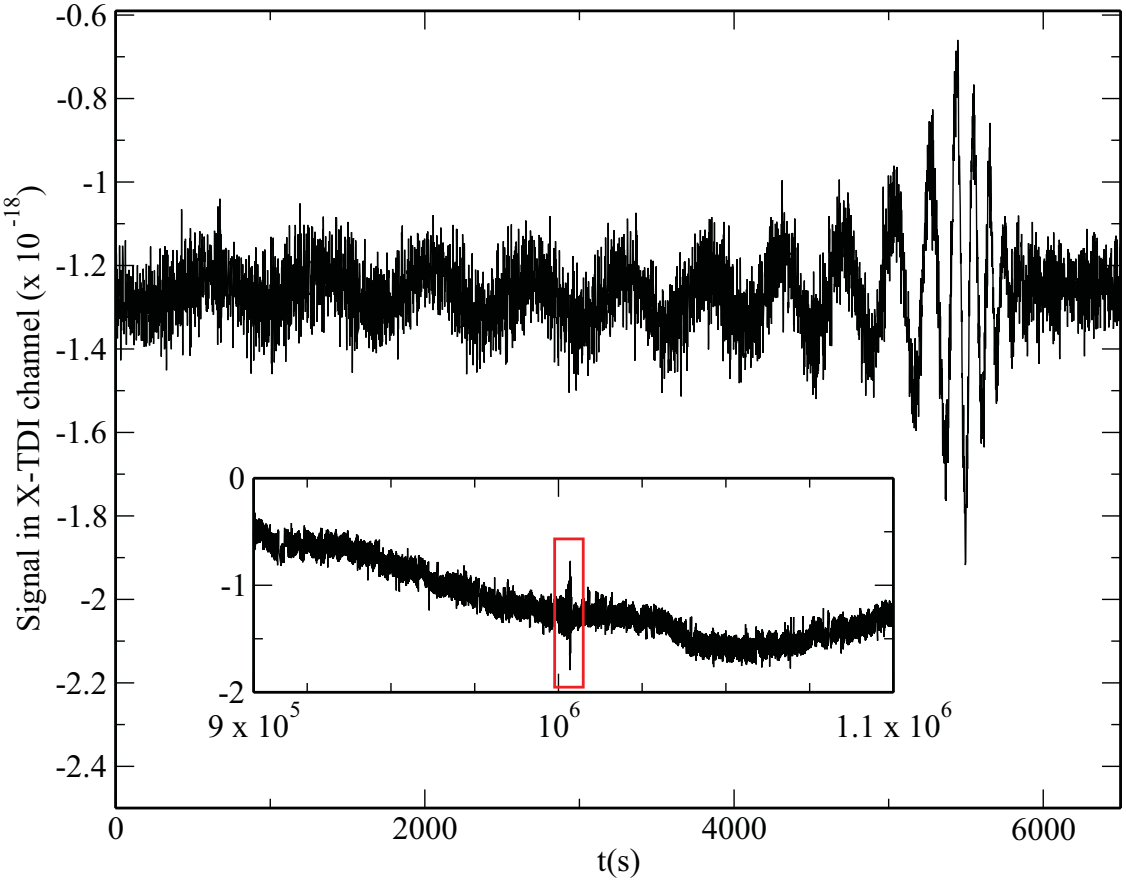

Figure 23: Gravitational wave signal for the final few orbits, plunge, merger and ringdown of a coalescing binary. The total mass of system $M(1+z) = 2 \times 10^6\,\mathrm{M}_\odot$, mass ratio $m_1/m_2 = 2$, spin magnitudes $a_1 = 0.6$ $a_2 = 0.55$, misalignment between spins and orbital angular momentum few degrees, the distance to the source $z = 5$. The inset shows the signal on a larger data span.

error bars (Weisberg and Taylor, 2005). Another double pulsar system, SR J0737-3039 A and B, allows additional tests of GR that were not available prior to its discovery (Kramer et al., 2006). In that system, the orbital period derivative is consistent with GR at the 0.3 % level, and the Shapiro delay agrees to within 0.05 % with the predictions of GR (Kramer and Wex, 2009).

However, the gravitational fields responsible for the orbital motion in known binary pulsars are not much stronger than those in the Solar System: the semimajor axis of the orbit of PSR 1913+16 is about $1.4\,\mathrm{R}_\odot$. Such weak fields limit the ability of binary pulsars to probe nonlinear GR *dynamics*. They do provide important tests of strong-field *static* gravity, as the redshift at the surface of a neutron star is of order 0.2.

eLISA observations of coalescing massive black hole binaries, or of stellar-mass compact objects spiralling into massive black holes, will allow us to confront GR with precision measurements of physical regimes and phenomena that are not accessible through Solar System or binary pulsar measurements. The merger of comparable-mass black hole binaries produces an enormously powerful burst of gravitational radiation, which eLISA will be able to measure with amplitude SNR as high as a few hundred, even at cosmological distances.

In the months prior to merger, eLISA will detect the gravitational waves emitted during the binary inspiral; from that inspiral waveform, the masses and spins of the two black holes can be determined to high accuracy. Given these physical parameters, numerical relativity will predict very accurately the shape of the merger waveform, and this can be compared directly with observations, providing an ideal test of pure GR in a highly dynamical, strong-field regime.

Stellar-mass compact objects spiralling into massive black holes will provide a qualitatively different test, but an equally exquisite one. The compact object travels on a near-geodesic of the spacetime of the massive black hole. As it spirals in, its emitted radiation effectively maps out the spacetime surrounding the massive black hole. Because the inspiralling body is so small compared to the central black hole, the inspiral time is long and eLISA will typically be able to observe of order 10^5 cycles of inspiral waveform, all of which are emitted as the compact object spirals from 10 horizon radii down to a few horizon radii. Encoded in these waves is an extremely high precision map of the spacetime metric just outside the central black hole. Better opportunities than these for confronting GR with actual strong-field observations could hardly be hoped for.

The LIGO and Virgo detectors should come online around 2015, and their sensitivity is large enough that they should routinely observe stellar mass black hole coalescences, where the binary components are of roughly comparable mass. However, even the brightest black hole mergers that LIGO and Virgo should observe will still have an amplitude SNR about 10 to 100 times smaller than the brightest massive black hole coalescences that eLISA will observe. The precision with which eLISA can measure the merger and ringdown waveforms will correspondingly be better by the same factor when compared to ground-based detectors. The situation is similar for the EMRI described in the previous section: while ground-based detectors may detect binaries with mass ratios of about 10^{-2} (e.g., a neutron star spiralling into a $100\,\mathrm{M}_\odot$ black hole), in observations lasting approximately $10^2 - 10^3$ cycles, the precision with which the spacetime can be mapped in such cases is at least two orders of magnitude worse than what is achievable with eLISA's EMRI sources. Thus eLISA will test our understanding of gravity in the most extreme conditions of strong and dynamical fields, and with a precision that is two orders of magnitude better than that achievable from the ground.

GR has been extraordinarily fruitful in correctly predicting new physical effects, including gravitational lensing, the gravitational redshift, black holes and gravitational waves. GR also provided the overall framework for modern cosmology, including the expansion of the Universe. However, our current understanding of the nonlinear, strong gravity regime of GR is quite limited. Exploring gravitational fields in the dynamical, strong-field regime could reveal new objects that are unexpected, but perfectly consistent with GR, or even show violations of GR.

The best opportunity for making such discoveries is with an instrument of high sensitivity. Ground-based detectors like LIGO and Virgo will almost certainly always have to detect signals by extracting them from deep in the instrumental noise, and they will therefore depend on prior predictions of waveforms. eLISA, on the other hand, will have enough sensitivity that many signals will show themselves well above noise; unexpected signals are much easier to recognize with such an instrument.

2 Testing strong-field gravity: The inspiral, merger, and ringdown of massive black hole binaries

eLISA's strongest sources are expected to be coalescing black hole binaries where the components have roughly comparable masses, $0.1 < m_2/m_1 < 1$. Their signal at coalescence will be visible by eye in the data stream, standing out well above the noise, as illustrated in figure 23.

As discussed in section 8, black hole binary coalescence can be schematically decomposed into three stages (inspiral, merger, and ringdown), all of which will be observable by eLISA for a typical source. The inspiral stage is a relatively slow, adiabatic process, well described by the analytic PN approximation. The inspiral is followed by the dynamical merger of the two black holes, that form a single, highly distorted black hole remnant. Close to merger, the black hole velocities approach $v/c \sim 1/3$ and the PN approximation breaks down, so the waveform must be computed by solving the full Einstein equations via advanced numerical techniques. The distorted remnant black hole settles down into a stationary rotating solution of Einstein's equations (a Kerr black hole) by emitting gravitational radiation. This is the so called "ringdown" phase, where the gravitational wave signal is a superposition of damped exponentials QNM, and therefore similar to the sound of a ringing bell.

While numerical relativity is required to understand the gravitational radiation emitted during merger, the post-merger evolution – i.e., the black hole "quasinormal ringing" – can be modelled using black hole perturbation theory. The final outcome of the ringdown is the Kerr geometry, with a stationary spacetime metric that is determined uniquely by its mass and spin, as required by the black hole"no-hair" theorem.

For equal-mass black hole binaries with total mass M in the range $2 \times 10^5\,\mathrm{M}_\odot < M(1+z) < 2 \times 10^6\,\mathrm{M}_\odot$, where z is the cosmological redshift of the source, the inspiral SNR and post-inspiral (merger plus ring-down) SNR are within an

order of magnitude of each other. From a typical eLISA observation of the inspiral part of the signal, it will be possible to determine the physical parameters of the binary to extremely high accuracy. Using these parameters, numerical relativity can predict very precisely the merger and ringdown waves. Measurements of the individual masses and spins will allow us to predict the mass and the spin of the remnant black hole (Rezzolla et al., 2008b), which can be directly tested against the corresponding parameters extracted from the ringdown. The merger and ringdown waveforms will typically have an SNR of 10^2 – 10^3 for binary black holes with total mass $10^5\,\mathrm{M}_\odot < M(1+z) < 6\times10^8\,\mathrm{M}_\odot$ at $z = 1$, so an extremely clean comparison will be possible between the observed waveforms and the predictions of GR.

The inspiral stage: comparing inspiral rate with predictions of General Relativity

With orbital velocities v/c typically in the range 0.05 – 0.3, most of the inspiral stage can be well described using high-order PN expansions of the Einstein equations. The inspiral waveform is a chirp: a sinusoid that increases in frequency and amplitude as the black holes spiral together. Depending on the source parameters, eLISA will be able to observe the final stages of the inspiral, for up to one year in some favourable cases. To give a practical reference, when the gravitational-wave frequency sweeps past 0.3 mHz, the time remaining until merger is approximately

$$t = 106.8\,\mathrm{days}\left(\frac{0.25}{\eta}\right)\left(\frac{M(1+z)}{2\times10^5\,\mathrm{M}_\odot}\right)^{-5/3}\left(\frac{f}{0.3\,\mathrm{mHz}}\right)^{-8/3} \tag{9}$$

where, as above, $M = m_1 + m_2$ is the total mass of the binary and $\eta = m_1 m_2/M^2$ is the symmetric mass ratio. eLISA will observe the last 10^2 – 10^4 gravitational wave inspiral cycles, depending on the total mass and distance of the source. Since the inspiral signal is quite well understood theoretically, matched filtering can be used to recognise these inspirals up to a year before the final merger, at a time when the total SNR is still small. Moreover, as the total SNR in the inspiral is quite large in many cases, and such signals are long lived, matched filtering based on the inspiral waveform alone can determine the system parameters to very high accuracy. Both masses can be determined to within a fractional error of about 10^{-2} – 10^{-1}, and the spin of the primary black hole can be measured to an accuracy of 10 % or better.

The nonlinear structure of GR (and possible deviations from GR) could be encoded in a phenomenological way by considering hypothetical modifications of the gravitational wave amplitude and phasing, as proposed by different authors (Arun et al., 2006, Yunes and Pretorius, 2009). The relatively large strength of the inspiral gravitational wave signal will allow a sensitive test of GR by comparing the rate of the observed inspiral (phase evolution) to predictions of the PN approximation to GR (Cornish et al., 2011, Huwyler et al., 2011, Li et al., 2011, Mishra et al., 2010).

The merger stage: spectacular bursts

The inspiral is followed by a dynamical merger that produces a burst of gravitational waves. This is a brief event, comprising a few cycles lasting about $5\times10^3\,\mathrm{s}\left(M/10^6\,\mathrm{M}_\odot\right)(0.25/\eta)$, yet very energetic: during the merger the gravitational wave luminosity is $L_{\mathrm{GW}} \sim 10^{23}\,\mathrm{L}_\odot$, emitting more power than all the stars in the observable Universe. The final merger of massive binaries occurs in the very strong-field, highly nonlinear and highly dynamical regime of GR, and is the strongest gravitational wave source that eLISA is expected to see. eLISA will be able to see the merger of two $10^4\,\mathrm{M}_\odot$ black hole beyond redshift $z = 20$, and for mergers of two $10^6\,\mathrm{M}_\odot$ black hole at $z = 1$ the SNR will be about 2000. As mentioned above, eLISA observations of the inspiral yield a good measurement of the masses and spins of the black holes. With these in hand, numerical relativity will make a very specific prediction for the merger and ringdown radiation from the system. Comparison with the waveform that eLISA actually observes will allow us to confront the predictions of GR with an ultra-high precision measurement in the fully nonlinear and dynamical regime of strong gravity for the first time.

The ringdown stage: black hole spectroscopy

Although numerical relativity waveforms from colliding holes naturally include the ringdown waves, these waves are also well understood analytically. GR predicts, as a consequence of the "no-hair" theorem, that every excited black hole emits gravitational waves until it reaches a time-independent state characterised entirely by its mass and spin. These ringdown waves consist of a set of superposed black hole QNM waves with exponentially damped sinusoidal time dependence, plus a far weaker "tail". The modes are strongly damped as their energy is radiated away to infinity, so the final ringdown stage is brief, lasting only a few cycles.

The QNM of Kerr black hole can be computed using perturbation theory: the spacetime metric is written as the Kerr metric plus a small perturbation, and Einstein's equations are expanded to first-order in that perturbation. The solutions can be decomposed into a sum of damped exponentials with complex eigenfrequencies (Chandrasekhar and Detweiler, 1975) that can be computed to essentially arbitrary accuracy (Leaver, 1985).

While there are infinitely many modes (corresponding to the angular order and overtone number of the perturbation from the stationary state), the lowest-order modes are the most readily excited and the least strongly damped, so in practice only a few modes are likely to be observed.

The frequencies and damping times of these ringdown QNM (tabulated in Berti et al., 2009) are completely determined by the mass and the spin of the remnant black hole.

A data analysis strategy based on multi-mode searches will be necessary for an accurate estimation of the mass and spin of the final black hole (Berti et al., 2007, 2006). Furthermore, if we can measure at least two different QNM in a ringdown signal, the ringdown radiation itself will provide a strong-field test of the hypothesis that the central massive objects in galactic nuclei are indeed Kerr black holes. The reason is that a two-mode signal contains four parameters (the frequencies and damping times of each mode), which must all be consistent with the *same* mass and spin values (Dreyer et al., 2004). Just like we can identify chemical elements via spectroscopic measurements, we can uniquely identify a black hole (determine its mass and spin) from the spectrum of its ringdown radiation.

If GR is correct but the observed radiation is emitted from a different source (exotic proposals include boson stars and gravastars, among others), the spectrum would most certainly be inconsistent with the QNM spectrum of Kerr black holes in GR (Berti and Cardoso, 2006, Chirenti and Rezzolla, 2007, Pani et al., 2009, Yoshida et al., 1994). The same should occur if GR does not correctly describe gravity in the extremes of strong fields and dynamical spacetimes. The fact that black hole oscillations should produce different radiation spectra in different theories of gravity is true in general (Barausse and Sotiriou, 2008), and the spectrum was studied in some specific extensions of GR, such as Einstein-dilaton-Gauss-Bonnet gravity (Pani and Cardoso, 2009). The possibility of testing the no-hair theorem with QNM depends on the accuracy with which frequencies and damping times can be measured, which in turn depends on the SNR of the ringdown signal. As shown in (Berti, 2006, Berti et al., 2007), SNR larger than 50 should be sufficient to identify the presence of a second mode and use it for tests of the no-hair theorem. This is only marginally achievable with advanced Earth-based detectors, but SNR of this order should be the norm for the black hole mergers detectable by eLISA. Furthermore, recent work showed that multi-mode ringdown waveforms could encode information on parameters of the binary *before merger*, such as the binary's mass ratio (Kamaretsos et al., 2011), and this would provide further consistency checks on the strong-field dynamics of general relativity.

3 Extreme mass ratio inspirals: precision probes of Kerr spacetime

EMRI are expected to be very clean astrophysical systems, except perhaps in the few percent of galaxies containing accreting massive black holes, where interactions with the accretion disk could possibly affect the EMRI dynamics. Over timescales of the order of a day, the orbits of the smaller body are essentially geodesics in the spacetime of the massive black hole. On longer timescales, the loss of energy and angular momentum due to gravitational-wave emission causes the smaller body to spiral in; i.e., the geodesic's "constants" of motion change slowly over time. Over a typical eLISA observation time (years), EMRI orbits are highly relativistic (radius smaller than 10 Schwarzschild radii) and display extreme forms of periastron and orbital plane precession due to the dragging of inertial frames by the massive black hole's spin. Figure 24 shows two sample waveforms, corresponding to short stretches of time.

Given the large amount of gravitational wave cycles collected in a typical EMRI observation (about 10^5), a fit of the observed gravitational waves to theoretically calculated templates will be very sensitive to small changes in the physical parameters of the system. As mentioned above, this sensitivity makes the search computationally challenging, but it allows an extremely accurate determination of the source parameters, once an EMRI signal is identified. Assuming that GR is correct and the central massive object is a black hole, eLISA should be able to determine the mass and spin of the massive black hole to fractional accuracy of about 10^{-4} – 10^{-3} for gravitational wave signals with an SNR of 20 (Barack and Cutler, 2004).

This level of precision suggests that we can use EMRI as a highly precise observational test of the "Kerr-ness" of the central massive object. That is, if we do *not* assume that the larger object is a black hole, we can use gravitational waves from an EMRI to map the spacetime of that object. The spacetime outside a stationary axisymmetric object is

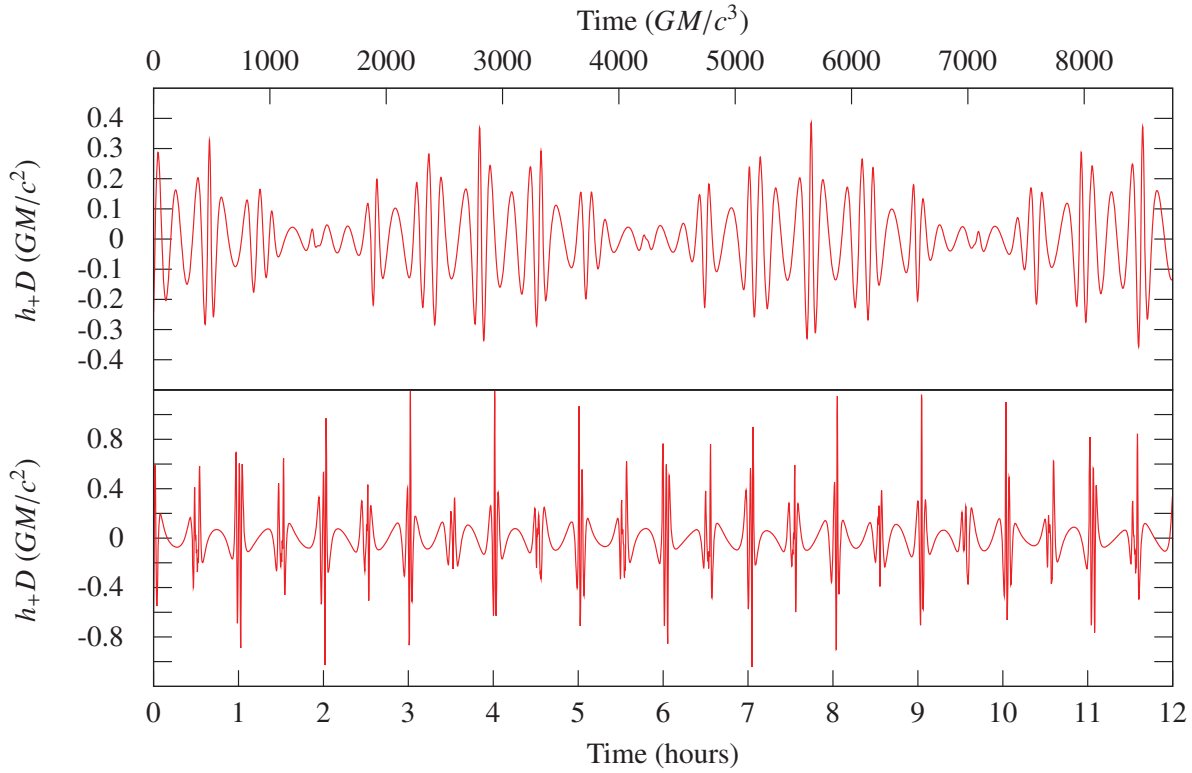

Figure 24: Segments of generic EMRI waveforms (Drasco and Hughes, 2006). These are the plus-polarised waves produced by a test mass orbiting a $10^6 M_\odot$ black hole that is spinning at 90 % of the maximal rate allowed by general relativity, a distance D from the observer. Top panel: Slightly eccentric and inclined retrograde orbit modestly far from the horizon. Bottom panel: Highly eccentric and inclined prograde orbit much closer to the horizon. The amplitude modulation visible in the top panel is mostly due to Lense-Thirring precession of the orbital plane. The bottom panel's more eccentric orbit produces sharp spikes at each pericentre passage.

fully determined by its mass moments M_l and current multipole moments S_l. Since these moments fully characterise the spacetime, the orbits of the smaller object and the gravitational waves it emits are determined by the multipolar structure of the spacetime. By observing these gravitational waves with eLISA we can therefore precisely characterise the spacetime of the central object. Extracting the moments from the EMRI waves is analogous to geodesy, in which the distribution of mass in the Earth is determined by studying the orbits of satellites. Black hole geodesy, also known as holiodesy, is very powerful because Kerr black holes have a very special multipolar structure. A Kerr black hole with mass $M_\bullet$ and spin parameter $a_\bullet$ (in units with $G = c = 1$) has multipole moments given by

$$M_l + \mathrm{i}S_l = (\mathrm{i}a_\bullet)^l M_\bullet^{l+1} \tag{10}$$

Thus, $M_0 = M_\bullet$, $S_1 = a_\bullet M_\bullet^2$, and $M_2 = -a_\bullet^2 M^3$, and similarly for all other multipole moments; they are all completely determined by the first two moments, the black hole mass and spin. This is nothing more than the black hole "no-hair" theorem: the properties of a black hole are entirely determined by its mass and spin.

For inspiraling trajectories that are slightly eccentric and slightly non-equatorial, in principle all the multipole moments are redundantly encoded in the emitted gravitational waves (Ryan, 1995), through the time-evolution of the three fundamental frequencies of the orbit: the fundamental frequencies associated with the r, θ, and ϕ motions (Drasco and Hughes, 2004), or, equivalently, the radial frequency and the two precession frequencies.

The mass quadrupole moment M_2 of a Kerr black hole can be measured to within $\Delta M_2 \approx 10^{-2}\, M_\bullet{}^3 - 10^{-4}\, M_\bullet{}^3$ for signals with an SNR of 30 (Barack and Cutler, 2004), At the same time $\Delta M_\bullet/M_\bullet$ and $\Delta S_1/M_\bullet^2$ will be estimated to an accuracy of $10^{-4} - 10^{-3}$.

Any inconsistency with the Kerr multipole structure could signal a failure of GR, the discovery of a new type of compact object, or a surprisingly strong perturbation from some other material or object. For a review of the different hypotheses regarding the nature of the central object see (Babak et al., 2011, Sopuerta, 2010).

Other tests of the Kerr nature of the central massive object have also been proposed. EMRI signals can be used to distinguish definitively between a central massive black hole and a boson star (Kesden et al., 2005). In the black hole case the gravitational wave signal "shuts off" shortly after the inspiraling body reaches the last stable orbit (and then plunges through the event horizon), while for a massive boson star, the signal does not fade, and its frequency derivative changes sign, as the body enters the boson star and spirals toward its centre. Similarly, if the central object's horizon is replaced by some kind of membrane (this is the case for the so-called gravastars) the orbital radiation produced by the orbiting body could resonantly excite the QNM of the gravastar, with characteristic signatures in the gravitational wave energy spectrum that would be detectable by eLISA (Pani et al., 2009).

Other studies within GR considered axisymmetric solutions of the Einstein field equations for which the multipole moments can differ from the Kerr metric, such as the Manko-Novikov solution. These studies revealed ergodic orbital motion in some parts of the parameter space (Gair, 2009b) as a result of the loss of the third integral of motion. A similar study suggested that the inspiralling body could experience an extended resonance in the orbital evolution when the ratio of intrinsic frequencies of the system is a rational number (Lukes-Gerakopoulos et al., 2010). If detected, these features would be a robust signature of a deviation from the Kerr metric.

These and similar studies of "bumpy" Kerr black holes – spacetime metrics with a multipolar stucture that deviates from the Kerr spacetime by some "tunable" amount (Collins and Hughes, 2004, Glampedakis and Babak, 2006, Hughes, 2006, Ryan, 1995, Vigeland et al., 2011, Vigeland and Hughes, 2010) – focussed on understanding whether the best fit to eLISA data is consistent with the Kerr solution *within general relativity*. However, an even more exciting prospect is that modifications in EMRI waveforms might arise because the true theory of gravity is in fact different from GR. For example, black holes in dynamical Chern-Simons theory (a parity-violating, quantum-gravity inspired extension of GR) deviate from Kerr black holes in the fourth multipole moment $\ell = 4$. This affects geodesic motion, and therefore the phasing of the gravitational wave signal (Pani et al., 2011, Sopuerta and Yunes, 2009).

Gravitational wave observations of black hole-black hole binaries cannot discriminate between GR and scalar-tensor theories of gravity. The reason is that black holes do not support scalar fields; i.e., they have no scalar hair. However, eLISA could place interesting bounds on scalar-tensor theories using observations of neutron stars spiralling into massive black holes (Berti et al., 2005, Yagi and Tanaka, 2010). These limits will be competitive with – but probably not much more stringent than – Solar System and binary pulsar measurements (Esposito-Farèse, 2004).

Finally, eLISA observations of compact binaries could provide interesting bounds on Randall-Sundrum inspired

braneworld models (McWilliams, 2010, Yagi et al., 2011). A general framework to describe deviations from GR in different alternative theories and their imprint on the gravitational wave signal from EMRI can be found in (Gair and Yunes, 2011).

Most high-energy modifications to GR predict the existence of light scalar fields (axions). If such scalar fields exist, as pointed out long ago by Detweiler and others (Detweiler, 1980), rotating black holes could undergo a superradiant "black hole bomb" instability for some values of their spin parameter. Depending on the mass of axions, string-theory motivated "string axiverse" scenarios predict that stable black holes cannot exist in certain regions of the mass/angular momentum plane (Arvanitaki and Dubovsky, 2011). Furthermore, this superradiant instability could produce a surprising result: close to the resonances corresponding to a superradiant instability the EMRI would stop, and the orbiting body would float around the central black hole. These "floating orbits" (for which the net gravitational energy loss at infinity is entirely provided by the black hole's rotational energy) are potentially observable by eLISA, and they could provide a smoking gun of high-energy deviations from general relativity (Cardoso et al., 2011, Yunes et al., 2011).

In conclusion we remark that, if GR must be modified, the "true" theory of gravity should lead to similar deviations in all observed EMRI. For this reason, statistical studies of EMRI to test GR would alleviate possible disturbances that may cause deviations in individual systems, such as interactions with an accretion disk (Barausse and Rezzolla, 2008, Barausse et al., 2007, Kocsis et al., 2011), perturbations due to a second nearby black hole (Yunes et al., 2011) or by a near-by star, which could allow us to investigate different models of how stars distribute around a massive black hole (Amaro-Seoane et al., 2012).

4 Intermediate mass ratio binaries

A loud gravitational wave source for eLISA would be the IMRI of binaries comprising a middleweight (or equivalently intermediate-mass) black hole, with mass in the range of a few times $10^2\,\mathrm{M}_\odot$ to a few times $10^4\,\mathrm{M}_\odot$, along with either a massive black hole ($10^6\,\mathrm{M}_\odot$) or a solar-mass black hole. Currently there is no fully convincing evidence for the existence of intermediate-mass black holes, primarily due to the enormous observational difficulties of resolving the central region of dwarf galaxies and/or globular clusters, the two most likely places where they might reside. eLISA is one of the most promising observatories for discovering these middleweight black holes.

The strength of the gravitational wave signal from an IMRI lies between that of massive black hole binaries and EMRI, and the signal itself carries features of both limiting types, including a relatively fast frequency evolution and comparable contribution of several harmonics to the total strength of the signal. According to the proposed eLISA sensitivity, IMRI could be seen up to redshift $z \sim 4$. There are good reasons to expect that IMRI orbits may have measurable eccentricity (Amaro-Seoane, 2006, Amaro-Seoane et al., 2010b, Amaro-Seoane and Freitag, 2006b, Amaro-Seoane et al., 2009, Amaro-Seoane and Santamaría, 2010, Sesana, 2010). It may also be possible in some cases to observe the gravitational spin-spin coupling between the two black holes (equivalent to the Lense-Thirring effect). The precision in the measurements of the source parameters will lie between that of EMRI and comparable-mass binaries.

5 The mass of the graviton

In GR, gravitational waves travel with the speed of light and the graviton is hence massless. Alternative theories with a massive graviton predict an additional frequency-dependent phase shift of the observed waveform. The dominant effect can be expressed at 1-PN order, and would change the PN coefficient ψ_2 in the stationary-phase approximation to the Fourier transform of the waveform as follows:

$$\psi_2 \to \psi_2 - \frac{128\pi^2}{3}\frac{G\eta^{3/5}M}{c^2}\frac{D}{\lambda_g^2(1+z)}, \tag{11}$$

where η is again the symmetric mass ratio. This term alters the time of arrival of waves of different frequencies, causing a dispersion, and a corresponding modulation in the phase of the signal that depends on the Compton wavelength λ_g and the distance D to the binary. Hence, by tracking the phase of the inspiral waves, eLISA should set bounds in the range $\lambda_g \in [2\times10^{16}\,\mathrm{km}, 10^{18}\,\mathrm{km}]$ on the graviton Compton wavelength (Berti et al., 2011, Huwyler et al., 2011), improving current Solar System bound on the graviton mass, $m_g < 4\times10^{-22}\,\mathrm{eV}$ ($\lambda_g > 3\times10^{12}\,\mathrm{m}$) by several orders of magnitude.

Statistical observations of an ensemble of black hole coalescence events could be used to yield stringent constraints on other theories whose deviations from GR are parametrized by a set of global parameters: examples considered so far in the literature include theories with an evolving gravitational constant (Yunes et al., 2010), massive Brans-Dicke theories (Alsing et al., 2011) and Lorentz-violating modifications of GR (Mirshekari et al., 2011).

7 Cosmology

1 New physics and the early Universe

Gravitational waves penetrate all of cosmic history, which allows eLISA to explore scales, epochs, and new physical effects not accessible in any other way (see figure 25). Indeed a detectable gravitational wave background in the eLISA band is predicted by a number of new physical ideas for early cosmological evolution (Hogan, 2006, Maggiore, 2000). Two important mechanisms for generating stochastic backgrounds are phase transitions in the early Universe and cosmic strings.

Gravitational waves produced after the Big Bang form a fossile radiation: expansion prevents them from reaching thermal equilibrium with the other components because of the weakness of the gravitational interaction. Important information on the first instants of the Universe is thus imprinted in these relics and can be decoded. The mechanical effect of expansion is simply to redshift the corresponding frequency. Assuming that the wavelength is set by the apparent horizon size $c/H_* = ca/\dot{a}$ at the time of production (when the temperature of the Universe is T_*), the redshifted frequency is

$$f_0 = \dot{a}(t) \approx 10^{-4}\,\mathrm{Hz}\sqrt{H_*(t) \times \frac{1\,\mathrm{mm}}{c}} \approx 10^{-4}\,\mathrm{Hz}\left(\frac{k_B T_*}{1\,\mathrm{TeV}}\right) \tag{12}$$

Thus, the eLISA frequency band of about 0.1 mHz to 100 mHz today corresponds to the horizon at and beyond the Terascale frontier of fundamental physics. This allows eLISA to probe bulk motions at times about $3 \times 10^{-18} - 3 \times 10^{-10}$ seconds after the Big Bang, a period not directly accessible with any other technique. Taking a typical broad spectrum into account, eLISA has the sensitivity to detect cosmological backgrounds caused by new physics active in the range of energy from 0.1 TeV to 1000 TeV, if more than a modest fraction Ω_{GW} of about 10^{-5} of the energy density is converted to gravitational radiation at the time of production.

Various sources of gravitational wave background of cosmological origin are presented in detail in Binétruy et al. (2012). Here we will only briefly summarize the main mechanisms leading to the potentially observable backgrounds.

A standard example of new physics is a first-order phase transition resulting in bubble nucleation and growth, and subsequent bubble collisions and turbulence. Phase transitions also often lead to the formation of one-dimensional topological defects known as cosmic strings. Among possible topological defects, cosmic strings are unique from a cosmological point of view because, whereas their energy density should grow with the expansion, they interact and form loops which decay into gravitational waves. Thus cosmic strings tend to form networks with a typical scaling behaviour, losing energy mainly through gravitational radiation with a very broad and uniquely identifiable spectrum. Besides topological defects, cosmic strings could also find their origin among the fundamental objects of string theory, the theory that is aiming at providing a unified framework for all particles and forces of nature. Indeed, although fundamental strings were devised as submicroscopic objects, it has been progressively realized (Copeland et al., 2004) that some of these strings could be stretched to astronomical size by the cosmic expansion. eLISA will be our most sensitive probe for these objects by several orders of magnitude and so offers the possibility of detecting direct evidence of fundamental strings.

In order to distinguish backgrounds of gravitational waves from those waves emitted by point sources, it is essential to make use of the successive positions of eLISA around the Sun, and thus to wait a sufficient amount of time (of the order of a few months). It is more difficult to disentangle an isotropic cosmological (or astrophysical) background from an instrumental one, all the more because the eLISA "Mother-Daughter" configuration, providing only two measurement arms, does not allow to use Sagnac calibration (Hogan and Bender, 2001). Luckily, in the case of phase transitions as well as cosmic strings, the spectral dependence of the signal is well predicted and may allow to distinguish cosmological backgrounds as long as they lie above the eLISA sensitivity curve.

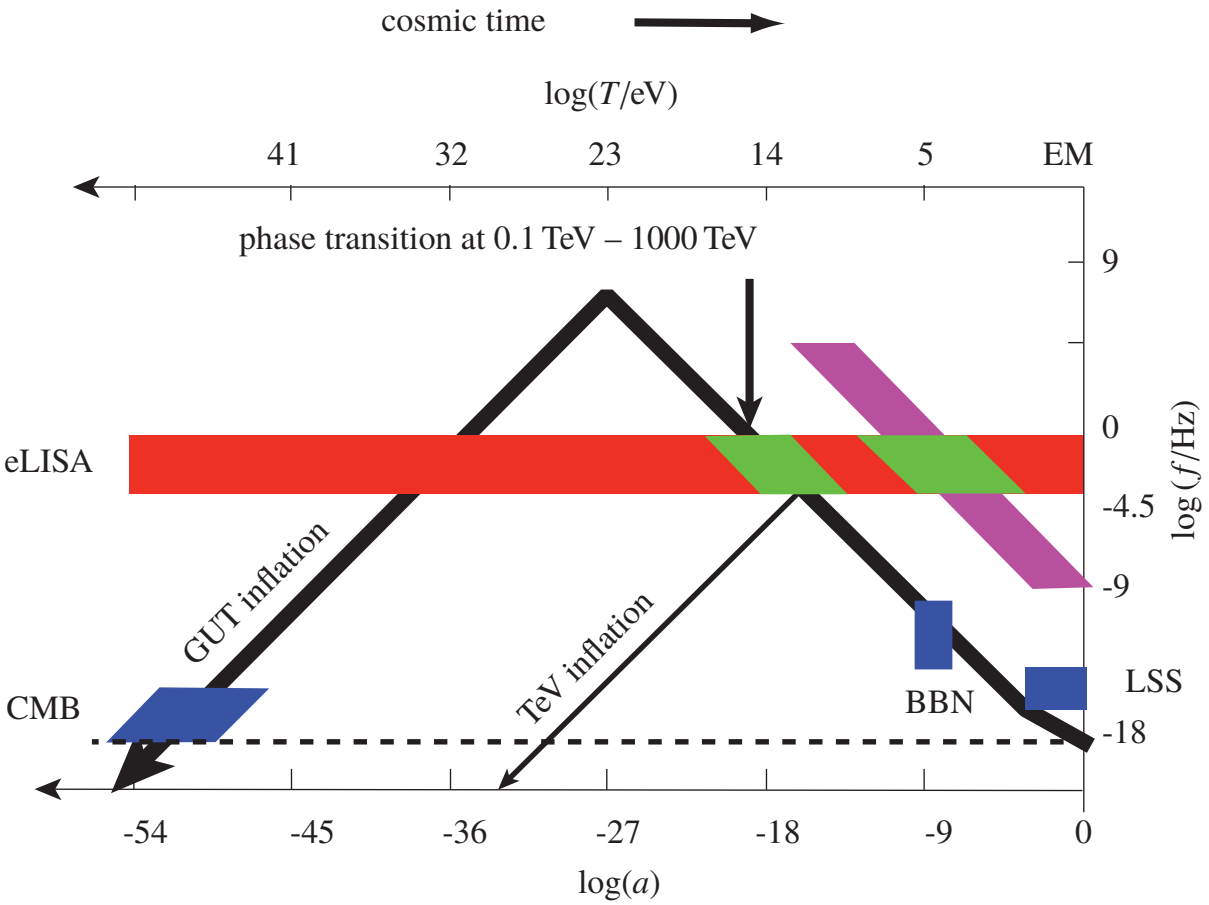

Figure 25: The observed (redshifted) frequency of wave-generating phenomena is shown as a function of cosmic scale factor a, with the present epoch at the right. The redshifted Hubble rate (horizon scale) is shown in black for a standard Grand Unified Theory (GUT) and a lower temperature Terascale (TeV) inflationary cosmology. Blue regions are accessible to electromagnetic (EM) observations: the Universe since recombination (right box) and cosmic microwave background (CMB) fluctuations (left box). The red bar shows the range of cosmic history accessible through eLISA from processes within the horizon up to about 1000 TeV.

First-order cosmological phase transitions: Bulk motion from bubble nucleation, cavitation, collisions, turbulence

Abundant evidence suggests that the physical vacuum was not always in its current state, but once had a significantly higher free energy. This idea is fundamental and general: it underlies symmetry breaking in theories such as the Standard Model and its supersymmetric extensions, and cosmological models including almost all versions of inflation. Common to all these schemes is the feature that a cold, nearly uniform free energy contained in the original (*false*) vacuum is liberated in a phase transition to a final (*true*) vacuum, and eventually converted into thermal energy of radiation and hot plasma.

In many theories beyond the Standard Model, the conversion between vacuum states corresponds to a first-order phase transition. In an expanding Universe this leads to a cataclysmic process. After supercooling below the critical temperature T_* for the transition, a thermal or quantum jump across an energy barrier leads to the formation of bubbles of the new phase. The bubbles rapidly expand and collide. The internal energy is thus converted to organised flows of mass-energy, whose bulk kinetic energy eventually dissipates via turbulence and finally thermalises. The initial bubble collision and subsequent turbulent cascade lead to relativistic flows and acceleration of matter that radiate gravitational waves on a scale not far below the horizon scale (Caprini et al., 2009, Hogan, 1986, Huber and Konstandin, 2008, Kamionkowski et al., 1994, Witten, 1984).

The gravitational wave energy density $\Omega_{\rm GW}$ typically depends on two parameters: H_*/β is the duration of the transition in Hubble units and α is the fraction of energy density available in the source (false vacuum, relativistic motion). Typically $\Omega_{\rm GW} \sim \Omega_{\rm rad}\,(H_*/\beta)^2\,(\kappa\,\alpha)^2/(1+\alpha)^2$, where $\Omega_{\rm rad}$ is the the fraction of radiation energy today, and κ the fraction of vacuum energy which is converted into bulk kinetic energy during the phase transition. Strong first order phase transitions are obtained for $\alpha \gg 1$ but, in the context of specific models, increasing α may increase β as well.

Dynamics of warped sub-millimetre extra dimensions

Superstring theory provides examples of strong first order phase transitions in the Terascale region. It requires, for mathematical consistency, several extra dimensions. The sizes of these dimensions, their shapes, and how they are stabilised are yet to be determined. If they exist, gravity can penetrate into them, so they must be small or warped – with a size below the sub-millimetre scale limit set by direct laboratory tests of the gravitational inverse-square law. The scales probed by Standard Model particles and fields are much smaller than this, but fields other than gravity might be confined to a 3-dimensional subspace or (mem)brane plunged in the higher dimensional space.

Since the the Hubble length at the Terascale is about a millimetre, the current threshold where possible new effects of extra dimensions might appear happens to be about the same for experimantal gravity in the laboratory as for the cosmological regime accessible to eLISA. It is even possible that new properties of gravity on this scale are related to cosmic dark energy, whose energy density is about $(0.1\,\mathrm{mm})^{-4}$ in particle physics units.

The dynamics associated with the stabilisation of extra dimensions at a certain size or warp radius might introduce a source of free internal energy released coherently on a *mesoscopic*, i.e. sub-millimetre to nanometre scale, leading to a detectable background (Hogan, 2000, Randall and Servant, 2007). If the extra dimensions are much smaller than the Hubble length when the stabilisation occurs, the behaviour of the extra dimensions is nearly equivalent to scalar field behaviour as viewed in conventional 3-dimensional space, with effects similar to the phase transitions discussed above (see figure 26).

Backgrounds, bursts, and harmonic notes from cosmic strings

As we have seen above, models of physics and cosmology based on string theory, as well as their field-theory counterparts, often predict the cosmological formation of cosmic superstrings (Copeland et al., 2004) that form after inflation and are stretched to enormous length by the cosmic expansion. In equivalent field-theory language, cosmic strings arise from certain types of phase transitions, and stable relics of the high-energy phase persist as topological defects: in the form of one-dimensional strings that resemble flux tubes or trapped vortex lines.

The primordial network of strings produces isolated, oscillating loops that ultimately radiate almost all of their energy into gravitational waves. Their gravitational radiation is mainly governed by a single dimensionless parameter $G\mu/c^4$ reflecting the fundamental physics of the strings, where G is Newton's constant and μ is the energy per unit length, or tension. This parameter is known to be very small, as current limits on gravitational wave backgrounds already indicate

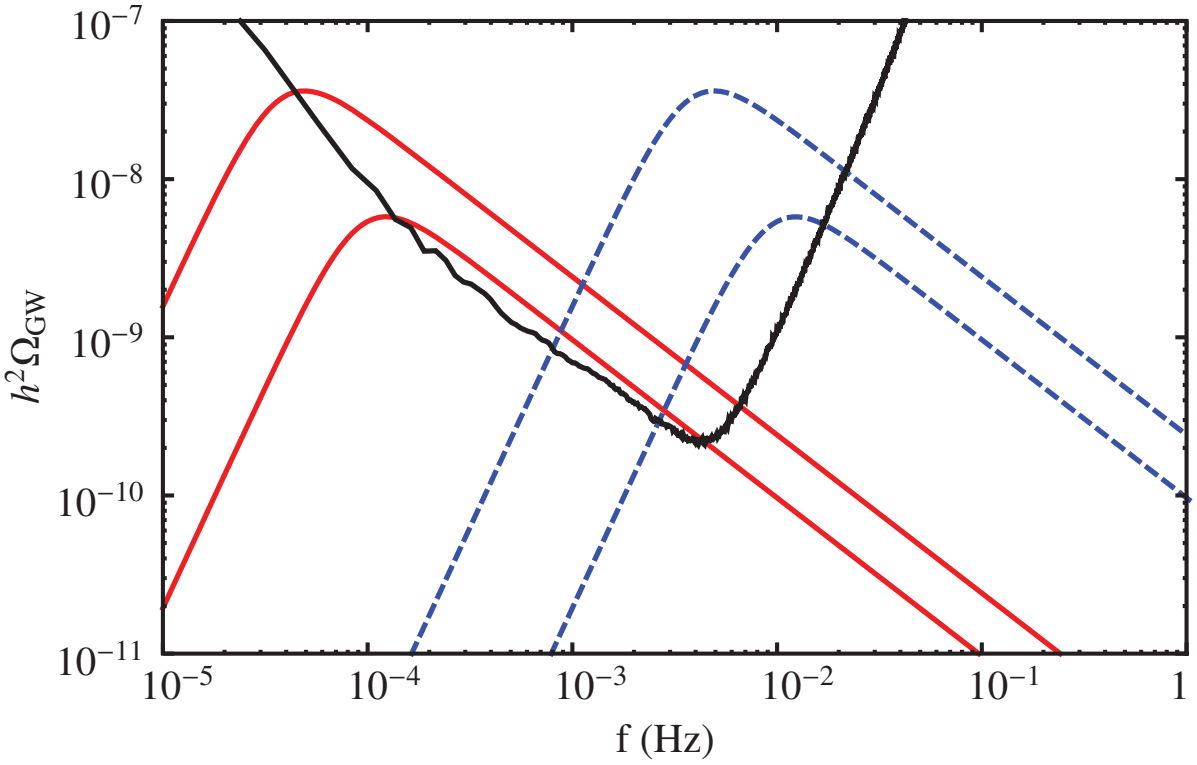

Figure 26: Predictions for the holographic phase transition (Konstandin et al., 2010) corresponding to the model of Randall and Sundrum with a TeV brane stabilized. In black, the sensitivity curve of eLISA expressed in terms of the gravitational wave background density Ω_{GW}. In red, signals corresponding to a phase transition temperature of 10^2 GeV. In dashed blue, a transition temperature of 10^4 GeV. From top to bottom, curves correspond to $\beta/H_* = 6$ and $\beta/H_* = 15$.

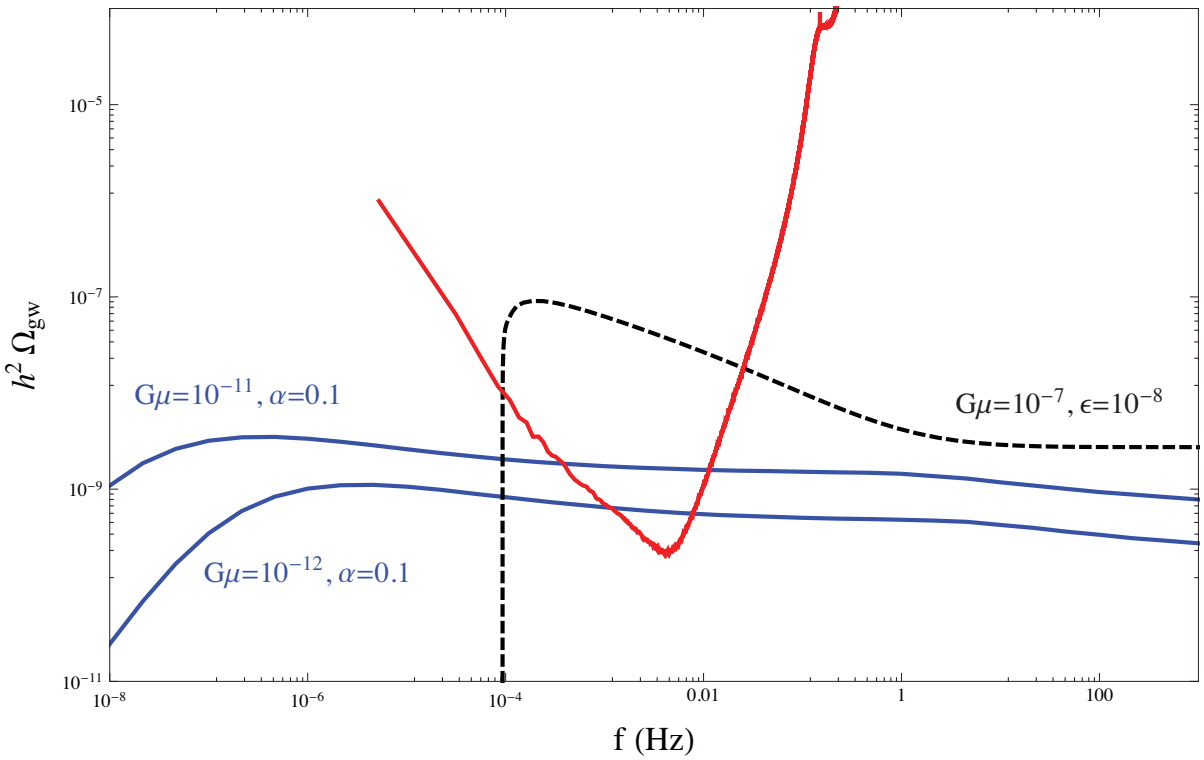

Figure 27: Typical string background expected for eLISA (whose sensitivity curve is in red) in the large loop scenario in blue (α determines the loop size as a fraction of the horizon size) and in the small loop scenario in dashed ($\epsilon \equiv \alpha/(50G\mu)$). See Binétruy et al. (2012) for more details.

that if cosmic strings exist, they must be so light that they would have few observable effects apart from their gravitational radiation.

Figure 27 compares eLISA sensitivity (in red) with predicted stochastic background spectra in two distinct scenarios: large loops in blue (where newly formed loops are about $\alpha = 0.1$ times the horizon size) for two values of $G\mu/c^4$ spanning a range of scenarios motivated by brane world inflation, and small loops in dashed (with $\alpha = 50\epsilon G\mu$) for one value of $G\mu/c^4$. We note that the spectrum from cosmic strings is distinguishably different from that of phase transitions or any other predicted source: it has nearly constant energy per logarithmic frequency interval over many decades at high frequencies, and falls off after a peak at low frequencies, since large string loops are rare and radiate slowly. In the small loop scenario, the peak frequency shifts to lower values when increasing ϵ, whereas the amplitude decreases with $G\mu/c^4$. This allows an interesting interplay between measurements at eLISA, ground interferometers and millisecond pulsar arrays: depending on the parameters, one may have detection of the string background at one, two or three of these different types of detectors. In the large loop scenario, eLISA sensitivity in terms of $G\mu/c^4$ is several orders of magnitude deeper than even the best possible future sensitivity from pulsar timing.

If the strings are not too much lighter than $G\mu/c^4 \sim 10^{-10}$, occasional distinctive bursts might be seen from loops, produced by a sharply bent bit of string moving at nearly the speed of light (Damour and Vilenkin, 2005, Siemens et al., 2006). These rare events, known as kinks or cusps, are recognisable, if they are intense enough to stand out above the background, from their universal waveform which derives just from the geometry of the string. Cusps are localized in time whereas kinks are propagating along the strings. In the case of fundamental strings, the presence of junctions between strings leads to a proliferation of kinks (Binétruy et al., 2010, Bohé, 2011).

Although individual burst events, if detected, give the clearest signature of a string source, the first detectable sign of a superstring loop population is likely their integrated stochastic background as shown in figure 27.

Terascale inflationary reheating

Inflation represents an extraordinarily coherent behaviour of an energetic scalar field that is nearly uniform across the observable Universe. After inflation, the internal potential energy of this field is converted into a thermal mix of relativistic particles, in a process known as reheating. The reheating temperature might be as cool as 1 TeV, especially in some brane-world models where the Planck scale is itself not far above the Terascale.

There is no reason to assume a quiet, orderly reheating process: the decay of the inflaton energy may be violently unstable. In many scenarios, the conversion begins with macroscopically coherent but inhomogeneous motions that eventually cascade to microscopic scales. Quantum coherent processes such as preheating transform the energy into coherent classical motions that can generate backgrounds on the order of 10^{-3} or more of the total energy density (Dufaux et al., 2007, 2009, Easther and Lim, 2006, Garcia-Bellido and Figueroa, 2007, Khlebnikov and Tkachev, 1997). The characteristic frequency of the background can fall in the eLISA band if the final reheating occurred at 0.1 TeV to 1000 TeV.

Exotic inflationary quantum vacuum fluctuations

The amplification of quantum vacuum fluctuations during inflation leads to a background of primordial gravitational waves. An optimistic estimate of this background in the case of conventional inflation limits these to less than about 10^{-10} of the CMB energy density, far below eLISA's sensitivity; in many inflation models it is much less (Chongchitnan and Efstathiou, 2006). However, some unconventional versions of inflation, particularly pre-Big-Bang or bouncing brane scenarios, predict possibly detectable backgrounds in the eLISA band (see e.g. Brustein et al., 1995, Buonanno, 2003, Buonanno et al., 1997). Although some key parameters remain unknown, which limits the predictive power of these models, they are significantly constrained by gravitational wave backgrounds. If such a background is detected, its spectrum also contains information about the Universe at the time perturbations re-enter the horizon (the second horizon intersection in figure 25).

2 Cosmological measurements with eLISA

As discussed in section 4 we can probe the assembly of cosmic structures through observations of black hole binaries up to high redshifts. In addition to that, gravitational wave sources could serve as standard sirens for cosmography (Holz and Hughes, 2005), because chirping binary systems allow direct measurements of the luminosity distance to the source. The principle is elegant and simple (Schutz, 1986): the chirping time τ of an inspiral/merger event, together with its orbital frequency ω and strain h, gives the absolute luminosity distance to the source, $D_L \sim c/(\omega^2 \tau h)$, with a numerical factor depending on details of the system that are precisely determined by the measured waveform. However, eLISA cannot independently determine the redshift of a source, since in gravitational wave astronomy, the measured source frequency and chirp time are always combined with cosmic redshift $\omega = \omega_{\rm source}/(1+z), \tau = (1+z)\tau_{\rm source}$, i.e., the redshift is degenerate with the source intrinsic parameters. An independent measurement of redshift is therefore needed. This may be accomplished by getting the optical redshift to the host galaxy, for instance by identifying an electromagnetic radiation counterpart to the event.

In the last decade, several mechanisms producing electromagnetic counterparts to black hole binary coalescences have been proposed (e.g., Armitage and Natarajan, 2002, Milosavljević and Phinney, 2005, Phinney, 2009); an exhaustive review can be found in (Schnittman, 2011). While there are still uncertainties in the nature and strength of such counterparts, we might expect some of them to be observable at least in the local Universe (say, $z \leq 1$). Our parameter estimation simulations show that, at low redshift, we could expect to localize at least 50 % of the inspiralling black holes to better than 400 square degrees and about 11 % to better than 10 square degrees. Merger and ringdown (if observed) should further improve those numbers. As a practical example, wide area surveys like LSST (LSST Science Collaborations et al., 2009) in optical or the VAST project using the Australian Square Kilometer Array Pathfinder (Johnston et al., 2007) in radio will have the capability of covering such large area in the sky to high depth several times per day during and right after the merger event, looking for distinctive transients. Any identified counterpart will provide precise measurements of the source redshift and sky location. We can use this information to perform directional search (fixing the sky location of the gravitational wave source) in the eLISA data and the resulting uncertainty in the luminosity distance drops to less than 1 % for 60 % (5 % for 87 %) of the sources. Those numbers are comparable with (or even lower than) the weak lensing error at these low redshifts (Wang et al., 2002). Ultra-precise measurements of the redshift and the luminosity distance will allow us to cross–check the SNIa measurements (Perlmutter and Riess, 1999, Riess et al., 1998), and because of the very

different systematics from the usual cosmological distance ladder estimates, will be a strong check on hidden systematic errors in these measurements. This will improve the estimation of cosmological parameters, such as H_0 and w.

Without electromagnetic identification of the host, we can check statistical consistency between all the possible hosts detected within the measurement error box, to infer cosmological parameters as suggested in (Petiteau et al., 2011). To realize this scheme one needs a rather good source sky location and distance determination, which is possible with eLISA only at low redshifts ($z < 2$). In the local Universe, the same technique applied to EMRI will allow precision measurement of H_0 (MacLeod and Hogan, 2008) at a level of a few percent.

8 Conclusions: science and observational requirements

In this document we have presented the science that eLISA will be able to do, which ranges from ultra-compact binaries to cosmology and tests of GR.

In particular, we note that eight of the known ultra-compact binaries will be detected by eLISA as verification binaries. Upcoming wide-field and synoptical surveys will most likely discover more verification binaries before eLISA's launch. eLISA will detect about 3,000 double white dwarf binaries individually. Most have orbital periods between 5 and 10 minutes and have experienced at least one common-envelope phase, so they will provide critical tests of physical models of the common-envelope phase. These sources are exactly the population which has been proposed as progenitors of normal as well as peculiar (type Ia) supernovae. eLISA will tell us if the formation of all ultra-compact binaries is enhanced in globular clusters by dynamical interactions. The millions of ultra-compact binaries that will not be individually detected by eLISA will form a detectable foreground from which the global properties of the whole population can be determined. The binaries detected by eLISA will improve our knowledge of tidal interactions in white dwarfs, mass-transfer stability and white dwarf mergers. eLISA will unravel the Galactic population of short-period neutron star and black hole binaries, and thus determine their local merger rate. eLISA will measure the sky position and distance of several hundred binaries, constraining the mass distribution in the Galaxy and providing an independent distance estimate to the Galactic centre. The level and shape of the Galactic foreground will constrain the relative contributions of thin disc, thick disc and halo populations and their properties. For several hundred sources the orbital inclination will be determined to better than 10 degrees, allowing to test if binaries are statistically aligned with the Galactic disc.

One of the most promising science goals of the mission are supermassive black holes, which appear to be a key component of galaxies. They are ubiquitous in near bright galaxies and share a common evolution. The intense accretion phase that supermassive black holes experience when shining as QSOs and AGN erases information on how and when the black holes formed. eLISA will unravel precisely this information. Very massive black holes are expected to transit into the mass interval to which eLISA is sensitive along the course of their cosmic evolution. eLISA will then map and mark the loci where galaxies form and cluster, using black holes as clean tracers of their assembly by capturing gravitational waves emitted during their coalescence, that travelled undisturbed from the sites where they originated. On the other hand, middleweight black holes of $10^5\,M_\odot$ are observed in the near universe, but our knowledge of these systems is rather incomplete. eLISA will investigate a mass interval that is not accessible to current electromagnetic techniques, and this is fundamental to understand the origin and growth of supermassive black holes. Due to the transparency of the universe to gravitational waves at any redshift, eLISA will explore black holes of $10^5\,M_\odot - 10^7\,M_\odot$ out to a redshift $z \lesssim 20$, tracing the growth of the black hole population.

eLISa will also shed light on the path of black holes to coalescence in a galaxy merger. This is a complex process, as various physical mechanisms involving the interaction of the black holes with stars and gas need to be at play and work effectively, acting on different scales (from kpc down to 10^{-3} pc). Only at the smallest scales gravitational waves are the dominant dissipative process driving the binary to coalescence. eLISA will trace the last phase of this evolution. Dual AGN, i.e. active black holes observed during their pairing phase, offer the view of what we may call the galactic precursors of black hole binary coalescences. They are now discovered in increasing numbers, in large surveys. By contrast, evidence of binary and recoiling AGN is poor, as the true nature of a number of candidates is not yet fully established. eLISA only will offer the unique view of an imminent binary merger by capturing its loud gravitational wave signal.

There exist major uncertainties in the physical mechanism(s) conducive to the gravitational collapse of a star (or perhaps of a very massive quasi-stars) leading to the formation of the first black holes in galaxies. The mass of seed black holes ranges from a few hundred to a few thousand solar masses. Seed black holes later grow, following different evolutions according to their different formation path and clustering inside dark matter halos, and eLISA aims at disentangling different routes of evolution. eLISA will considerably reduce uncertainties on the nature of the seed population, as the

number of observed mergers and the inferred masses will allow to decide among the different models or, in the case of concurrent models, determine their prevalence.

According to the theoretical findings we have presented, massive black hole masses and spins evolve through coalescence and accretion events. Black hole spins offers the best opportunity to determine whether accretion episodes prior to coalescence are coherent or chaotic. Masses and spins are directly encoded into the gravitational waves emitted during the the merger process. eLISA will measure the masses and spins of the black holes prior to coalescence, offering unprecedented details on how black hole binaries have been evolving via mergers and accretion along cosmic history. At present, coalescence rates, as a function of redshift and in different mass bins, can only be inferred theoretically, using statistical models for the hierarchical build-up of cosmic structures. These models, firmly anchored to low redshift observations, indicate that the expected detection rates for eLISA range between few and few hundred per year.

Current electromagnetic observations are probing only the tip of the massive black hole distribution in the universe, targeting black holes with large masses, between $10^7\,M_\odot - 10^9\,M_\odot$. Conversely, eLISA will be able to detect the gravitational waves emitted by black hole binaries with total mass (in the source rest frame) as small as $10^4\,\mathrm{M}_\odot$ and up to $10^7\,\mathrm{M}_\odot$, out to a redshift as remote as $z \sim 20$. eLISA will detect fiducial sources out to redshift $z \lesssim 10$ with SNR $\gtrsim 10$ and so it will explore almost all the mass-redshift parameter space relevant for addressing scientific questions on the evolution of the black hole population. Redshifted masses will be measured to an unprecedented accuracy, up to the 0.1–1% level, whereas absolute errors in the spin determination are expected to be in the range 0.01–0.1, allowing us to reconstruct the cosmic evolution of massive black holes. eLISA observations hence have the potential of constraining the astrophysics of massive black holes along their entire cosmic history, in a mass and redshift range inaccessible to conventional electromagnetic observations.

On smaller scales, eLISA will also bring a new revolutionary perspective, in this case relative to the study of galactic nuclei. eLISA will offer the deepest view of galactic nuclei, exploring regions to which we are blind using current electromagnetic techniques and probing the dynamics of stars in the space-time of a Kerr black hole, by capturing the gravitational waves emitted by stellar black holes orbiting the massive black hole. EMRI detections will allow us to infer properties of the stellar environment around a massive black hole, so that our understanding of stellar dynamics in galactic nuclei will be greatly improved. Detection of EMRIs from black holes in the eLISA mass range, that includes black holes similar to the Milky Way's, will enable us to probe the population of central black holes in an interval of masses where electromagnetic observations are challenging. eLISA's EMRIs can be detected up to $z \simeq 0.5 - 0.7$ allowing to explore a volume of several tens of Gpc^3 and discover massive black holes in dwarf galaxies that are still elusive to electromagnetic observations. eLISA may also measure the mass of stellar-mass black holes. This will provide invaluable information on the mass spectrum of stellar black holes, and on the processes giving rise to compact stars. eLISA will detect EMRI events out to redshift $z \sim 0.7$, in normal galaxies with high SNR, and in the mass interval, $10^4\,\mathrm{M}_\odot \lesssim M \lesssim 5 \times 10^6\,\mathrm{M}_\odot$. eLISA will measure the mass and spin of the large, massive black hole with a precision to better than a part in 10^4. This will enable us to characterise the population of massive black holes in nuclei in an interval of masses where electromagnetic observations are poor, incomplete or even missing, providing information also on their spins. eLISA will also measure with equivalent precision the mass of the stellar black hole in the EMRI event, and also the orbital eccentricity at plunge. These observations will provide insight on the way stars and their remnants are forming and evolving in the extreme environment of a galactic nucleus. The estimated detection rates based on the best available models of the black hole population and the EMRI rate per galaxy, are about 50 events with a two year eLISA mission, with a factor of $\lesssim 2$ uncertainty from the waveform modelling and lack of knowledge about the likely system parameters (larger uncertainties are of astrophysical nature). Even with a handful of events, EMRIs will be a powerful astrophysical probe of the formation and evolution of massive and stellar black holes. We also note that the detection with eLISA of even a single coalescence event involving two intermediate mass black holes in colliding star clusters, present in the very local universe, would be a major discovery, and it would have a strong impact in the field of stellar dynamics and stellar evolution in star forming regions.

General Relativity has been extensively tested in the weak field regime both in the solar system and by using binary pulsars. eLISA will provide a unique opportunity of confronting GR in the highly dynamical strong field regime of massive black holes. eLISA will be capable of detecting inspiral and/or merger plus ring-down parts of the gravitational wave signal from coalescing massive black holes binaries of comparable mass. For the nearby events ($z \sim 1$) the last several hours of the gravitational wave signal will be clearly seen in the data, allowing direct comparison with the waveforms predicted by GR. The inspiral phase could be observed by eLISA up to a year before the final merger with relatively large SNR. Comparison of the observed inspiral rate with the predictions of GR will provide a valuable test of the theory in the regime of strong, dynamical gravitational fields.

The merger of two black holes could be observed by eLISA throughout the Universe if it falls into the detector band.

The observation of the merger could be confronted directly with the predictions of GR and, if the inspiral is also observed, could be used for a consistency check between the two parts of the gravitational wave signal. According to GR the merger leads to a single ringing Kerr black hole characterised by its mass and spin. Detecting two or more quasinormal modes (the individual damped exponential components of the so-called ringdown radiation) will allow us to check whether the final object indeed is described only by two parameters in accord with the no-hair theorem of GR. eLISA will give us a unique opportunity to observe middleweight mass black holes in the local Universe. If observed, these systems would provide an additional testbed for GR.

eLISA will be capable of setting an upper limit on the mass of graviton that is at least four orders of magnitude better than the current limit based on observations in the Solar System. The discovery of coalescing binary black holes, signposts of (pre-)galactic mergers, will test, albeit indirectly, the hypothesis which is at the heart of the current paradigm of galaxy formation, i.e. their assembly in a bottom-up fashion. Furthermore coalescing binary black holes can be regarded as standard sirens, and they may allow a direct measurement of the luminosity distance to the source. If coalescence is accompanied by an electromagnetic signal that permits the measurement of the optical redshift of the source eLISA will improve upon the estimation of cosmological parameters, such as the Hubble constant and the dark-energy parameter w. eLISA will have unique capabilities in detecting signatures from (or setting meaningful constraints on) a wide range of cosmological phenomena and fundamental physics. Gravitational radiation backgrounds are predicted in cosmological models that include first order phase transitions, late-ending inflation, and dynamically active mesoscopic extra dimensions. eLISA will provide the most sensitive direct probes of such phenomena near TeV energies.

We state now the eLISA science requirements (SR) which summarize the research needed to fulfill the eLISA objectives. For each science requirement, one or more observational requirements (OR) are defined. The observational requirements are stated in terms of observable quantities necessary to meet the science requirements, and in terms of the precision with which such quantities must be measured.

- ***Galactic binaries***
  - ***SR 1.1*** *: Elucidate the formation and evolution of Galactic stellar-mass compact binaries and thus constrain the outcome of the common envelope phase and the progenitors of (type Ia) supernovae.*
    - **OR 1.1.1** : eLISA shall have the capability to detect at least 1000 binaries at SNR > 10 with orbital periods shorter than approximately six hours and determine their period. eLISA shall maintain this detection capability for at least one year.
    - **OR 1.1.2** : eLISA shall detect all neutron star and black hole binaries in the Milky Way with periods shorter than 35 minutes if they exist.
    - **OR 1.1.3** : eLISA shall have the capability to measure the level of the unresolved Galactic foreground. eLISA shall maintain this detection capability for at least one year.
  - ***SR 1.2*** *: Determine the spatial distribution of stellar mass binaries in the Milky Way.*
    - **OR 1.2.1** : eLISA shall have the capability to determine the position of at least 500 sources with better than ten square degree angular resolution and the frequency derivative to a fractional uncertainty of 10 %.
    - **OR 1.2.2** : eLISA shall measure the inclination of at least 500 binaries to better than 10 degrees.
  - ***SR 1.3*** *: Improve our understanding of white dwarfs, their masses, and their interactions in binaries, and enable combined gravitational and electromagnetic observations.*
    - **OR 1.3** : eLISA shall have the capability to measure the frequency derivative of all detected binary systems with gravitational wave frequencies above 10 mHz to better than 10 %.
- ***Massive black hole binaries***
  - ***SR 2.1*** *: Trace the formation, growth and merger history of massive black hole with masses* $10^5 M_\odot - 10^7 M_\odot$ *during the epoch of growth of QSO and widespread star formation (*$0 < z < 5$*) through their coalescence in galactic halos.*
    - **OR 2.1.1** : eLISA shall have the capability to detect the mergers of similar masses massive black hole (mass ratio $m_2/m_1 > 0.1$) with total mass in the range $10^5\,M_\odot < m_1 + m_2 < 10^7\,M_\odot$ up to redshift $z = 20$. The SNR of those sources with redshift $z < 5$ should be sufficient to enable determination of the massive black hole masses (relative errors smaller than 1 %) and the spin of the largest massive black hole (error smaller than 0.1) and an estimation of the luminosity distance (relative error smaller than 50 %).

  - ∗ **OR 2.1.1** : eLISA shall have the capability to detect the mergers of massive black hole with total mass in the range $10^5 M_\odot < m_1 + m_2 < 10^7 M_\odot$ and mass ratio m_2/m_1 about 0.01 up to redshift $z = 8$. The SNR of those sources with redshift $z < 5$ shall be sufficient to enable determination of the massive black hole masses (relative errors smaller than a few percents).

- ***SR 2.2*** *: Capture the signal of coalescing massive black hole binaries with masses* $2\times10^4\,M_\odot - 10^5\,M_\odot$ *in the range of* $5 < z < 10$ *when the universe is less than 1 Gyr old.*
  - ∗ **OR 2.2.1** : eLISA shall have the capability to detect the mergers of comparable mass massive black hole (mass ratio $m_2/m_1 > 0.1$) with total mass in the range $2 \times 10^4\,M_\odot < m_1 + m_2 < 10^5\,M_\odot$ beyond redhift $z = 5$ and up to $z = 15$ for equal mass systems with sufficient SNR to enable determination of the massive black hole masses (relative errors smaller than 1 %) and the spin of the largest massive black hole (error smaller than 0.1) and an estimation of the luminosity distance (relative error smaller than 50 %).
  - ∗ **OR 2.2.2** : eLISA shall have the capability to detect some of the mergers of massive black hole with total mass in the range $2 \times 10^4\,M_\odot < m_1 + m_2 < 10^5\,M_\odot$ and mass ratio $0.01 < m_1/m_2 < 0.1$ beyond redshift $z = 5$ with sufficient SNR to enable determination of the massive black hole masses with relative errors smaller than a few percent.

- ***Extreme (and intermediate) mass ratio inspiral***
  - ***SR 3.1*** *: Characterise the immediate environment of massive black hole in* $z < 0.7$ *galactic nuclei from EMRI capture signals.*
    - ∗ **OR 3.1** : eLISA shall have the capability to detect gravitational waves emitted during the last two years of inspiral for a stellar-mass compact object ($m_2 \sim 5\,M_\odot - 20\,M_\odot$) orbiting a massive black hole ($m_1 \sim 10^5\,M_\odot - 10^6\,M_\odot$) up to $z = 0.7$ with an SNR > 20 . The detection of those sources shall be sufficient to determine the mass of the massive black hole with an relative error smaller than 0.1 %, the spin of the massive black hole with an error smaller than 10^{-3}, and the mass of the compact object with a relative error smaller than 0.1 %, as well as the orbital eccentricity before the plunge with an error smaller than 10^{-3}.
  - ***SR 3.2*** *: Discovery of intermediate-mass black holes from their captures by massive black hole.*
    - ∗ **OR 3.2** : eLISA shall have the capability to detect gravitational waves emitted by a $10^2\,M_\odot - 10^4 M_\odot$ intermediate-mass black hole spiralling into an massive black hole with mass $3\times10^5 M_\odot - 10^7 M_\odot$ out to $z \sim 2 - 4$ (for a mass ratio around 10^{-2} to 10^{-3}).

- ***Confronting General Relativity with Precision Measurements of Strong Gravity***
  - ***SR 4.1*** *: Detect gravitational waves directly and measure their properties precisely.*
    - ∗ **OR 4.1.1** : eLISA shall have capability to detect and study three or more optically observable verification binaries between 1 mHz and 10 mHz with SNR > 10 in two years of mission lifetime.
    - ∗ **OR 4.1.2** : eLISA shall be capable of observing the gravitational waves from at least 50 % of all $z \sim 2$ coalescing binary systems consisting of compact objects with masses between $10^5\,M_\odot$ and $10^6\,M_\odot$ and mass ratios between 1 : 1 and 1 : 3. eLISA shall detect these systems with SNR ≥ 5 in each of five equal logarithmic frequency bands between 0.1 mHz (or the lowest observed frequency) and the highest inspiral frequency.
  - ***SR 4.2*** *Test whether the central massive objects in galactic nuclei are consistent with the Kerr black holes of General Relativity.*
    - ∗ **OR 4.2** : eLISA shall have the capability to detect gravitational waves emitted during the last year of inspiral for a $10\,M_\odot$ black hole orbiting a $10^5\,M_\odot$ and $10^6\,M_\odot$ black hole up to $z = 0.7$ with SNR > 20. eLISA shall have a science mission duration with adequate observation time for extreme mass-ratio inspirals (EMRIs) to sweep over a range of r/M to map space-time.
  - ***SR 4.3*** *: Perform precision tests of dynamical strong-field gravity.*
    - ∗ **OR 4.3.1** : eLISA shall have the capability to observe the inspiral radiation from massive black hole with masses between $10^5\,M_\odot - 10^6\,M_\odot$ and mass ratio $m_2/m_1 > 1/3$ to $z \leq 5$ with an average SNR > 30, measuring the mass to better than 1 % and spin parameters to better than 0.1. The SNR should be sufficient to check consistency of the inspiral waveform with the predictions of the General Theory of Relativity.

    - **OR 4.3.2** : eLISA shall have the capability to observe the merger and ring-down radiation from massive black hole with masses between $10^5\,M_\odot - 10^6\,M_\odot$ and mass ratio $m_2/m_1 > 1/3$ to $z \leq 8$ with an average SNR > 60, measuring the mass to better than 1 % and spin parameters to better than 0.3. The SNR should be sufficient to check consistency with the predictions of the General Theory of Relativity based on inspiral measurements.

- ***Cosmology***
  - ***SR 5.1*** *: Measure the spectrum of cosmological backgrounds, or set upper limits on them in the* $10^{-4}Hz - 10^{-1}Hz$ *band.*
    - **OR 5.1** : eLISA shall be capable of setting an upper limit on the spectrum of a stochastic gravitational wave background in the 10^{-4}Hz – 10^{-1}Hz band.
  - ***SR 5.2*** *: Search for gravitational wave bursts from cosmic string cusps and kinks.*
    - **OR 5.2** : eLISA shall be capable of detecting gravitational wave bursts from cusps or kinks, or of setting cosmologically interesting constraints on cosmic (super-)strings.

- ***Discovery***
  - ***SR 6.1*** *: Search for unforeseen sources of gravitational waves*
    - **OR 6.1** : eLISA shall be sensitive over discovery space for unforeseen effects (e.g. even at frequencies where we cannot predict likely signals from known classes of astrophysical sources). eLISA shall allow for reliable separation of real strain signals from instrumental and environmental artifacts.

Acknowledgements

The following scientists contributed significantly through work regarding the previous study (in alphabetical order): Berangere Argence (APC), Stuart Aston (Birmingham), Gerard Auger (APC), John Baker (GSFC), Simon Barke (AEI), Matthew Benacquista (UTB), Iouri Bykov (AEI), Martin Caldwell (RAL), Jordan Camp (GSFC), John Conklin (Stanford), Dan deBra (Stanford), Luciano Di Fiore (Naples), Christian Diekmann (AEI), Juan Jose Esteban Delgado (AEI), Roland Fleddermann (AEI), Antonio Garcia (AEI), Catia Grimani (Urbino) Felipe Guzman (AEI/GSFC), Hubert Halloin (APC), Tupper Hyde (GSFC), Ian Harris (JPL), Gerhard Heinzel (AEI), Martin Hewitson (AEI) Steven Hochman (U Florida), Daniel Hollington (Imperial College), Nick Jedrich (GSFC), Mac Keiser (Stanford), Christian Killow (Glasgow), William Klipstein (JPL), Joachim Kullmann (AEI), Jeffrey Livas (GSFC), Achmed Mansoor (GSFC), Kirk McKenzie (JPL), Stephen Merkowitz (GSFC), Shawn Mitryk (U Florida), Anneke Monsky (AEI), Guido Müller (U Florida), Miquel Nofrarias (AEI), Kenji Numata (GSFC), Frank Ohme (AEI), Eric Plagnol (APC), Moshe Pniel (JPL), Scott Pollack (University of Washington), Alix Preston (UF), Volker Quetschke (UTB), Emma Robinson (AEI), Dave Robertson (Glasgow), Albrecht Rüdiger (AEI), Josep Sanjuan (IEEC Barcelona), B. Sathyaprakash (U Cardiff), Daniel Shaddock (ANU), Diana Shaul (Imperial College), Ben Sheard (AEI), Robert Spero (JPL), Frank Steier (AEI), Ke-Xun Sun (Stanford), Dylan Sweeney (U Florida), David Tanner (UF), Michael Troebs (AEI), Glenn de Vine (JPL), Vinzenz Wand (AEI), Gudrun Wanner (AEI), Brent Ware (JPL), Peter Wass (U Trento/Imperial College), Bill Weber (U Trento), Yinan Yu (U Florida), Alberto Vecchio (U Birmingham), and Andreas Zoellner (Stanford).

We acknowledge the rest of the members of the former joint science team for LISA, whose work constituted a crucial starting point for our article, even if they are not included in the authorship list of this paper: Thomas A Prince (JPL), Peter Bender (JILA), Sasha Buchman (Stanford University), Joan Centrella (NASA GFSC), Massimo Cerdonio (INFN Padua), Mike Cruise (University of Birmingham), Curt J Cutler (JPL), Lee Sam Finn (PennState University), Jens Gundlach (University of Washington), Craig Hogan (Fermilab), Jim Hough (University of Glasgow), Scott A. Hughes (MIT), Piero Madau (UC Santa Cruz), Yannick Mellier (IAP), Sterl Phinney (Caltech), Douglas O. Richstone (University of Michigan), Kip Thorne (Caltech), and Jean-Yves Vinet (Observatoire de Côte d'Azur).

It is a pleasure for P.A.S to thank Antón for the very interesting discussions about black holes and astrophysics. This work has been supported by the Transregio 7 "Gravitational Wave Astronomy" financed by the Deutsche Forschungsgemeinschaft DFG (German Research Foundation). E.Berti was supported by NSF Grant PHY-0900735 and by NSF CAREER Grant PHY-1055103. A. Klein was supported by the Swiss National Science Foundation. T. B. Littenberg was supported by NASA Grant 08-ATFP08-0126. R. N. Lang was supported by an appointment to the NASA Postdoctoral Program at the Goddard Space Flight Center, administered by Oak Ridge Associated Universities through a contract with NASA. M. Vallisneri performed this work at the Jet Propulsion Laboratory, California Institute of Technology, under contract with the National Aeronautics and Space Administration.

References

Abel, T., Bryan, G. L., and Norman, M. L. (2002). The Formation of the First Star in the Universe. *Science*, 295:93–98.

Alexander, T. (2005). Stellar processes near the massive black hole in the Galactic center [review article]. *Phys. Rep.*, 419:65–142.

Aller, M. C. and Richstone, D. (2002). The Cosmic Density of Massive Black Holes from Galaxy Velocity Dispersions. *AJ*, 124:3035–3041.

Alsing, J., Berti, E., Will, C., and Zaglauer, H. (2011). Gravitational radiation from compact binary systems in the massive Brans-Dicke theory of gravity. *ArXiv e-prints*.

Amaro-Seoane, P. (2006). Gravitational waves from coalescing massive black holes in young dense clusters. In S. M. Merkovitz & J. C. Livas, editor, *Laser Interferometer Space Antenna: 6th International LISA Symposium*, volume 873 of *American Institute of Physics Conference Series*, pages 250–256.

Amaro-Seoane, P., Brem, P., Cuadra, J., and Armitage, P. J. (2012). The Butterfly Effect in the Extreme-mass Ratio Inspiral Problem. *ApJ Letts*, 744:L20.

Amaro-Seoane, P., Eichhorn, C., Porter, E. K., and Spurzem, R. (2010a). Binaries of massive black holes in rotating clusters: dynamics, gravitational waves, detection and the role of eccentricity. *MNRAS*, 401:2268–2284.

Amaro-Seoane, P., Eichhorn, C., Porter, E. K., and Spurzem, R. (2010b). Binaries of massive black holes in rotating clusters: dynamics, gravitational waves, detection and the role of eccentricity. *MNRAS*, 401:2268–2284.

Amaro-Seoane, P. and Freitag, M. (2006a). Intermediate-Mass Black Holes in Colliding Clusters: Implications for Lower Frequency Gravitational-Wave Astronomy. *ApJ*, 653:L53–L56.

Amaro-Seoane, P. and Freitag, M. (2006b). Intermediate-Mass Black Holes in Colliding Clusters: Implications for Lower Frequency Gravitational-Wave Astronomy. *ApJ Letts*, 653:L53–L56.

Amaro-Seoane, P., Gair, J. R., Freitag, M., Miller, M. C., Mandel, I., Cutler, C. J., and Babak, S. (2007). TOPICAL REVIEW: Intermediate and extreme mass-ratio inspirals — astrophysics, science applications and detection using LISA. *Class. Quantum Grav.*, 24:113–+.

Amaro-Seoane, P., Miller, M. C., and Freitag, M. (2009). Gravitational Waves from Eccentric Intermediate-Mass Black Hole Binaries. *ApJ Letts*, 692:L50–L53.

Amaro-Seoane, P. and Preto, M. (2011). The impact of realistic models of mass segregation on the event rate of extreme-mass ratio inspirals and cusp re-growth. *Class. Quantum Grav.*, 28(9):094017–+.

Amaro-Seoane, P. and Santamaría, L. (2010). Detection of IMBHs with Ground-based Gravitational Wave Observatories: A Biography of a Binary of Black Holes, from Birth to Death. *ApJ*, 722:1197–1206.

Armitage, P. J. and Natarajan, P. (2002). Accretion during the Merger of Supermassive Black Holes. *ApJ*, 567:L9–L12.

Armitage, P. J. and Natarajan, P. (2005). Eccentricity of Supermassive Black Hole Binaries Coalescing from Gas-rich Mergers. *ApJ*, 634:921–927.

Arun, K. G., Babak, S., Berti, E., Cornish, N., Cutler, C., Gair, J., Hughes, S. A., Iyer, B. R., Lang, R. N., Mandel, I., Porter, E. K., Sathyaprakash, B. S., Sinha, S., Sintes, A. M., Trias, M., Van Den Broeck, C., and Volonteri, M. (2009). Massive black-hole binary inspirals: results from the LISA parameter estimation taskforce. *Class. Quantum Grav.*, 26(9):094027–+.

Arun, K. G., Iyer, B. R., Qusailah, M. S. S., and Sathyaprakash, B. S. (2006). Probing the nonlinear structure of general relativity with black hole binaries. *Phys. Rev. D*, 74(2):024006–+.

Arvanitaki, A. and Dubovsky, S. (2011). Exploring the string axiverse with precision black hole physics. *Phys. Rev. D*, 83(4):044026–+.

Babak, S., Baker, J. G., Benacquista, M. J., Cornish, N. J., Larson, S. L., Mandel, I., McWilliams, S. T., Petiteau, A., Porter, E. K., Robinson, E. L., Vallisneri, M., Vecchio, A., Data Challenge Task Force, t. M. L., Adams, M., Arnaud, K. A., Błaut, A., Bridges, M., Cohen, M., Cutler, C., Feroz, F., Gair, J. R., Graff, P., Hobson, M., Shapiro Key, J., Królak, A., Lasenby, A., Prix, R., Shang, Y., Trias, M., Veitch, J., Whelan, J. T., and participants, t. C. . (2010). The Mock LISA Data Challenges: from challenge 3 to challenge 4. *Class. Quantum Grav.*, 27(8):084009–+.

Babak, S., Gair, J. R., Petiteau, A., and Sesana, A. (2011). Fundamental physics and cosmology with LISA. *Class. Quantum Grav.*, 28(11):114001–+.

Bahcall, J. N. and Wolf, R. A. (1976). Star distribution around a massive black hole in a globular cluster. *ApJ*, 209:214–232.

Bahcall, J. N. and Wolf, R. A. (1977). The star distribution around a massive black hole in a globular cluster. II Unequal star masses. *ApJ*, 216:883–907.

Baker, J. G., Boggs, W. D., Centrella, J., Kelly, B. J., McWilliams, S. T., Miller, M. C., and van Meter, J. R. (2008). Modeling Kicks from the Merger of Generic Black Hole Binaries. *ApJ*, 682:L29–L32.

Baker, J. G., Centrella, J., Choi, D.-I., Koppitz, M., and van Meter, J. (2006). Gravitational-Wave Extraction from an

Inspiraling Configuration of Merging Black Holes. *Phys. Rev. Lett.*, 96(11):111102–+.

Ballo, L., Braito, V., Della Ceca, R., Maraschi, L., Tavecchio, F., and Dadina, M. (2004). Arp 299: A Second Merging System with Two Active Nuclei? *ApJ*, 600:634–639.

Barack, L. and Cutler, C. (2004). LISA capture sources: Approximate waveforms, signal-to-noise ratios, and parameter estimation accuracy. *Phys. Rev. D*, 69:082005–+.

Barausse, E. and Rezzolla, L. (2008). Influence of the hydrodynamic drag from an accretion torus on extreme mass-ratio inspirals. *Phys. Rev. D*, 77(10):104027–+.

Barausse, E., Rezzolla, L., Petroff, D., and Ansorg, M. (2007). Gravitational waves from extreme mass ratio inspirals in nonpure Kerr spacetimes. *Phys. Rev. D*, 75(6):064026–+.

Barausse, E. and Sotiriou, T. P. (2008). Perturbed Kerr Black Holes can probe deviations from General Relativity. *Phys.Rev.Lett.*, 101:099001.

Barclay, T., Ramsay, G., Hakala, P., Napiwotzki, R., Nelemans, G., Potter, S., and Todd, I. (2011). Stellar variability on time-scales of minutes: results from the first 5 yr of the Rapid Temporal Survey. *MNRAS*, 413:2696–2708.

Bardeen, J. M. (1970). Kerr Metric Black Holes. *Nature*, 226:64–65.

Bardeen, J. M. and Petterson, J. A. (1975). The Lense-Thirring Effect and Accretion Disks around Kerr Black Holes. *ApJ*, 195:L65+.

Barrows, R. S., Lacy, C. H. S., Kennefick, D., Kennefick, J., and Seigar, M. S. (2011). Unusual double-peaked emission in the SDSS quasar J093201.60 + 031858.7. *NewA*, 16:122–127.

Barth, A. J., Ho, L. C., Rutledge, R. E., and Sargent, W. L. W. (2004). POX 52: A Dwarf Seyfert 1 Galaxy with an Intermediate-Mass Black Hole. *ApJ*, 607:90–102.

Barth, A. J., Strigari, L. E., Bentz, M. C., Greene, J. E., and Ho, L. C. (2009). Dynamical Constraints on the Masses of the Nuclear Star Cluster and Black Hole in the Late-Type Spiral Galaxy NGC 3621. *ApJ*, 690:1031–1044.

Begelman, M. C., Blandford, R. D., and Rees, M. J. (1980). Massive black hole binaries in active galactic nuclei. *Nature*, 287:307–309.

Begelman, M. C. and Shlosman, I. (2009). Angular Momentum Transfer and Lack of Fragmentation in Self-Gravitating Accretion Flows. *ApJ*, 702:L5–L8.

Begelman, M. C., Volonteri, M., and Rees, M. J. (2006). Formation of supermassive black holes by direct collapse in pre-galactic haloes. *MNRAS*, 370:289–298.

Bekki, K. and Graham, A. W. (2010). On the Transition from Nuclear-cluster- to Black-hole-dominated Galaxy Cores. *ApJ*, 714:L313–L317.

Belczynski, K., Benacquista, M., and Bulik, T. (2010). Double Compact Objects as Low-frequency Gravitational Wave Sources. *ApJ*, 725:816–823.

Belczynski, K., Kalogera, V., and Bulik, T. (2002). A Comprehensive Study of Binary Compact Objects as Gravitational Wave Sources: Evolutionary Channels, Rates, and Physical Properties. *ApJ*, 572:407–431.

Bell, E. F., Phleps, S., Somerville, R. S., Wolf, C., Borch, A., and Meisenheimer, K. (2006). The Merger Rate of Massive Galaxies. *ApJ*, 652:270–276.

Benacquista, M. and Holley-Bockelmann, K. (2006). Consequences of Disk Scale Height on LISA Confusion Noise from Close White Dwarf Binaries. *ApJ*, 645:589–596.

Berczik, P., Merritt, D., and Spurzem, R. (2005). Long-Term Evolution of Massive Black Hole Binaries. II. Binary Evolution in Low-Density Galaxies. *ApJ*, 633:680–687.

Berczik, P., Merritt, D., Spurzem, R., and Bischof, H. (2006). Efficient Merger of Binary Supermassive Black Holes in Nonaxisymmetric Galaxies. *ApJ*, 642:L21–L24.

Berti, E. (2006). LISA observations of massive black hole mergers: event rates and issues in waveform modelling. *Class. Quantum Grav.*, 23:785–+.

Berti, E., Buonanno, A., and Will, C. M. (2005). Estimating spinning binary parameters and testing alternative theories of gravity with LISA. *Phys. Rev. D*, 71:084025–+.

Berti, E., Cardoso, J., Cardoso, V., and Cavaglià, M. (2007). Matched filtering and parameter estimation of ringdown waveforms. *Phys. Rev. D*, 76(10):104044–+.

Berti, E. and Cardoso, V. (2006). Supermassive black holes or boson stars? Hair counting with gravitational wave detectors. *Int.J.Mod.Phys.*, D15:2209–2216.

Berti, E., Cardoso, V., and Starinets, A. O. (2009). TOPICAL REVIEW: Quasinormal modes of black holes and black branes. *Class. Quantum Grav.*, 26(16):163001.

Berti, E., Cardoso, V., and Will, C. M. (2006). Gravitational-wave spectroscopy of massive black holes with the space interferometer LISA. *Phys. Rev. D*, 73:064030–+.

Berti, E., Gair, J., and Sesana, A. (2011). Graviton mass bounds from space-based gravitational-wave observations of massive black hole populations. *ArXiv e-prints*.

Berti, E. and Volonteri, M. (2008). Cosmological Black Hole Spin Evolution by Mergers and Accretion. *ApJ*, 684:822–828.

Bertone, S., De Lucia, G., and Thomas, P. A. (2007). The recycling of gas and metals in galaxy formation: predictions of a dynamical feedback model. *MNRAS*, 379:1143–1154.

Bhattacharya, D. and van den Heuvel, E. P. J. (1991). Formation and evolution of binary and millisecond radio pulsars. *Phys. Rep.*, 203:1–124.

Bildsten, L. (1998). Gravitational Radiation and Rotation of Accreting Neutron Stars. *ApJ*, 501:L89+.

Binétruy, P., Bohé, A., Caprini, C., and Dufaux, J.-F. (2012). Cosmological Backgrounds of Gravitational Waves and eLISA/NGO: Phase Transitions, Cosmic Strings and Other Sources. *ArXiv e-prints*.

Binétruy, P., Bohé, A., Hertog, T., and Steer, D. A. (2010). Gravitational wave signatures from kink proliferation on cosmic (super-) strings. *Phys. Rev. D*, 82(12):126007–+.

Blanchet, L. (2006). Gravitational radiation from post-newtonian sources and inspiralling compact binaries. *Living Reviews in Relativity*, 9(4).

Blecha, L., Cox, T. J., Loeb, A., and Hernquist, L. (2011). Recoiling black holes in merging galaxies: relationship to active galactic nucleus lifetimes, starbursts and the M_{BH}-σ_* relation. *MNRAS*, 412:2154–2182.

Blecha, L. and Loeb, A. (2008). Effects of gravitational-wave recoil on the dynamics and growth of supermassive black holes. *MNRAS*, 390:1311–1325.

Bogdanović, T., Eracleous, M., and Sigurdsson, S. (2009). SDSS J092712.65+294344.0: Recoiling Black Hole or a Subparsec Binary Candidate? *ApJ*, 697:288–292.

Bogdanović, T., Smith, B. D., Sigurdsson, S., and Eracleous, M. (2008). Modeling of Emission Signatures of Massive Black Hole Binaries. I. Methods. *ApJS*, 174:455–480.

Bohé, A. (2011). Gravitational power from cosmic string loops with many kinks. *Phys. Rev. D*, 84(6):065016–+.

Boroson, T. A. and Lauer, T. R. (2009). A candidate sub-parsec supermassive binary black hole system. *Nature*, 458:53–55.

Boylan-Kolchin, M., Ma, C.-P., and Quataert, E. (2004). Core Formation in Galactic Nuclei due to Recoiling Black Holes. *ApJ*, 613:L37–L40.

Boyle, B. J. and Terlevich, R. J. (1998). The cosmological evolution of the QSO luminosity density and of the star formation rate. *MNRAS*, 293:L49–L51.

Bromm, V., Coppi, P. S., and Larson, R. B. (2002). The Formation of the First Stars. I. The Primordial Star-forming Cloud. *ApJ*, 564:23–51.

Bromm, V. and Loeb, A. (2003). Formation of the First Supermassive Black Holes. *ApJ*, 596:34–46.

Brown, W. R., Geller, M. J., Kenyon, S. J., and Bromley, B. C. (2009). The Anisotropic Spatial Distribution of Hypervelocity Stars. *ApJ*, 690:L69–L71.

Brown, W. R., Kilic, M., Hermes, J. J., Allende Prieto, C., Kenyon, S. J., and Winget, D. E. (2011). A 12 Minute Orbital Period Detached White Dwarf Eclipsing Binary. *ApJ*, 737:L23+.

Brustein, R., Gasperini, M., Giovannini, M., and Veneziano, G. (1995). Relic gravitational waves from string cosmology. *Physics Letters B*, 361:45–51.

Bullock, J. S., Dekel, A., Kolatt, T. S., Kravtsov, A. V., Klypin, A. A., Porciani, C., and Primack, J. R. (2001). A Universal Angular Momentum Profile for Galactic Halos. *ApJ*, 555:240–257.

Buonanno, A. (2003). TASI Lectures on Gravitational Waves from the Early Universe. *ArXiv e-prints*.

Buonanno, A., Maggiore, M., and Ungarelli, C. (1997). Spectrum of relic gravitational waves in string cosmology. *Phys. Rev. D*, 55:3330–3336.

Callegari, S., Kazantzidis, S., Mayer, L., Colpi, M., Bellovary, J. M., Quinn, T., and Wadsley, J. (2011). Growing Massive Black Hole Pairs in Minor Mergers of Disk Galaxies. *ApJ*, 729:85–+.

Callegari, S., Mayer, L., Kazantzidis, S., Colpi, M., Governato, F., Quinn, T., and Wadsley, J. (2009). Pairing of Supermassive Black Holes in Unequal-Mass Galaxy Mergers. *ApJ*, 696:L89–L92.

Campanelli, M., Lousto, C. O., Marronetti, P., and Zlochower, Y. (2006). Accurate Evolutions of Orbiting Black-Hole Binaries without Excision. *Phys. Rev. Lett.*, 96(11):111101–+.

Campanelli, M., Lousto, C. O., Zlochower, Y., and Merritt, D. (2007). Maximum Gravitational Recoil. *Phys. Rev. Lett.*, 98(23):231102–+.

Caprini, C., Durrer, R., and Servant, G. (2009). The stochastic gravitational wave background from turbulence and magnetic fields generated by a first-order phase transition. *JCAP*, 0912:024.

Cardoso, V., Chakrabarti, S., Pani, P., Berti, E., and Gualtieri, L. (2011). Floating and sinking: The Imprint of massive scalars around rotating black holes. *Phys.Rev.Lett.*, 107:241101.

Centrella, J., Baker, J. G., Kelly, B. J., and van Meter, J. R. (2010). The Final Merger of Black-Hole Binaries. *Annual Review of Nuclear and Particle Science*, 60:75–100.

Chakrabarty, D., Morgan, E. H., Muno, M. P., Galloway, D. K., Wijnands, R., van der Klis, M., and Markwardt, C. B. (2003). Nuclear-powered millisecond pulsars and the maximum spin frequency of neutron stars. *Nature*, 424:42–44.

Chandrasekhar, S. (1943). Dynamical Friction. I. General Considerations: the Coefficient of Dynamical Friction. *ApJ*, 97:255–+.

Chandrasekhar, S. and Detweiler, S. (1975). The quasi-normal modes of the Schwarzschild black hole. *Royal Soc. of London Proc. Series A*, 344:441–452.

Chirenti, C. B. M. H. and Rezzolla, L. (2007). How to tell a gravastar from a black hole. *Class. Quantum Grav.*, 24:4191–4206.

Chongchitnan, S. and Efstathiou, G. (2006). Prospects for direct detection of primordial gravitational waves. *Phys. Rev. D*, 73(8):083511–+.

Ciotti, L., Ostriker, J. P., and Proga, D. (2010). Feedback from Central Black Holes in Elliptical Galaxies. III. Models with Both Radiative and Mechanical Feedback. *ApJ*, 717:708–723.

Civano, F., Elvis, M., Lanzuisi, G., Jahnke, K., Zamorani, G., Blecha, L., Bongiorno, A., Brusa, M., Comastri, A., Hao, H., Leauthaud, A., Loeb, A., Mainieri, V., Piconcelli, E., Salvato, M., Scoville, N., Trump, J., Vignali, C., Aldcroft, T., Bolzonella, M., Bressert, E., Finoguenov, A., Fruscione, A., Koekemoer, A. M., Cappelluti, N., Fiore, F., Giodini, S., Gilli, R., Impey, C. D., Lilly, S. J., Lusso, E., Puccetti, S., Silverman, J. D., Aussel, H., Capak, P., Frayer, D., Le Floch, E., McCracken, H. J., Sanders, D. B., Schiminovich, D., and Taniguchi, Y. (2010). A Runaway Black Hole in COSMOS: Gravitational Wave or Slingshot Recoil? *ApJ*, 717:209–222.

Clark, P. C., Glover, S. C. O., Klessen, R. S., and Bromm, V. (2011). Gravitational Fragmentation in Turbulent Primordial Gas and the Initial Mass Function of Population III Stars. *ApJ*, 727:110–+.

Collins, N. A. and Hughes, S. A. (2004). Towards a formalism for mapping the spacetimes of massive compact objects: Bumpy black holes and their orbits. *Phys. Rev. D*, 69(12):124022–+.

Colpi, M. and Dotti, M. (2011). Massive binary black holes in the cosmic landscape. *Advanced Science Letters*, 4(2):181–203.

Colpi, M., Mayer, L., and Governato, F. (1999). Dynamical Friction and the Evolution of Satellites in Virialized Halos: The Theory of Linear Response. *ApJ*, 525:720–733.

Colpi, M., Shapiro, S. L., and Wasserman, I. (1986). Boson stars - Gravitational equilibria of self-interacting scalar fields. *Phys. Rev. Lett.*, 57:2485–2488.

Copeland, E. J., Myers, R. C., and Polchinski, J. (2004). Cosmic F- and D-strings. *Journal of High Energy Physics*, 6:13–+.

Cornish, N., Sampson, L., Yunes, N., and Pretorius, F. (2011). Gravitational wave tests of general relativity with the parameterized post-Einsteinian framework. *Phys. Rev. D*, 84(6):062003–+.

Cornish, N. J. (2011). Detection strategies for extreme mass ratio inspirals. *Class. Quantum Grav.*, 28(9):094016–+.

Cornish, N. J. and Porter, E. K. (2006). MCMC exploration of supermassive black hole binary inspirals. *Class. Quantum Grav.*, 23:761–+.

Cox, T. J. and Loeb, A. (2008). The collision between the Milky Way and Andromeda. *MNRAS*, 386:461–474.

Croton, D. J., Springel, V., White, S. D. M., De Lucia, G., Frenk, C. S., Gao, L., Jenkins, A., Kauffmann, G., Navarro, J. F., and Yoshida, N. (2006). The many lives of active galactic nuclei: cooling flows, black holes and the luminosities and colours of galaxies. *MNRAS*, 365:11–28.

Cuadra, J., Armitage, P. J., Alexander, R. D., and Begelman, M. C. (2009). Massive black hole binary mergers within subparsec scale gas discs. *MNRAS*, 393:1423–1432.

Damour, T., Nagar, A., and Trias, M. (2011). Accuracy and effectualness of closed-form, frequency-domain waveforms for nonspinning black hole binaries. *Phys. Rev. D*, 83(2):024006–+.

Damour, T. and Vilenkin, A. (2005). Gravitational radiation from cosmic (super)strings: Bursts, stochastic background, and observational windows. *Phys. Rev. D*, 71(6):063510–+.

Dan, M., Rosswog, S., Guillochon, J., and Ramirez-Ruiz, E. (2011). Prelude to A Double Degenerate Merger: The Onset of Mass Transfer and Its Impact on Gravitational Waves and Surface Detonations. *ApJ*, 737:89–+.

Davies, M. B., Miller, M. C., and Bellovary, J. M. (2011). Supermassive Black Hole Formation Via Gas Accretion in Nuclear Stellar Clusters. *ApJ*, 740:L42+.

De Lucia, G., Springel, V., White, S. D. M., Croton, D., and Kauffmann, G. (2006). The formation history of elliptical galaxies. *MNRAS*, 366:499–509.

De Marco, O., Passy, J.-C., Moe, M., Herwig, F., Mac Low, M.-M., and Paxton, B. (2011). On the α formalism for the common envelope interaction. *MNRAS*, 411:2277–2292.

De Propris, R., Conselice, C. J., Liske, J., Driver, S. P., Patton, D. R., Graham, A. W., and Allen, P. D. (2007). The Millennium Galaxy Catalogue: The Connection between Close Pairs and Asymmetry; Implications for the Galaxy Merger Rate. *ApJ*, 666:212–221.

de Ravel, L., Le Fèvre, O., Tresse, L., Bottini, D., Garilli, B., Le Brun, V., Maccagni, D., Scaramella, R., Scodeggio, M., Vettolani, G., Zanichelli, A., Adami, C., Arnouts, S., Bardelli, S., Bolzonella, M., Cappi, A., Charlot, S., Ciliegi, P., Contini, T., Foucaud, S., Franzetti, P., Gavignaud, I., Guzzo, L., Ilbert, O., Iovino, A., Lamareille, F., McCracken, H. J., Marano, B., Marinoni, C., Mazure, A., Meneux, B., Merighi, R., Paltani, S., Pellò, R., Pollo, A., Pozzetti, L., Radovich, M., Vergani, D., Zamorani, G., Zucca, E., Bondi, M., Bongiorno, A., Brinchmann, J., Cucciati, O., de La Torre, S., Gregorini, L., Memeo, P., Perez-Montero, E., Mellier, Y., Merluzzi, P., and Temporin, S. (2009). The VIMOS VLT Deep Survey. Evolution of the major merger rate since z ˜ 1 from spectroscopically confirmed galaxy pairs. *A&A*, 498:379–397.

Decarli, R., Dotti, M., Montuori, C., Liimets, T., and Ederoclite, A. (2010). The Peculiar Optical Spectrum of 4C+22.25: Imprint of a Massive Black Hole Binary? *ApJ*, 720:L93–L96.

Detweiler, S. (1980). Klein-Gordon equation and rotating black holes. *Phys. Rev. D*, 22:2323–2326.

Devecchi, B., Rasia, E., Dotti, M., Volonteri, M., and Colpi, M. (2009). Imprints of recoiling massive black holes on the hot gas of early-type galaxies. *MNRAS*, 394:633–640.

Devecchi, B. and Volonteri, M. (2009). Formation of the First Nuclear Clusters and Massive Black Holes at High Redshift. *ApJ*, 694:302–313.

Di Matteo, T., Colberg, J., Springel, V., Hernquist, L., and Sijacki, D. (2008). Direct Cosmological Simulations of the Growth of Black Holes and Galaxies. *ApJ*, 676:33–53.

Di Matteo, T., Springel, V., and Hernquist, L. (2005). Energy input from quasars regulates the growth and activity of black holes and their host galaxies. *Nature*, 433:604–607.

Dijkstra, M., Haiman, Z., Mesinger, A., and Wyithe, J. S. B. (2008). Fluctuations in the high-redshift Lyman-Werner background: close halo pairs as the origin of supermassive black holes. *MNRAS*, 391:1961–1972.

Dotan, C., Rossi, E. M., and Shaviv, N. J. (2011). A lower limit on the halo mass to form supermassive black holes. *MNRAS*, pages 1661–+.

Dotti, M., Colpi, M., and Haardt, F. (2006). Laser Interferometer Space Antenna double black holes: dynamics in gaseous nuclear discs. *mnras*, 367:103–112.

Dotti, M., Colpi, M., Haardt, F., and Mayer, L. (2007). Supermassive black hole binaries in gaseous and stellar circum-nuclear discs: orbital dynamics and gas accretion. *MNRAS*, 379:956–962.

Dotti, M., Montuori, C., Decarli, R., Volonteri, M., Colpi, M., and Haardt, F. (2009a). SDSSJ092712.65+294344.0: a candidate massive black hole binary. *MNRAS*, 398:L73–L77.

Dotti, M., Ruszkowski, M., Paredi, L., Colpi, M., Volonteri, M., and Haardt, F. (2009b). Dual black holes in merger remnants - I. Linking accretion to dynamics. *MNRAS*, 396:1640–1646.

Dotti, M., Volonteri, M., Perego, A., Colpi, M., Ruszkowski, M., and Haardt, F. (2010). Dual black holes in merger remnants - II. Spin evolution and gravitational recoil. *MNRAS*, 402:682–690.

Drasco, S. and Hughes, S. A. (2004). Rotating black hole orbit functionals in the frequency domain. *Phys. Rev. D*, 69(4):044015–+.

Drasco, S. and Hughes, S. A. (2006). Gravitational wave snapshots of generic extreme mass ratio inspirals. *Phys. Rev. D*, 73(2):024027–+.

Dreyer, O., Kelly, B., Krishnan, B., Finn, L. S., Garrison, D., and Lopez-Aleman, R. (2004). Black-hole spectroscopy: testing general relativity through gravitational-wave observations. *Class. Quantum Grav.*, 21:787–803.

D'Souza, M. C. R., Motl, P. M., Tohline, J. E., and Frank, J. (2006). Numerical Simulations of the Onset and Stability of Dynamical Mass Transfer in Binaries. *ApJ*, 643:381–401.

Dufaux, J. F., Bergman, A., Felder, G. N., Kofman, L., and Uzan, J.-P. (2007). Theory and Numerics of Gravitational Waves from Preheating after Inflation. *Phys. Rev.*, D76:123517.

Dufaux, J.-F., Felder, G., Kofman, L., and Navros, O. (2009). Gravity Waves from Tachyonic Preheating after Hybrid Inflation. *JCAP*, 0903:001.

Easther, R. and Lim, E. A. (2006). Stochastic gravitational wave production after inflation. *Journal of Cosmology and Astro-Particle Physics*, 4:10–+.

Edlund, J. A., Tinto, M., Królak, A., and Nelemans, G. (2005). White-dwarf white-dwarf galactic background in the LISA data. *Phys. Rev. D*, 71:122003–+.

Eisenhauer, F., Genzel, R., Alexander, T., Abuter, R., Paumard, T., Ott, T., Gilbert, A., Gillessen, S., Horrobin, M., Trippe, S., Bonnet, H., Dumas, C., Hubin, N., Kaufer, A., Kissler-Patig, M., Monnet, G., Ströbele, S., Szeifert, T., Eckart, A., Schödel, R., and Zucker, S. (2005). SINFONI in the Galactic Center: Young Stars and Infrared Flares in the Central Light-Month. *ApJ*, 628:246–259.

Enoki, M., Inoue, K. T., Nagashima, M., and Sugiyama, N. (2004). Gravitational Waves from Supermassive Black Hole Coalescence in a Hierarchical Galaxy Formation Model. *ApJ*, 615:19–28.

Eracleous, M., Boroson, T. A., Halpern, J. P., and Liu, J. (2011). A Large Systematic Search for Recoiling and Close

Supermassive Binary Black Holes. *ArXiv e-prints*.

Escala, A., Larson, R. B., Coppi, P. S., and Mardones, D. (2004). The Role of Gas in the Merging of Massive Black Holes in Galactic Nuclei. I. Black Hole Merging in a Spherical Gas Cloud. *ApJ*, 607:765–777.

Esposito-Farèse, G. (2004). Tests of Scalar-Tensor Gravity. In C. J. A. P. Martins, P. P. Avelino, M. S. Costa, K. Mack, M. F. Mota, & M. Parry, editor, *Phi in the Sky: The Quest for Cosmological Scalar Fields*, volume 736 of *AIP Conf. Series*, pages 35–52. AIP.

Fabbiano, G., Wang, J., Elvis, M., and Risaliti, G. (2011). A close nuclear black-hole pair in the spiral galaxy NGC3393. *Nature*, 477:431–434.

Fan, X., Hennawi, J. F., Richards, G. T., Strauss, M. A., Schneider, D. P., Donley, J. L., Young, J. E., Annis, J., Lin, H., Lampeitl, H., Lupton, R. H., Gunn, J. E., Knapp, G. R., Brandt, W. N., Anderson, S., Bahcall, N. A., Brinkmann, J., Brunner, R. J., Fukugita, M., Szalay, A. S., Szokoly, G. P., and York, D. G. (2004). A Survey of $z > 5.7$ Quasars in the Sloan Digital Sky Survey. III. Discovery of Five Additional Quasars. *AJ*, 128:515–522.

Fan, X., Narayanan, V. K., Lupton, R. H., Strauss, M. A., Knapp, G. R., Becker, R. H., White, R. L., Pentericci, L., Leggett, S. K., Haiman, Z., Gunn, J. E., Ivezić, Ž., Schneider, D. P., Anderson, S. F., Brinkmann, J., Bahcall, N. A., Connolly, A. J., Csabai, I., Doi, M., Fukugita, M., Geballe, T., Grebel, E. K., Harbeck, D., Hennessy, G., Lamb, D. Q., Miknaitis, G., Munn, J. A., Nichol, R., Okamura, S., Pier, J. R., Prada, F., Richards, G. T., Szalay, A., and York, D. G. (2001). A Survey of $z > 5.8$ Quasars in the Sloan Digital Sky Survey. I. Discovery of Three New Quasars and the Spatial Density of Luminous Quasars at z˜6. *AJ*, 122:2833–2849.

Fan, X., Strauss, M. A., Becker, R. H., White, R. L., Gunn, J. E., Knapp, G. R., Richards, G. T., Schneider, D. P., Brinkmann, J., and Fukugita, M. (2006a). Constraining the Evolution of the Ionizing Background and the Epoch of Reionization with z˜6 Quasars. II. A Sample of 19 Quasars. *AJ*, 132:117–136.

Fan, X., Strauss, M. A., Richards, G. T., Hennawi, J. F., Becker, R. H., White, R. L., Diamond-Stanic, A. M., Donley, J. L., Jiang, L., Kim, J. S., Vestergaard, M., Young, J. E., Gunn, J. E., Lupton, R. H., Knapp, G. R., Schneider, D. P., Brandt, W. N., Bahcall, N. A., Barentine, J. C., Brinkmann, J., Brewington, H. J., Fukugita, M., Harvanek, M., Kleinman, S. J., Krzesinski, J., Long, D., Neilsen, Jr., E. H., Nitta, A., Snedden, S. A., and Voges, W. (2006b). A Survey of $z > 5.7$ Quasars in the Sloan Digital Sky Survey. IV. Discovery of Seven Additional Quasars. *AJ*, 131:1203–1209.

Fan, X., Strauss, M. A., Schneider, D. P., Becker, R. H., White, R. L., Haiman, Z., Gregg, M., Pentericci, L., Grebel, E. K., Narayanan, V. K., Loh, Y.-S., Richards, G. T., Gunn, J. E., Lupton, R. H., Knapp, G. R., Ivezić, Ž., Brandt, W. N., Collinge, M., Hao, L., Harbeck, D., Prada, F., Schaye, J., Strateva, I., Zakamska, N., Anderson, S., Brinkmann, J., Bahcall, N. A., Lamb, D. Q., Okamura, S., Szalay, A., and York, D. G. (2003). A Survey of $z > 5.7$ Quasars in the Sloan Digital Sky Survey. II. Discovery of Three Additional Quasars at $z > 6$. *AJ*, 125:1649–1659.

Farmer, A. J. and Phinney, E. S. (2003). The gravitational wave background from cosmological compact binaries. *MNRAS*, 346:1197–1214.

Ferrarese, L., Côté, P., Dalla Bontà, E., Peng, E. W., Merritt, D., Jordán, A., Blakeslee, J. P., Haşegan, M., Mei, S., Piatek, S., Tonry, J. L., and West, M. J. (2006). A Fundamental Relation between Compact Stellar Nuclei, Supermassive Black Holes, and Their Host Galaxies. *ApJ*, 644:L21–L24.

Ferrarese, L. and Ford, H. (2005). Supermassive Black Holes in Galactic Nuclei: Past, Present and Future Research. *Space Science Reviews*, 116:523–624.

Ferrarese, L. and Merritt, D. (2000). A Fundamental Relation between Supermassive Black Holes and Their Host Galaxies. *ApJ*, 539:L9–L12.

Finn, L. S. and Thorne, K. S. (2000). Gravitational waves from a compact star in a circular, inspiral orbit, in the equatorial plane of a massive, spinning black hole, as observed by LISA. *Phys. Rev. D*, 6212:124021–+.

Flanagan, É. É. and Hughes, S. A. (1998). Measuring gravitational waves from binary black hole coalescences. I. Signal to noise for inspiral, merger, and ringdown. *Phys. Rev. D*, 57:4535–4565.

Freitag, M., Amaro-Seoane, P., and Kalogera, V. (2006a). Models of mass segregation at the Galactic Centre. *JPCS*, 54:252–258.

Freitag, M., Amaro-Seoane, P., and Kalogera, V. (2006b). Stellar Remnants in Galactic Nuclei: Mass Segregation. *ApJ*, 649:91–117.

Freitag, M., Rasio, F. A., and Baumgardt, H. (2006c). Runaway collisions in young star clusters - I. Methods and tests. *MNRAS*, 368:121–140.

Fuller, J. and Lai, D. (2011). Dynamical Tides in Compact White Dwarf Binaries: Tidal Synchronization and Dissipation. *ArXiv e-prints*.

Gair, J. and Yunes, N. (2011). Approximate waveforms for extreme-mass-ratio inspirals in modified gravity spacetimes. *Phys. Rev. D*, 84(6):064016–+.

Gair, J. R. (2009a). Probing black holes at low redshift using LISA EMRI observations. *Class. Quantum Grav.*, 26(9):094034–+.

Gair, J. R. (2009b). Probing black holes at low redshift using LISA EMRI observations. *Class. Quantum Grav.*,

26(9):094034–+.

Gair, J. R., Barack, L., Creighton, T., Cutler, C., Larson, S. L., Phinney, E. S., and Vallisneri, M. (2004). Event rate estimates for LISA extreme mass ratio capture sources. *Class. Quantum Grav.*, 21:S1595–S1606.

Gair, J. R., Porter, E., Babak, S., and Barack, L. (2008). A constrained Metropolis Hastings search for EMRIs in the Mock LISA Data Challenge 1B. *Class. Quantum Grav.*, 25(18):184030–+.

Gair, J. R., Tang, C., and Volonteri, M. (2010). LISA extreme-mass-ratio inspiral events as probes of the black hole mass function. *Phys. Rev. D*, 81(10):104014–+.

Galloway, D. K., Chakrabarty, D., Morgan, E. H., and Remillard, R. A. (2002). Discovery of a High-Latitude Accreting Millisecond Pulsar in an Ultracompact Binary. *ApJ*, 576:L137–L140.

Gammie, C. F., Shapiro, S. L., and McKinney, J. C. (2004). Black Hole Spin Evolution. *ApJ*, 602:312–319.

Garcia-Bellido, J. and Figueroa, D. G. (2007). A stochastic background of gravitational waves from hybrid preheating. *Phys. Rev. Lett.*, 98:061302.

Gebhardt, K., Bender, R., Bower, G., Dressler, A., Faber, S. M., Filippenko, A. V., Green, R., Grillmair, C., Ho, L. C., Kormendy, J., Lauer, T. R., Magorrian, J., Pinkney, J., Richstone, D., and Tremaine, S. (2000). A Relationship between Nuclear Black Hole Mass and Galaxy Velocity Dispersion. *ApJ*, 539:L13–L16.

Genzel, R., Eisenhauer, F., and Gillessen, S. (2010). The Galactic Center massive black hole and nuclear star cluster. *Reviews of Modern Physics*, 82:3121–3195.

Genzel, R., Pichon, C., Eckart, A., Gerhard, O. E., and Ott, T. (2000). Stellar dynamics in the Galactic Centre: proper motions and anisotropy. *MNRAS*, 317:348–374.

Genzel, R., Tacconi, L. J., Eisenhauer, F., Förster Schreiber, N. M., Cimatti, A., Daddi, E., Bouché, N., Davies, R., Lehnert, M. D., Lutz, D., Nesvadba, N., Verma, A., Abuter, R., Shapiro, K., Sternberg, A., Renzini, A., Kong, X., Arimoto, N., and Mignoli, M. (2006). The rapid formation of a large rotating disk galaxy three billion years after the Big Bang. *Nature*, 442:786–789.

Ghez, A. M., Duchêne, G., Matthews, K., Hornstein, S. D., Tanner, A., Larkin, J., Morris, M., Becklin, E. E., Salim, S., Kremenek, T., Thompson, D., Soifer, B. T., Neugebauer, G., and McLean, I. (2003). The First Measurement of Spectral Lines in a Short-Period Star Bound to the Galaxy's Central Black Hole: A Paradox of Youth. *ApJ*, 586:L127–L131.

Ghez, A. M., Salim, S., Hornstein, S. D., Tanner, A., Lu, J. R., Morris, M., Becklin, E. E., and Duchêne, G. (2005). Stellar Orbits around the Galactic Center Black Hole. *ApJ*, 620:744–757.

Ghez, A. M., Salim, S., Weinberg, N. N., Lu, J. R., Do, T., Dunn, J. K., Matthews, K., Morris, M. R., Yelda, S., Becklin, E. E., Kremenek, T., Milosavljevic, M., and Naiman, J. (2008). Measuring Distance and Properties of the Milky Way's Central Supermassive Black Hole with Stellar Orbits. *ApJ*, 689:1044–1062.

Gillessen, S., Eisenhauer, F., Trippe, S., Alexander, T., Genzel, R., Martins, F., and Ott, T. (2009). Monitoring Stellar Orbits Around the Massive Black Hole in the Galactic Center. *ApJ*, 692:1075–1109.

Glampedakis, K. and Babak, S. (2006). Mapping spacetimes with LISA: inspiral of a test body in a 'quasi-Kerr' field. *Class. Quantum Grav.*, 23:4167–4188.

González, J. A., Hannam, M., Sperhake, U., Brügmann, B., and Husa, S. (2007). Supermassive Recoil Velocities for Binary Black-Hole Mergers with Antialigned Spins. *Phys. Rev. Lett.*, 98(23):231101–+.

Gould, A. and Rix, H.-W. (2000). Binary Black Hole Mergers from Planet-like Migrations. *ApJ*, 532:L29–L32.

Graham, A. W., Onken, C. A., Athanassoula, E., and Combes, F. (2011). An expanded M_{bh}-σ diagram, and a new calibration of active galactic nuclei masses. *MNRAS*, 412:2211–2228.

Graham, A. W. and Spitler, L. R. (2009). Quantifying the coexistence of massive black holes and dense nuclear star clusters. *MNRAS*, 397:2148–2162.

Greene, J. E. and Ho, L. C. (2004). Active Galactic Nuclei with Candidate Intermediate-Mass Black Holes. *ApJ*, 610:722–736.

Greene, J. E., Ho, L. C., and Barth, A. J. (2008). Black Holes in Pseudobulges and Spheroidals: A Change in the Black Hole-Bulge Scaling Relations at Low Mass. *ApJ*, 688:159–179.

Gualandris, A. and Merritt, D. (2008). Ejection of Supermassive Black Holes from Galaxy Cores. *ApJ*, 678:780–797.

Guedes, J., Madau, P., Kuhlen, M., Diemand, J., and Zemp, M. (2009). Simulations of Recoiling Massive Black Holes in the Via Lactea Halo. *ApJ*, 702:890–900.

Guedes, J., Madau, P., Mayer, L., and Callegari, S. (2011). Recoiling Massive Black Holes in Gas-rich Galaxy Mergers. *ApJ*, 729:125–+.

Gültekin, K., Richstone, D. O., Gebhardt, K., Lauer, T. R., Tremaine, S., Aller, M. C., Bender, R., Dressler, A., Faber, S. M., Filippenko, A. V., Green, R., Ho, L. C., Kormendy, J., Magorrian, J., Pinkney, J., and Siopis, C. (2009). The M-σ and M-L Relations in Galactic Bulges, and Determinations of Their Intrinsic Scatter. *ApJ*, 698:198–221.

Guo, Q., White, S., Boylan-Kolchin, M., De Lucia, G., Kauffmann, G., Lemson, G., Li, C., Springel, V., and Weinmann, S. (2011). From dwarf spheroidals to cD galaxies: simulating the galaxy population in a ΛCDM cosmology. *MNRAS*,

413:101–131.

Gürkan, M. A., Fregeau, J. M., and Rasio, F. A. (2006). Massive Black Hole Binaries from Collisional Runaways. *ApJ*, 640:L39–L42.

Gürkan, M. A., Freitag, M., and Rasio, F. A. (2004). Formation of Massive Black Holes in Dense Star Clusters. I. Mass Segregation and Core Collapse. *ApJ*, 604:632–652.

Gürkan, M. A. and Hopman, C. (2007). Resonant relaxation near a massive black hole: the dependence on eccentricity. *MNRAS*, 379:1083–1088.

Haehnelt, M. G. (1994). Low-Frequency Gravitational Waves from Supermassive Black-Holes. *MNRAS*, 269:199–+.

Haehnelt, M. G., Natarajan, P., and Rees, M. J. (1998). High-redshift galaxies, their active nuclei and central black holes. *MNRAS*, 300:817–827.

Haehnelt, M. G. and Rees, M. J. (1993). The formation of nuclei in newly formed galaxies and the evolution of the quasar population. *MNRAS*, 263:168–178.

Haiman, Z. and Loeb, A. (1998). Observational Signatures of the First Quasars. *ApJ*, 503:505–+.

Haiman, Z., Thoul, A. A., and Loeb, A. (1996). Cosmological Formation of Low-Mass Objects. *ApJ*, 464:523–+.

Häring, N. and Rix, H.-W. (2004). On the Black Hole Mass-Bulge Mass Relation. *ApJ*, 604:L89–L92.

Hayasaki, K., Mineshige, S., and Ho, L. C. (2008). A Supermassive Binary Black Hole with Triple Disks. *ApJ*, 682:1134–1140.

Hayasaki, K. and Okazaki, A. T. (2009). A New Approach for Probing Circumbinary Disks. *ApJ*, 691:L5–L8.

Heger, A., Fryer, C. L., Woosley, S. E., Langer, N., and Hartmann, D. H. (2003). How Massive Single Stars End Their Life. *ApJ*, 591:288–300.

Hogan, C. J. (1986). Gravitational radiation from cosmological phase transitions. *MNRAS*, 218:629–636.

Hogan, C. J. (2000). Gravitational Waves from Mesoscopic Dynamics of the Extra Dimensions. *Phys. Rev. Lett.*, 85:2044–2047.

Hogan, C. J. (2006). Gravitational Wave Sources from New Physics. In *Laser Interferometer Space Antenna: 6th International LISA Symposium*, volume 873 of *AIP Conf. Proc.*, pages 30–40. AIP.

Hogan, C. J. and Bender, P. L. (2001). Estimating stochastic gravitational wave backgrounds with the Sagnac calibration. *Phys. Rev. D*, 64(6):062002–+.

Holz, D. E. and Hughes, S. A. (2005). Using Gravitational-Wave Standard Sirens. *ApJ*, 629:15–22.

Hopkins, P. F., Hernquist, L., Cox, T. J., Di Matteo, T., Robertson, B., and Springel, V. (2006). A Unified, Merger-driven Model of the Origin of Starbursts, Quasars, the Cosmic X-Ray Background, Supermassive Black Holes, and Galaxy Spheroids. *ApJS*, 163:1–49.

Hopkins, P. F., Hernquist, L., Cox, T. J., and Kereš, D. (2008). A Cosmological Framework for the Co-Evolution of Quasars, Supermassive Black Holes, and Elliptical Galaxies. I. Galaxy Mergers and Quasar Activity. *ApJS*, 175:356–389.

Hopkins, P. F., Murray, N., and Thompson, T. A. (2009). The small scatter in BH-host correlations and the case for self-regulated BH growth. *MNRAS*, 398:303–311.

Hopman, C. (2009). Extreme mass ratio inspiral rates: dependence on the massive black hole mass. *Class. Quantum Grav.*, 26(9):094028–+.

Hopman, C. and Alexander, T. (2006a). Resonant Relaxation near a Massive Black Hole: The Stellar Distribution and Gravitational Wave Sources. *ApJ*, 645:1152–1163.

Hopman, C. and Alexander, T. (2006b). The Effect of Mass Segregation on Gravitational Wave Sources near Massive Black Holes. *ApJ*, 645:L133–L136.

Huber, S. J. and Konstandin, T. (2008). Gravitational Wave Production by Collisions: More Bubbles. *JCAP*, 0809:022.

Huerta, E. A. and Gair, J. R. (2009). Influence of conservative corrections on parameter estimation for extreme-mass-ratio inspirals. *Phys. Rev. D*, 79(8):084021–+.

Hughes, S. A. (2006). A brief survey of lisa sources and science. In Merkowitz, S. M. and Livas, J. C., editors, *Laser Interferometer Space Antenna: 6th International LISA Symposium*, volume 873 of *AIP Conf. Series*, pages 13–20. AIP.

Hughes, S. A. and Blandford, R. D. (2003). Black Hole Mass and Spin Coevolution by Mergers. *ApJ*, 585:L101–L104.

Huwyler, C., Klein, A., and Jetzer, P. (2011). Testing General Relativity with LISA including Spin Precession and Higher Harmonics in the Waveform. *ArXiv e-prints*.

Ivanov, P. B., Papaloizou, J. C. B., and Polnarev, A. G. (1999). The evolution of a supermassive binary caused by an accretion disc. *MNRAS*, 307:79–90.

Jiang, Y.-F., Greene, J. E., and Ho, L. C. (2011a). Black Hole Mass and Bulge Luminosity for Low-mass Black Holes. *ApJ*, 737:L45+.

Jiang, Y.-F., Greene, J. E., Ho, L. C., Xiao, T., and Barth, A. J. (2011b). The Host Galaxies of Low-mass Black Holes. *ArXiv e-prints*.

Johansson, P. H., Naab, T., and Burkert, A. (2009). Equal- and Unequal-Mass Mergers of Disk and Elliptical Galaxies with Black Holes. *ApJ*, 690:802–821.

Johnston, S., Bailes, M., Bartel, N., Baugh, C., Bietenholz, M., Blake, C., Braun, R., Brown, J., Chatterjee, S., Darling, J., Deller, A., Dodson, R., Edwards, P. G., Ekers, R., Ellingsen, S., Feain, I., Gaensler, B. M., Haverkorn, M., Hobbs, G., Hopkins, A., Jackson, C., James, C., Joncas, G., Kaspi, V., Kilborn, V., Koribalski, B., Kothes, R., Landecker, T. L., Lenc, E., Lovell, J., Macquart, J.-P., Manchester, R., Matthews, D., McClure-Griffiths, N. M., Norris, R., Pen, U.-L., Phillips, C., Power, C., Protheroe, R., Sadler, E., Schmidt, B., Stairs, I., Staveley-Smith, L., Stil, J., Taylor, R., Tingay, S., Tzioumis, A., Walker, M., Wall, J., and Wolleben, M. (2007). Science with the Australian Square Kilometre Array Pathfinder. *PASA*, 24:174–188.

Jonker, P. G., Bassa, C. G., Nelemans, G., Steeghs, D., Torres, M. A. P., Maccarone, T. J., Hynes, R. I., Greiss, S., Clem, J., Dieball, A., Mikles, V. J., Britt, C. T., Gossen, L., Collazzi, A. C., Wijnands, R., In't Zand, J. J. M., Méndez, M., Rea, N., Kuulkers, E., Ratti, E. M., van Haaften, L. M., Heinke, C., Özel, F., Groot, P. J., and Verbunt, F. (2011). The Galactic Bulge Survey: Outline and X-ray Observations. *ApJS*, 194:18–+.

Jonker, P. G., Torres, M. A. P., Fabian, A. C., Heida, M., Miniutti, G., and Pooley, D. (2010). A bright off-nuclear X-ray source: a type IIn supernova, a bright ULX or a recoiling supermassive black hole in CXOJ122518.6+144545. *MNRAS*, 407:645–650.

Kamaretsos, I., Hannam, M., Husa, S., and Sathyaprakash, B. S. (2011). Black-hole hair loss: learning about binary progenitors from ringdown signals. *ArXiv e-prints*.

Kamionkowski, M., Kosowsky, A., and Turner, M. S. (1994). Gravitational radiation from first order phase transitions. *Phys. Rev.*, D49:2837–2851.

Kasliwal, M. M., Kulkarni, S. R., Gal-Yam, A., Yaron, O., Quimby, R. M., Ofek, E. O., Nugent, P., Poznanski, D., Jacobsen, J., Sternberg, A., Arcavi, I., Howell, D. A., Sullivan, M., Rich, D. J., Burke, P. F., Brimacombe, J., Milisavljevic, D., Fesen, R., Bildsten, L., Shen, K., Cenko, S. B., Bloom, J. S., Hsiao, E., Law, N. M., Gehrels, N., Immler, S., Dekany, R., Rahmer, G., Hale, D., Smith, R., Zolkower, J., Velur, V., Walters, R., Henning, J., Bui, K., and McKenna, D. (2010). Rapidly Decaying Supernova 2010X: A Candidate ".Ia" Explosion. *ApJ*, 723:L98–L102.

Kauffmann, G. and Haehnelt, M. (2000). A unified model for the evolution of galaxies and quasars. *MNRAS*, 311:576–588.

Kesden, M., Gair, J., and Kamionkowski, M. (2005). Gravitational-wave signature of an inspiral into a supermassive horizonless object. *Phys. Rev. D*, 71(4):044015–+.

Kesden, M., Sperhake, U., and Berti, E. (2010). Relativistic Suppression of Black Hole Recoils. *ApJ*, 715:1006–1011.

Khan, F. M., Just, A., and Merritt, D. (2011). Efficient Merger of Binary Supermassive Black Holes in Merging Galaxies. *ApJ*, 732:89–+.

Khlebnikov, S. and Tkachev, I. (1997). Relic gravitational waves produced after preheating. *Phys. Rev. D*, 56:653–660.

King, A. (2003). Black Holes, Galaxy Formation, and the M_{BH}-σ Relation. *ApJ*, 596:L27–L29.

King, A. R., Lubow, S. H., Ogilvie, G. I., and Pringle, J. E. (2005). Aligning spinning black holes and accretion discs. *MNRAS*, 363:49–56.

King, A. R. and Pringle, J. E. (2006). Growing supermassive black holes by chaotic accretion. *MNRAS*, 373:L90–L92.

King, A. R. and Pringle, J. E. (2007). Fuelling active galactic nuclei. *MNRAS*, 377:L25–L28.

Kocsis, B., Yunes, N., and Loeb, A. (2011). Observable signatures of extreme mass-ratio inspiral black hole binaries embedded in thin accretion disks. *Phys. Rev. D*, 84(2):024032–+.

Komossa, S., Burwitz, V., Hasinger, G., Predehl, P., Kaastra, J. S., and Ikebe, Y. (2003). Discovery of a Binary Active Galactic Nucleus in the Ultraluminous Infrared Galaxy NGC 6240 Using Chandra. *ApJ*, 582:L15–L19.

Komossa, S., Zhou, H., and Lu, H. (2008). A Recoiling Supermassive Black Hole in the Quasar SDSS J092712.65+294344.0? *ApJ*, 678:L81–L84.

Konstandin, T., Nardini, G., and Quiros, M. (2010). Gravitational backreaction effects on the holographic phase transition. *Phys. Rev. D*, 82(8):083513–+.

Konstantinidis, S., Amaro-Seoane, P., and Kokkotas, K. D. (2011). Kicking massive black holes off clusters: Intermediate-mass ratio inspirals. *ArXiv e-prints*.

Kormendy, J. and Bender, R. (2009). Correlations between Supermassive Black Holes, Velocity Dispersions, and Mass Deficits in Elliptical Galaxies with Cores. *ApJ*, 691:L142–L146.

Koushiappas, S. M., Bullock, J. S., and Dekel, A. (2004). Massive black hole seeds from low angular momentum material. *MNRAS*, 354:292–304.

Koushiappas, S. M. and Zentner, A. R. (2006). Testing Models of Supermassive Black Hole Seed Formation through Gravity Waves. *ApJ*, 639:7–22.

Kramer, M., Stairs, I. H., Manchester, R. N., McLaughlin, M. A., Lyne, A. G., Ferdman, R. D., Burgay, M., Lorimer, D. R., Possenti, A., D'Amico, N., Sarkissian, J. M., Hobbs, G. B., Reynolds, J. E., Freire, P. C. C., and Camilo, F.

(2006). Tests of General Relativity from Timing the Double Pulsar. *Science*, 314:97–102.

Kramer, M. and Wex, N. (2009). TOPICAL REVIEW: The double pulsar system: a unique laboratory for gravity. *Class. Quantum Grav.*, 26(7):073001–+.

Krolik, J. H. (1999). *Active galactic nuclei: from the central black hole to the galactic environment*. Princeton University Press, Princeton, N.J.

Kuo, C. Y., Braatz, J. A., Condon, J. J., Impellizzeri, C. M. V., Lo, K. Y., Zaw, I., Schenker, M., Henkel, C., Reid, M. J., and Greene, J. E. (2011). The Megamaser Cosmology Project. III. Accurate Masses of Seven Supermassive Black Holes in Active Galaxies with Circumnuclear Megamaser Disks. *ApJ*, 727:20–+.

Lacey, C. and Cole, S. (1993). Merger rates in hierarchical models of galaxy formation. *MNRAS*, 262:627–649.

Lamastra, A., Menci, N., Maiolino, R., Fiore, F., and Merloni, A. (2010). The building up of the black hole-stellar mass relation. *MNRAS*, 405:29–40.

Lauer, T. R., Faber, S. M., Richstone, D., Gebhardt, K., Tremaine, S., Postman, M., Dressler, A., Aller, M. C., Filippenko, A. V., Green, R., Ho, L. C., Kormendy, J., Magorrian, J., and Pinkney, J. (2007). The Masses of Nuclear Black Holes in Luminous Elliptical Galaxies and Implications for the Space Density of the Most Massive Black Holes. *ApJ*, 662:808–834.

Leaver, E. W. (1985). An analytic representation for the quasi-normal modes of Kerr black holes. *Royal Society of London Proceedings Series A*, 402:285–298.

Levan, A. J., Wynn, G. A., Chapman, R., Davies, M. B., King, A. R., Priddey, R. S., and Tanvir, N. R. (2006). Short gamma-ray bursts in old populations: magnetars from white dwarf-white dwarf mergers. *MNRAS*, 368:L1–L5.

Levin, Y. (2007). Starbursts near supermassive black holes: young stars in the Galactic Centre, and gravitational waves in LISA band. *MNRAS*, 374:515–524.

Levitan, D., Fulton, B. J., Groot, P. J., Kulkarni, S. R., Ofek, E. O., Prince, T. A., Shporer, A., Bloom, J. S., Cenko, S. B., Kasliwal, M. M., Law, N. M., Nugent, P. E., Poznanski, D., Quimby, R. M., Horesh, A., Sesar, B., and Sternberg, A. (2011). PTF1 J071912.13+485834.0: An Outbursting AM CVn System Discovered by a Synoptic Survey. *ApJ*, 739:68–+.

Li, T. G. F., Del Pozzo, W., Vitale, S., Van Den Broeck, C., Agathos, M., Veitch, J., Grover, K., Sidery, T., Sturani, R., and Vecchio, A. (2011). Towards a generic test of the strong field dynamics of general relativity using compact binary coalescence. *ArXiv e-prints*.

Lin, L., Koo, D. C., Willmer, C. N. A., Patton, D. R., Conselice, C. J., Yan, R., Coil, A. L., Cooper, M. C., Davis, M., Faber, S. M., Gerke, B. F., Guhathakurta, P., and Newman, J. A. (2004). The DEEP2 Galaxy Redshift Survey: Evolution of Close Galaxy Pairs and Major-Merger Rates up to z ˜ 1.2. *ApJ*, 617:L9–L12.

Lin, L., Patton, D. R., Koo, D. C., Casteels, K., Conselice, C. J., Faber, S. M., Lotz, J., Willmer, C. N. A., Hsieh, B. C., Chiueh, T., Newman, J. A., Novak, G. S., Weiner, B. J., and Cooper, M. C. (2008). The Redshift Evolution of Wet, Dry, and Mixed Galaxy Mergers from Close Galaxy Pairs in the DEEP2 Galaxy Redshift Survey. *ApJ*, 681:232–243.

Liu, F. K. (2004). X-shaped radio galaxies as observational evidence for the interaction of supermassive binary black holes and accretion disc at parsec scale. *MNRAS*, 347:1357–1369.

Lodato, G. and Natarajan, P. (2006). Supermassive black hole formation during the assembly of pre-galactic discs. *MNRAS*, 371:1813–1823.

Lodato, G., Nayakshin, S., King, A. R., and Pringle, J. E. (2009). Black hole mergers: can gas discs solve the 'final parsec' problem? *MNRAS*, 398:1392–1402.

Loeb, A. (2007). Observable Signatures of a Black Hole Ejected by Gravitational-Radiation Recoil in a Galaxy Merger. *Phys. Rev. Lett.*, 99(4):041103–+.

Loeb, A. and Rasio, F. A. (1994). Collapse of primordial gas clouds and the formation of quasar black holes. *ApJ*, 432:52–61.

Lorimer, D. R. (2008). Binary and Millisecond Pulsars. *Living Reviews in Relativity*, 11:8–+.

Lousto, C. O. and Zlochower, Y. (2011a). Hangup Kicks: Still Larger Recoils by Partial Spin/Orbit Alignment of Black-Hole Binaries. *ArXiv e-prints*.

Lousto, C. O. and Zlochower, Y. (2011b). Modeling maximum astrophysical gravitational recoil velocities. *Phys. Rev. D*, 83(2):024003–+.

LSST Science Collaborations, Abell, P. A., Allison, J., Anderson, S. F., Andrew, J. R., Angel, J. R. P., Armus, L., Arnett, D., Asztalos, S. J., Axelrod, T. S., and et al. (2009). LSST Science Book, Version 2.0. *ArXiv e-prints*.

Lukes-Gerakopoulos, G., Apostolatos, T. A., and Contopoulos, G. (2010). Observable signature of a background deviating from the Kerr metric. *Phys. Rev. D*, 81(12):124005–+.

MacFadyen, A. I. and Milosavljević, M. (2008). An Eccentric Circumbinary Accretion Disk and the Detection of Binary Massive Black Holes. *ApJ*, 672:83–93.

MacLeod, C. L. and Hogan, C. J. (2008). Precision of Hubble constant derived using black hole binary absolute distances

and statistical redshift information. *Phys. Rev. D*, 77(4):043512–+.

Madau, P. and Rees, M. J. (2001). Massive Black Holes as Population III Remnants. *ApJ*, 551:L27–L30.

Maggiore, M. (2000). Gravitational wave experiments and early universe cosmology. *Phys. Rep.*, 331:283–367.

Magorrian, J., Tremaine, S., Richstone, D., Bender, R., Bower, G., Dressler, A., Faber, S. M., Gebhardt, K., Green, R., Grillmair, C., Kormendy, J., and Lauer, T. (1998). The Demography of Massive Dark Objects in Galaxy Centers. *AJ*, 115:2285–2305.

Makino, J. and Funato, Y. (2004). Evolution of Massive Black Hole Binaries. *ApJ*, 602:93–102.

Maoz, E. (1998). Dynamical Constraints on Alternatives to Supermassive Black Holes in Galactic Nuclei. *ApJ*, 494:L181+.

Marconi, A. and Hunt, L. K. (2003). The Relation between Black Hole Mass, Bulge Mass, and Near-Infrared Luminosity. *ApJ*, 589:L21–L24.

Marconi, A., Risaliti, G., Gilli, R., Hunt, L. K., Maiolino, R., and Salvati, M. (2004). Local supermassive black holes, relics of active galactic nuclei and the X-ray background. *MNRAS*, 351:169–185.

Marronetti, P., Tichy, W., Brügmann, B., González, J., and Sperhake, U. (2008). High-spin binary black hole mergers. *Phys. Rev. D*, 77(6):064010–+.

Marsh, T. R. (2011). Double white dwarfs and LISA. *Class. Quantum Grav.*, 28(9):094019–+.

Marsh, T. R., Nelemans, G., and Steeghs, D. (2004). Mass transfer between double white dwarfs. *MNRAS*, 350:113–128.

Marsh, T. R. and Steeghs, D. (2002). V407 Vul: a direct impact accretor. *MNRAS*, 331:L7–L11.

Mathur, S. and Grupe, D. (2005). The Locus of Highly Accreting Active Galactic Nuclei on the M_{BH}-σ Plane: Selections, Limitations, and Implications. *ApJ*, 633:688–692.

Mayer, L., Kazantzidis, S., Escala, A., and Callegari, S. (2010). Direct formation of supermassive black holes via multi-scale gas inflows in galaxy mergers. *Nature*, 466:1082–1084.

Mayer, L., Kazantzidis, S., Madau, P., Colpi, M., Quinn, T., and Wadsley, J. (2007). Rapid Formation of Supermassive Black Hole Binaries in Galaxy Mergers with Gas. *Science*, 316:1874–.

McWilliams, S. T. (2010). Constraining the Braneworld with Gravitational Wave Observations. *Phys. Rev. Lett.*, 104(14):141601–+.

Merloni, A. (2004). The anti-hierarchical growth of supermassive black holes. *MNRAS*, 353:1035–1047.

Merritt, D. (2006). Mass Deficits, Stalling Radii, and the Merger Histories of Elliptical Galaxies. *ApJ*, 648:976–986.

Merritt, D., Alexander, T., Mikkola, S., and Will, C. M. (2011). Stellar dynamics of extreme-mass-ratio inspirals. *Phys. Rev. D*, 84(4):044024–+.

Merritt, D. and Ekers, R. D. (2002). Tracing Black Hole Mergers Through Radio Lobe Morphology. *Science*, 297:1310–1313.

Merritt, D., Gualandris, A., and Mikkola, S. (2009a). Explaining the Orbits of the Galactic Center S-Stars. *ApJ*, 693:L35–L38.

Merritt, D., Mikkola, S., and Szell, A. (2007). Long-Term Evolution of Massive Black Hole Binaries. III. Binary Evolution in Collisional Nuclei. *ApJ*, 671:53–72.

Merritt, D. and Milosavljević, M. (2005). Massive Black Hole Binary Evolution. *Living Reviews in Relativity*, 8:8–+.

Merritt, D. and Poon, M. Y. (2004). Chaotic Loss Cones and Black Hole Fueling. *ApJ*, 606:788–798.

Merritt, D., Schnittman, J. D., and Komossa, S. (2009b). Hypercompact Stellar Systems Around Recoiling Supermassive Black Holes. *ApJ*, 699:1690–1710.

Mihos, J. C. and Hernquist, L. (1996). Gasdynamics and Starbursts in Major Mergers. *ApJ*, 464:641–+.

Miller, M. C. (2009). Intermediate-mass black holes as LISA sources. *Class. Quantum Grav.*, 26(9):094031–+.

Miller, M. C. and Colbert, E. J. M. (2004). Intermediate-Mass Black Holes. *International Journal of Modern Physics D*, 13:1–64.

Miller, M. C., Freitag, M., Hamilton, D. P., and Lauburg, V. M. (2005). Binary Encounters with Supermassive Black Holes: Zero-Eccentricity LISA Events. *ApJ*, 631:L117–L120.

Milosavljević, M. and Merritt, D. (2001). Formation of Galactic Nuclei. *ApJ*, 563:34–62.

Milosavljević, M. and Phinney, E. S. (2005). The Afterglow of Massive Black Hole Coalescence. *ApJ*, 622:L93–L96.

Miralda-Escude, J. (1998). Reionization of the Intergalactic Medium and the Damping Wing of the Gunn-Peterson Trough. *ApJ*, 501:15–+.

Miralda-Escudé, J. and Gould, A. (2000). A Cluster of Black Holes at the Galactic Center. *ApJ*, 545:847–853.

Mirshekari, S., Yunes, N., and Will, C. M. (2011). Constraining Generic Lorentz Violation and the Speed of the Graviton with Gravitational Waves. *ArXiv e-prints*.

Mishra, C. K., Arun, K. G., Iyer, B. R., and Sathyaprakash, B. S. (2010). Parametrized tests of post-Newtonian theory using Advanced LIGO and Einstein Telescope. *Phys. Rev. D*, 82(6):064010–+.

Mo, H., van den Bosch, F. C., and White, S. (2010). *Galaxy Formation and Evolution*. Cambridge University Press.

Moderski, R., Sikora, M., and Lasota, J.-P. (1998). On the spin paradigm and the radio dichotomy of quasars. *MNRAS*, 301:142–148.

Montero, P. J., Janka, H.-T., and Mueller, E. (2011). Relativistic collapse and explosion of rotating supermassive stars with thermonuclear effects. *ArXiv e-prints*.

Montuori, C., Dotti, M., Colpi, M., Decarli, R., and Haardt, F. (2011). Search for sub-parsec massive binary black holes through line diagnosis. *MNRAS*, 412:26–32.

Mortlock, D. J., Warren, S. J., Venemans, B. P., Patel, M., Hewett, P. C., McMahon, R. G., Simpson, C., Theuns, T., Gonzáles-Solares, E. A., Adamson, A., Dye, S., Hambly, N. C., Hirst, P., Irwin, M. J., Kuiper, E., Lawrence, A., and Röttgering, H. J. A. (2011). A luminous quasar at a redshift of z = 7.085. *Nature*, 474:616–619.

Mouawad, N., Eckart, A., Pfalzner, S., Schödel, R., Moultaka, J., and Spurzem, R. (2005). Weighing the cusp at the Galactic Centre. *Astronomische Nachrichten*, 326:83–95.

Nelemans, G., Portegies Zwart, S. F., Verbunt, F., and Yungelson, L. R. (2001). Population synthesis for double white dwarfs. II. Semi-detached systems: AM CVn stars. *A&A*, 368:939–949.

Nelemans, G. and Tout, C. A. (2005). Reconstructing the evolution of white dwarf binaries: further evidence for an alternative algorithm for the outcome of the common-envelope phase in close binaries. *MNRAS*, 356:753–764.

Nelemans, G., Yungelson, L. R., and Portegies Zwart, S. F. (2004). Short-period AM CVn systems as optical, X-ray and gravitational-wave sources. *MNRAS*, 349:181–192.

O'Leary, R. M. and Loeb, A. (2009). Star clusters around recoiled black holes in the Milky Way halo. *MNRAS*, 395:781–786.

Omukai, K. and Palla, F. (2001). On the Formation of Massive Primordial Stars. *ApJ*, 561:L55–L58.

Omukai, K. and Palla, F. (2003). Formation of the First Stars by Accretion. *ApJ*, 589:677–687.

Orosz, J. A. (2003). Inventory of black hole binaries. In K. van der Hucht, A. Herrero, & C. Esteban, editor, *A Massive Star Odyssey: From Main Sequence to Supernova*, volume 212 of *IAU Symposium*, pages 365–+.

Ostriker, E. C. (1999). Dynamical Friction in a Gaseous Medium. *ApJ*, 513:252–258.

Paczynski, B. (1976). Common Envelope Binaries. In P. Eggleton, S. Mitton, & J. Whelan, editor, *Structure and Evolution of Close Binary Systems*, volume 73 of *IAU Symposium*, pages 75–+.

Pakmor, R., Kromer, M., Röpke, F. K., Sim, S. A., Ruiter, A. J., and Hillebrandt, W. (2010). Sub-luminous type Ia supernovae from the mergers of equal-mass white dwarfs with mass ˜0.9$M_{\rm solar}$. *Nature*, 463:61–64.

Pan, Y., Buonanno, A., Boyle, M., Buchman, L. T., Kidder, L. E., Pfeiffer, H. P., and Scheel, M. A. (2011). Inspiral-merger-ringdown multipolar waveforms of nonspinning black-hole binaries using the effective-one-body formalism. *ArXiv e-prints*.

Pani, P., Berti, E., Cardoso, V., Chen, Y., and Norte, R. (2009). Gravitational wave signatures of the absence of an event horizon: Nonradial oscillations of a thin-shell gravastar. *Phys. Rev. D*, 80(12):124047–+.

Pani, P. and Cardoso, V. (2009). Are black holes in alternative theories serious astrophysical candidates? The case for Einstein-dilaton-Gauss-Bonnet black holes. *Phys. Rev. D*, 79(8):084031.

Pani, P., Cardoso, V., and Gualtieri, L. (2011). Gravitational waves from extreme mass-ratio inspirals in dynamical Chern-Simons gravity. *Phys. Rev. D*, 83(10):104048–+.

Patruno, A., Haskell, B., and D'Angelo, C. (2011). Gravitational Waves and the Maximum Spin Frequency of Neutron Stars. *ArXiv e-prints*.

Patton, D. R., Pritchet, C. J., Carlberg, R. G., Marzke, R. O., Yee, H. K. C., Hall, P. B., Lin, H., Morris, S. L., Sawicki, M., Shepherd, C. W., and Wirth, G. D. (2002). Dynamically Close Galaxy Pairs and Merger Rate Evolution in the CNOC2 Redshift Survey. *ApJ*, 565:208–222.

Peng, C. Y. (2007). How Mergers May Affect the Mass Scaling Relation between Gravitationally Bound Systems. *ApJ*, 671:1098–1107.

Perego, A., Dotti, M., Colpi, M., and Volonteri, M. (2009). Mass and spin co-evolution during the alignment of a black hole in a warped accretion disc. *MNRAS*, 399:2249–2263.

Perets, H. B. and Alexander, T. (2008). Massive Perturbers and the Efficient Merger of Binary Massive Black Holes. *ApJ*, 677:146–159.

Perets, H. B., Badenes, C., Arcavi, I., Simon, J. D., and Gal-yam, A. (2011). An Emerging Class of Bright, Fast-evolving Supernovae with Low-mass Ejecta. *ApJ*, 730:89–+.

Perets, H. B., Gal-Yam, A., Mazzali, P. A., Arnett, D., Kagan, D., Filippenko, A. V., Li, W., Arcavi, I., Cenko, S. B., Fox, D. B., Leonard, D. C., Moon, D.-S., Sand, D. J., Soderberg, A. M., Anderson, J. P., James, P. A., Foley, R. J., Ganeshalingam, M., Ofek, E. O., Bildsten, L., Nelemans, G., Shen, K. J., Weinberg, N. N., Metzger, B. D., Piro, A. L., Quataert, E., Kiewe, M., and Poznanski, D. (2010). A faint type of supernova from a white dwarf with a helium-rich companion. *Nature*, 465:322–325.

Perlmutter, S. and Riess, A. (1999). Cosmological parameters from supernovae: Two groups' results agree. In D. O. Cald-

well, editor, *COSMO-98*, volume 478 of *AIP Conf. Series*, pages 129–142.

Peters, P. C. (1964). Gravitational Radiation and the Motion of Two Point Masses. *Physical Review*, 136:1224–1232.

Peterson, B. M., Bentz, M. C., Desroches, L.-B., Filippenko, A. V., Ho, L. C., Kaspi, S., Laor, A., Maoz, D., Moran, E. C., Pogge, R. W., and Quillen, A. C. (2005). Multiwavelength Monitoring of the Dwarf Seyfert 1 Galaxy NGC 4395. I. A Reverberation-based Measurement of the Black Hole Mass. *ApJ*, 632:799–808.

Petiteau, A., Auger, G., Halloin, H., Jeannin, O., Plagnol, E., Pireaux, S., Regimbau, T., and Vinet, J.-Y. (2008). LISACode: A scientific simulator of LISA. *Phys. Rev. D*, 77(2):023002.

Petiteau, A., Babak, S., and Sesana, A. (2011). Constraining the Dark Energy Equation of State Using LISA Observations of Spinning Massive Black Hole Binaries. *ApJ*, 732:82–+.

Phinney, E. S. (2009). Finding and Using Electromagnetic Counterparts of Gravitational Wave Sources. In *astro2010: The Astronomy and Astrophysics Decadal Survey*, volume 2010 of *Astronomy*, pages 235–+.

Piro, A. L. (2011). Tidal Interactions in Merging White Dwarf Binaries. *ApJ*, 740:L53+.

Popham, R. and Gammie, C. F. (1998). Advection-dominated Accretion Flows in the Kerr Metric. II. Steady State Global Solutions. *ApJ*, 504:419–+.

Portegies Zwart, S. F., Baumgardt, H., Hut, P., Makino, J., and McMillan, S. L. W. (2004). Formation of massive black holes through runaway collisions in dense young star clusters. *Nature*, 428:724–726.

Portegies Zwart, S. F. and McMillan, S. L. W. (2000). Black Hole Mergers in the Universe. *ApJ*, 528:L17–L20.

Portegies Zwart, S. F. and McMillan, S. L. W. (2002). The Runaway Growth of Intermediate-Mass Black Holes in Dense Star Clusters. *ApJ*, 576:899–907.

Porter, E. K. (2009). An Overview of LISA Data Analysis Algorithms. *GW Notes*, 1:4–+.

Press, W. H. and Schechter, P. (1974). Formation of Galaxies and Clusters of Galaxies by Self-Similar Gravitational Condensation. *ApJ*, 187:425–438.

Preto, M. and Amaro-Seoane, P. (2010). On Strong Mass Segregation Around a Massive Black Hole: Implications for Lower-Frequency Gravitational-Wave Astrophysics. *ApJ*, 708:L42–L46.

Preto, M., Berentzen, I., Berczik, P., and Spurzem, R. (2011). Fast Coalescence of Massive Black Hole Binaries from Mergers of Galactic Nuclei: Implications for Low-frequency Gravitational-wave Astrophysics. *ApJ*, 732:L26+.

Pretorius, F. (2005). Evolution of Binary Black-Hole Spacetimes. *Phys. Rev. Lett.*, 95(12):121101–+.

Quinlan, G. D. (1996). The dynamical evolution of massive black hole binaries I. Hardening in a fixed stellar background. *NewA*, 1:35–56.

Racine, É., Phinney, E. S., and Arras, P. (2007). Non-dissipative tidal synchronization in accreting binary white dwarf systems. *MNRAS*, 380:381–398.

Randall, L. and Servant, G. (2007). Gravitational Waves from Warped Spacetime. *Journal of High Energy Physics*, 5:54–+.

Rau, A., Roelofs, G. H. A., Groot, P. J., Marsh, T. R., Nelemans, G., Steeghs, D., Salvato, M., and Kasliwal, M. M. (2010). A Census of AM CVn Stars: Three New Candidates and One Confirmed 48.3-Minute Binary. *ApJ*, 708:456–461.

Rezzolla, L., Barausse, E., Dorband, E. N., Pollney, D., Reisswig, C., Seiler, J., and Husa, S. (2008a). Final spin from the coalescence of two black holes. *Phys. Rev. D*, 78(4):044002–+.

Rezzolla, L., Diener, P., Dorband, E. N., Pollney, D., Reisswig, C., Schnetter, E., and Seiler, J. (2008b). The Final Spin from the Coalescence of Aligned-Spin Black Hole Binaries. *ApJ*, 674:L29–L32.

Rhook, K. J. and Wyithe, J. S. B. (2005). Realistic event rates for detection of supermassive black hole coalescence by LISA. *MNRAS*, 361:1145–1152.

Riess, A. G., Nugent, P., Filippenko, A. V., Kirshner, R. P., and Perlmutter, S. (1998). Snapshot Distances to Type IA Supernovae: All in "One" Night's Work. *ApJ*, 504:935–+.

Ripamonti, E., Haardt, F., Ferrara, A., and Colpi, M. (2002). Radiation from the first forming stars. *MNRAS*, 334:401–418.

Robertson, B., Hernquist, L., Cox, T. J., Di Matteo, T., Hopkins, P. F., Martini, P., and Springel, V. (2006). The Evolution of the M_{BH}-σ Relation. *ApJ*, 641:90–102.

Rodriguez, C., Taylor, G. B., Zavala, R. T., Peck, A. B., Pollack, L. K., and Romani, R. W. (2006). A Compact Supermassive Binary Black Hole System. *ApJ*, 646:49–60.

Rodriguez, C., Taylor, G. B., Zavala, R. T., Pihlström, Y. M., and Peck, A. B. (2009). H I Observations of the Supermassive Binary Black Hole System in 0402+379. *ApJ*, 697:37–44.

Roelofs, G. H. A., Groot, P. J., Nelemans, G., Marsh, T. R., and Steeghs, D. (2006). Kinematics of the ultracompact helium accretor AM Canum Venaticorum. *MNRAS*, 371:1231–1242.

Roelofs, G. H. A., Nelemans, G., and Groot, P. J. (2007). The population of AM CVn stars from the Sloan Digital Sky Survey. *MNRAS*, 382:685–692.

Roelofs, G. H. A., Rau, A., Marsh, T. R., Steeghs, D., Groot, P. J., and Nelemans, G. (2010). Spectroscopic Evidence for a 5.4 Minute Orbital Period in HM Cancri. *ApJ*, 711:L138–L142.

Ruiter, A. J., Belczynski, K., Benacquista, M., and Holley-Bockelmann, K. (2009). The Contribution of Halo White Dwarf Binaries to the Laser Interferometer Space Antenna Signal. *ApJ*, 693:383–387.

Ruiter, A. J., Belczynski, K., Benacquista, M., Larson, S. L., and Williams, G. (2010). The LISA Gravitational Wave Foreground: A Study of Double White Dwarfs. *ApJ*, 717:1006–1021.

Ryan, F. D. (1995). Gravitational waves from the inspiral of a compact object into a massive, axisymmetric body with arbitrary multipole moments. *Phys. Rev. D*, 52:5707–5718.

Salpeter, E. E. (1964). Accretion of Interstellar Matter by Massive Objects. *ApJ*, 140:796–800.

Santamaría, L., Ohme, F., Ajith, P., Brügmann, B., Dorband, N., Hannam, M., Husa, S., Mösta, P., Pollney, D., Reisswig, C., Robinson, E. L., Seiler, J., and Krishnan, B. (2010). Matching post-Newtonian and numerical relativity waveforms: Systematic errors and a new phenomenological model for nonprecessing black hole binaries. *Phys. Rev. D*, 82(6):064016–+.

Schawinski, K., Dowlin, N., Thomas, D., Urry, C. M., and Edmondson, E. (2010). The Role of Mergers in Early-type Galaxy Evolution and Black Hole Growth. *ApJ*, 714:L108–L112.

Schawinski, K., Treister, E., Urry, C. M., Cardamone, C. N., Simmons, B., and Yi, S. K. (2011). HST WFC3/IR Observations of Active Galactic Nucleus Host Galaxies at z ˜ 2: Supermassive Black Holes Grow in Disk Galaxies. *ApJ*, 727:L31+.

Scheel, M. A., Boyle, M., Chu, T., Kidder, L. E., Matthews, K. D., and Pfeiffer, H. P. (2009). High-accuracy waveforms for binary black hole inspiral, merger, and ringdown. *Phys. Rev. D*, 79(2):024003–+.

Scheuer, P. A. G. and Feiler, R. (1996). The realignment of a black hole misaligned with its accretion disc. *MNRAS*, 282:291–+.

Schnittman, J. D. (2007). Retaining Black Holes with Very Large Recoil Velocities. *ApJ*, 667:L133–L136.

Schnittman, J. D. (2011). Electromagnetic counterparts to black hole mergers. *Class. Quantum Grav.*, 28(9):094021–+.

Schnittman, J. D. and Buonanno, A. (2007). The Distribution of Recoil Velocities from Merging Black Holes. *ApJ*, 662:L63–L66.

Schödel, R., Ott, T., Genzel, R., Eckart, A., Mouawad, N., and Alexander, T. (2003). Stellar Dynamics in the Central Arcsecond of Our Galaxy. *ApJ*, 596:1015–1034.

Schutz, B. F. (1986). Determining the Hubble constant from gravitational wave observations. *Nature*, 323:310–+.

Sesana, A. (2010). Self Consistent Model for the Evolution of Eccentric Massive Black Hole Binaries in Stellar Environments: Implications for Gravitational Wave Observations. *ApJ*, 719:851–864.

Sesana, A., Gair, J., Berti, E., and Volonteri, M. (2011). Reconstructing the massive black hole cosmic history through gravitational waves. *Phys. Rev. D*, 83(4):044036–+.

Sesana, A., Haardt, F., and Madau, P. (2006). Interaction of Massive Black Hole Binaries with Their Stellar Environment. I. Ejection of Hypervelocity Stars. *ApJ*, 651:392–400.

Sesana, A., Haardt, F., and Madau, P. (2007a). Interaction of Massive Black Hole Binaries with Their Stellar Environment. II. Loss Cone Depletion and Binary Orbital Decay. *ApJ*, 660:546–555.

Sesana, A., Haardt, F., and Madau, P. (2008a). Interaction of Massive Black Hole Binaries with Their Stellar Environment. III. Scattering of Bound Stars. *ApJ*, 686:432–447.

Sesana, A., Haardt, F., Madau, P., and Volonteri, M. (2004). Low-Frequency Gravitational Radiation from Coalescing Massive Black Hole Binaries in Hierarchical Cosmologies. *ApJ*, 611:623–632.

Sesana, A., Haardt, F., Madau, P., and Volonteri, M. (2005). The Gravitational Wave Signal from Massive Black Hole Binaries and Its Contribution to the LISA Data Stream. *ApJ*, 623:23–30.

Sesana, A., Vecchio, A., and Colacino, C. N. (2008b). The stochastic gravitational-wave background from massive black hole binary systems: implications for observations with Pulsar Timing Arrays. *MNRAS*, 390:192–209.

Sesana, A., Vecchio, A., and Volonteri, M. (2009). Gravitational waves from resolvable massive black hole binary systems and observations with Pulsar Timing Arrays. *MNRAS*, 394:2255–2265.

Sesana, A., Volonteri, M., and Haardt, F. (2007b). The imprint of massive black hole formation models on the LISA data stream. *MNRAS*, 377:1711–1716.

Seth, A., Agüeros, M., Lee, D., and Basu-Zych, A. (2008). The Coincidence of Nuclear Star Clusters and Active Galactic Nuclei. *ApJ*, 678:116–130.

Shakura, N. I. and Sunyaev, R. A. (1973). Black holes in binary systems. Observational appearance. *A&A*, 24:337–355.

Shapiro, S. L. and Teukolsky, S. A. (1979). Gravitational collapse of supermassive stars to black holes - Numerical solution of the Einstein equations. *ApJ*, 234:L177–L181.

Shapiro, S. L. and Teukolsky, S. A. (1986). *Black Holes, White Dwarfs and Neutron Stars: The Physics of Compact Objects*. Wiley-VCH.

Shen, Y. and Loeb, A. (2010). Identifying Supermassive Black Hole Binaries with Broad Emission Line Diagnosis. *ApJ*, 725:249–260.

Sheth, R. K. and Tormen, G. (1999). Large-scale bias and the peak background split. *MNRAS*, 308:119–126.

Shibata, M. and Shapiro, S. L. (2002). Collapse of a Rotating Supermassive Star to a Supermassive Black Hole: Fully Relativistic Simulations. *ApJ*, 572:L39–L43.

Shields, G. A., Rosario, D. J., Smith, K. L., Bonning, E. W., Salviander, S., Kalirai, J. S., Strickler, R., Ramirez-Ruiz, E., Dutton, A. A., Treu, T., and Marshall, P. J. (2009). The quasar sdss j105041.35+345631.3: Black hole recoil or extreme double-peaked emitter? *ApJ*, 707(2):936.

Shlosman, I., Frank, J., and Begelman, M. C. (1989). Bars within bars - A mechanism for fuelling active galactic nuclei. *Nature*, 338:45–47.

Siemens, X., Creighton, J., Maor, I., Majumder, S. R., Cannon, K., and Read, J. (2006). Gravitational wave bursts from cosmic (super)strings: Quantitative analysis and constraints. *Phys. Rev. D*, 73(10):105001–+.

Sigurdsson, S. and Rees, M. J. (1997). Capture of stellar mass compact objects by massive black holes in galactic cusps. *MNRAS*, 284:318–326.

Silk, J. and Rees, M. J. (1998). Quasars and galaxy formation. *A&A*, 331:L1–L4.

Soltan, A. (1982). Masses of quasars. *MNRAS*, 200:115–122.

Somerville, R. S., Hopkins, P. F., Cox, T. J., Robertson, B. E., and Hernquist, L. (2008). A semi-analytic model for the co-evolution of galaxies, black holes and active galactic nuclei. *MNRAS*, 391:481–506.

Sopuerta, C. F. (2010). A Roadmap to Fundamental Physics from LISA EMRI Observations. *GW Notes*, 4:3–47.

Sopuerta, C. F. and Yunes, N. (2009). Extreme- and intermediate-mass ratio inspirals in dynamical Chern-Simons modified gravity. *Phys. Rev. D*, 80(6):064006–+.

Springel, V., White, S. D. M., Jenkins, A., Frenk, C. S., Yoshida, N., Gao, L., Navarro, J., Thacker, R., Croton, D., Helly, J., Peacock, J. A., Cole, S., Thomas, P., Couchman, H., Evrard, A., Colberg, J., and Pearce, F. (2005). Simulations of the formation, evolution and clustering of galaxies and quasars. *Nature*, 435:629–636.

Stroeer, A., Benacquista, M., and Ceballos, F. (2011). Detecting Double Degenerate Progenitors of SNe Ia with LISA. *ArXiv e-prints*.

Stroeer, A. and Nelemans, G. (2009). The influence of short-term variations in AM CVn systems on LISA measurements. *MNRAS*, 400:L24–L28.

Stroeer, A. and Vecchio, A. (2006). The LISA verification binaries. *Class. Quantum Grav.*, 23:809–+.

Sullivan, M., Kasliwal, M. M., Nugent, P. E., Howell, D. A., Thomas, R. C., Ofek, E. O., Arcavi, I., Blake, S., Cooke, J., Gal-Yam, A., Hook, I. M., Mazzali, P., Podsiadlowski, P., Quimby, R., Bildsten, L., Bloom, J. S., Cenko, S. B., Kulkarni, S. R., Law, N., and Poznanski, D. (2011). The Subluminous and Peculiar Type Ia Supernova PTF 09dav. *ApJ*, 732:118–+.

Taam, R. E. and Ricker, P. M. (2010). Common envelope evolution. *NewAR*, 54:65–71.

Taam, R. E. and Sandquist, E. L. (2000). Common Envelope Evolution of Massive Binary Stars. *ARA&A*, 38:113–141.

Tegmark, M., Silk, J., Rees, M. J., Blanchard, A., Abel, T., and Palla, F. (1997). How Small Were the First Cosmological Objects? *ApJ*, 474:1–+.

Teukolsky, S. A. (1973). Perturbations of a Rotating Black Hole. I. Fundamental Equations for Gravitational, Electromagnetic, and Neutrino-Field Perturbations. *ApJ*, 185:635–648.

Thorne, K. S. (1974). Disk-Accretion onto a Black Hole. II. Evolution of the Hole. *ApJ*, 191:507–520.

Tremaine, S., Gebhardt, K., Bender, R., Bower, G., Dressler, A., Faber, S. M., Filippenko, A. V., Green, R., Grillmair, C., Ho, L. C., Kormendy, J., Lauer, T. R., Magorrian, J., Pinkney, J., and Richstone, D. (2002). The Slope of the Black Hole Mass versus Velocity Dispersion Correlation. *ApJ*, 574:740–753.

Treu, T., Woo, J.-H., Malkan, M. A., and Blandford, R. D. (2007). Cosmic Evolution of Black Holes and Spheroids. II. Scaling Relations at z=0.36. *ApJ*, 667:117–130.

Tsalmantza, P., Decarli, R., Dotti, M., and Hogg, D. W. (2011). A Systematic Search for Massive Black Hole Binaries in the Sloan Digital Sky Survey Spectroscopic Sample. *ApJ*, 738:20–+.

Tundo, E., Bernardi, M., Hyde, J. B., Sheth, R. K., and Pizzella, A. (2007). On the Inconsistency between the Black Hole Mass Function Inferred from $M_\bullet$-σ and $M_\bullet$-L Correlations. *ApJ*, 663:53–60.

Valsecchi, F., Farr, W. M., Willems, B., Deloye, C. . J., and Kalogera, V. (2011). Tidally-Induced Apsidal Precession in Double White Dwarfs: a new mass measurement tool with LISA. *ArXiv e-prints*.

Valtonen, M. J., Lehto, H. J., Nilsson, K., Heidt, J., Takalo, L. O., Sillanpää, A., Villforth, C., Kidger, M., Poyner, G., Pursimo, T., Zola, S., Wu, J.-H., Zhou, X., Sadakane, K., Drozdz, M., Koziel, D., Marchev, D., Ogloza, W., Porowski, C., Siwak, M., Stachowski, G., Winiarski, M., Hentunen, V.-P., Nissinen, M., Liakos, A., and Dogru, S. (2008). A massive binary black-hole system in OJ287 and a test of general relativity. *Nature*, 452:851–853.

Valtonen, M. J., Lehto, H. J., Takalo, L. O., and Sillanpää, A. (2011). Testing the 1995 Binary Black Hole Model of OJ287. *ApJ*, 729:33–+.

Valtonen, M. J., Mikkola, S., Merritt, D., Gopakumar, A., Lehto, H. J., Hyvönen, T., Rampadarath, H., Saunders, R.,

Basta, M., and Hudec, R. (2010). Measuring the Spin of the Primary Black Hole in OJ287. *ApJ*, 709:725–732.

Valtonen, M. J., Nilsson, K., Sillanpää, A., Takalo, L. O., Lehto, H. J., Keel, W. C., Haque, S., Cornwall, D., and Mattingly, A. (2006). The 2005 November Outburst in OJ 287 and the Binary Black Hole Model. *ApJ*, 643:L9–L12.

van der Marel, R. P., Rix, H. W., Carter, D., Franx, M., White, S. D. M., and de Zeeuw, T. (1994). Velocity Profiles of Galaxies with Claimed Black-Holes - Part One - Observations of M31 M32 NGC3115 and NGC4594. *MNRAS*, 268:521–+.

Vigeland, S., Yunes, N., and Stein, L. C. (2011). Bumpy black holes in alternative theories of gravity. *Phys. Rev. D*, 83(10):104027–+.

Vigeland, S. J. and Hughes, S. A. (2010). Spacetime and orbits of bumpy black holes. *Phys. Rev. D*, 81(2):024030–+.

Volonteri, M. (2010). Formation of supermassive black holes. *A&A Rev.*, 18:279–315.

Volonteri, M. and Begelman, M. C. (2010). Quasi-stars and the cosmic evolution of massive black holes. *MNRAS*, 409:1022–1032.

Volonteri, M., Gültekin, K., and Dotti, M. (2010). Gravitational recoil: effects on massive black hole occupation fraction over cosmic time. *MNRAS*, 404:2143–2150.

Volonteri, M., Haardt, F., and Madau, P. (2003). The Assembly and Merging History of Supermassive Black Holes in Hierarchical Models of Galaxy Formation. *ApJ*, 582:559–573.

Volonteri, M., Lodato, G., and Natarajan, P. (2008). The evolution of massive black hole seeds. *MNRAS*, 383:1079–1088.

Volonteri, M., Miller, J. M., and Dotti, M. (2009). Sub-Parsec Supermassive Binary Quasars: Expectations at $z < 1$. *ApJ*, 703:L86–L89.

Volonteri, M. and Natarajan, P. (2009). Journey to the M_{BH}-σ relation: the fate of low-mass black holes in the Universe. *MNRAS*, 400:1911–1918.

Volonteri, M., Sikora, M., and Lasota, J. (2007). Black Hole Spin and Galactic Morphology. *ApJ*, 667:704–713.

Waldman, R., Sauer, D., Livne, E., Perets, H., Glasner, A., Mazzali, P., Truran, J. W., and Gal-Yam, A. (2011). Helium Shell Detonations on Low-mass White Dwarfs as a Possible Explanation for SN 2005E. *ApJ*, 738:21–+.

Wang, Y., Holz, D. E., and Munshi, D. (2002). A Universal Probability Distribution Function for Weak-lensing Amplification. *ApJ*, 572:L15–L18.

Watts, A. L., Krishnan, B., Bildsten, L., and Schutz, B. F. (2008). Detecting gravitational wave emission from the known accreting neutron stars. *MNRAS*, 389:839–868.

Webbink, R. F. (1984). Double white dwarfs as progenitors of R Coronae Borealis stars and Type I supernovae. *ApJ*, 277:355–360.

Webbink, R. F. (2010). Watch This Space: Observing Merging White Dwarfs. *AIP Conf. Series*, 1314:217–222.

Wehner, E. H. and Harris, W. E. (2006). From Supermassive Black Holes to Dwarf Elliptical Nuclei: A Mass Continuum. *ApJ*, 644:L17–L20.

Weisberg, J. M. and Taylor, J. H. (2005). The Relativistic Binary Pulsar B1913+16: Thirty Years of Observations and Analysis. In F. A. Rasio & I. H. Stairs, editor, *Binary Radio Pulsars*, volume 328 of *Astronomical Society of the Pacific Conference Series*, pages 25–+.

White, S. D. M. and Rees, M. J. (1978). Core condensation in heavy halos - A two-stage theory for galaxy formation and clustering. *MNRAS*, 183:341–358.

Wijnands, R. (2010). Accreting millisecond X-ray pulsars: recent developments. *Highlights of Astronomy*, 15:121–125.

Will, C. M. (2006). The Confrontation between General Relativity and Experiment. *Living Reviews in Relativity*, 9:3–+.

Willems, B., Deloye, C. J., and Kalogera, V. (2010). Energy Dissipation Through Quasi-static Tides in White Dwarf Binaries. *ApJ*, 713:239–256.

Witten, E. (1984). Cosmic separation of phases. *Phys. Rev. D*, 30:272–285.

Woo, J.-H., Treu, T., Malkan, M. A., and Blandford, R. D. (2008). Cosmic Evolution of Black Holes and Spheroids. III. The M_{BH}-σ_* Relation in the Last Six Billion Years. *ApJ*, 681:925–930.

Wyithe, J. S. B. and Loeb, A. (2002). A Physical Model for the Luminosity Function of High-Redshift Quasars. *ApJ*, 581:886–894.

Wyithe, J. S. B. and Loeb, A. (2003). Low-frequency gravitational waves from massive black hole binaries: Predictions for LISA and pulsar timing arrays. *ApJ*, 590:691–706.

Wyithe, J. S. B. and Loeb, A. (2003). Self-regulated Growth of Supermassive Black Holes in Galaxies as the Origin of the Optical and X-Ray Luminosity Functions of Quasars. *ApJ*, 595:614–623.

Xiao, T., Barth, A. J., Greene, J. E., Ho, L. C., Bentz, M. C., Ludwig, R. R., and Jiang, Y. (2011). Exploring the Low-mass End of the M_{BH}-σ_* Relation with Active Galaxies. *ApJ*, 739:28–+.

Xu, C. K., Zhao, Y., Scoville, N., Capak, P., Drory, N., and Gao, Y. (2011). Galaxy Pairs in COSMOS – Merger Rate Evolution Since z=1. *ArXiv e-prints*.

Yagi, K., Tanahashi, N., and Tanaka, T. (2011). Probing the size of extra dimensions with gravitational wave astronomy.

Phys. Rev. D, 83(8):084036–+.

Yagi, K. and Tanaka, T. (2010). Constraining alternative theories of gravity by gravitational waves from precessing eccentric compact binaries with LISA. *Phys. Rev. D*, 81(6):064008–+.

Yoshida, S., Eriguchi, Y., and Futamase, T. (1994). Quasinormal modes of boson stars. *Phys. Rev. D*, 50:6235–6246.

Yu, Q. and Tremaine, S. (2002). Observational constraints on growth of massive black holes. *MNRAS*, 335:965–976.

Yu, S. and Jeffery, C. S. (2010). The gravitational wave signal from diverse populations of double white dwarf binaries in the Galaxy. *A&A*, 521:A85+.

Yunes, N., Coleman Miller, M., and Thornburg, J. (2011). Effect of massive perturbers on extreme mass-ratio inspiral waveforms. *Phys. Rev. D*, 83(4):044030–+.

Yunes, N., Pani, P., and Cardoso, V. (2011). Gravitational Waves from Extreme Mass-Ratio Inspirals as Probes of Scalar-Tensor Theories. *ArXiv e-prints*.

Yunes, N. and Pretorius, F. (2009). Fundamental theoretical bias in gravitational wave astrophysics and the parametrized post-Einsteinian framework. *Phys. Rev. D*, 80(12):122003–+.

Yunes, N., Pretorius, F., and Spergel, D. (2010). Constraining the evolutionary history of Newton's constant with gravitational wave observations. *Phys. Rev. D*, 81(6):064018–+.

Yungelson, L. R., Nelemans, G., and van den Heuvel, E. P. J. (2002). On the formation of neon-enriched donor stars in ultracompact X-ray binaries. *A&A*, 388:546–551.

Zel'dovich, Y. B. and Novikov, I. D. (1964). The Radiation of Gravity Waves by Bodies Moving in the Field of a Collapsing Star. *Soviet Physics Doklady*, 9:246–+.

Zinnecker, H. and Yorke, H. W. (2007). Toward Understanding Massive Star Formation. *ARA&A*, 45:481–563.